DESIGN AND PERFORMANCE OF POROUS ASPHALT MIXTURE FOR PEDESTRIAN/CYCLIST APPLICATIONS IN SINGAPORE

CHEN MENGJIA

SCHOOL OF CIVIL AND ENVIRONMENTAL ENGINEERING

A thesis submitted to the Nanyang Technological University
in partial fulfilment of the requirements for the degree of
Doctor of Philosophy

2016

Acknowledgements

I would love to express my heart-felt gratitude to my supervisor, Associate Professor Wong Yiik Diew, for his valuable suggestions and continuous encouragement in the research work. Without his great support, this thesis report would not have been done.

I also would also love to extend the gratitude to all the technicians in Transport & Geospatial Laboratory: Mrs. Ng-Ho Choo Hiang, Mr. Andrew Liew Kai Liang, and Mr. Choi Siew Pheng, for their technical support in the experimental work.

I also need to thank my family and friends for the constant love and unconditional support.

Lastly, I want to acknowledge the School of Civil and Environmental Engineering, Nanyang Technological University for providing scholarship for this study.

Contents

Abstract

Porous asphalt mixture (PAM) is a particular type of asphalt mixture with high content of air voids (usually ≥ 18%), which is attributed to the open-graded design, namely coarse aggregate dominates the aggregate gradation while fine fraction is strictly limited. The benefits of PAM include driving safety (e.g. aquaplaning alleviation, splash and spray mitigation, glare reduction and skid resistance enhancement) and environmental friendliness (e.g. cooling effect and noise reduction), while the two major drawbacks are ravelling and clogging. With the rapid development in non-motorised traffic facility, it is appropriate to apply PAM in Singapore, a tropical country with frequent thunderstorms during monsoon periods, for low-strength pavement application, such as walking and cycling pathways.

The main objective of the research is to design appropriate PAM for specific application, namely low-strength pavement in Singapore. Firstly, the impact of three critical design factors, namely aggregate gradation (G), gyration compaction level (GCL), and asphalt binder type (ABT), on PAM's properties is investigated. The evaluation shows that all three factors can significantly influence PAM's air voids content, which is the most important volumetric parameter directly related to PAM's permeability and mixture strength. Generally desired air voids content is achieved by a proper open-graded design, while modified asphalt binder and sufficient compaction during preparation are needed to achieve adequate strength and durability.

As the packing structure created by the coarse aggregates is the major contributor of PAM's mixture strength, packing mechanism is analysed via both laboratory measurement and Discrete Element Method (DEM) simulation. Coarse aggregates within different size ranges are divided into three components: main-coarse (19.0-

6.3 mm aggregates), interceptor (6.3-4.75 mm aggregates), and quasi-fine (4.75-2.36 mm aggregates).

Subsequently, 7% fine fraction (namely aggregates passing 2.36 mm sieve) is selected in the open-graded design that meets the required permeability in Singapore, namely 130 $\times 10^{-3}$ cm/s, based on the gradation-permeability relationship. Four potential PAMs are designed with different aggregate gradations: (a) G_cont, the overall coarse fraction is generally continuously distributed, (b) G_coarse, main-coarse aggregates are dominant in the coarse fraction, (c) G_inter, interceptor aggregates are dominant in the coarse fraction, and (d) G_fine, quasi-fine aggregates are dominant in the coarse fraction.

Test results show that all the four PAM designs can meet the required mixture strength for low-strength pavement (namely possessing Marshall stability no lower than 4.0 kN), while only G_coarse and G_inter can achieve adequate permeability. Packing condition in the designed PAMs is subsequently evaluated via two kinds of PFC3D simulation models, a model of compacted coarse aggregate blend and a model of compacted PAM specimen. It is found that stable contact as well as chain contact is gradually developed with assistance of finer fraction in the coarse fraction, and large forces carried by the large-size particles (e.g. main-coarse and interceptor components) are partially transferred by the support of finer fraction (e.g. quasi-fine component). A simulation parameter, porosity_CP ratio is proposed, which is defined as the ratio of porosity within the coarse particles in the PFC3D model of compacted coarse aggregate blend and that in the PFC3D model of compacted PAM specimen. It turns out that porosity_CP ratio is an effective and useful parameter to assess PAM's packing degree.

Based on modified experiment methods for ravelling resistance and clogging resistance in three testing scenarios (namely unconditioned, ageing-conditioned, and moisture-conditioned), G_inter has the better performance generally. On the whole, open-graded design with a low content of fine fraction (e.g. 7%) and a high content of interceptor aggregates in the coarse fraction is suggested in the PAM design for the low-strength pavement application, while modified asphalt binder and sufficient compaction application are needed in order to achieve adequate performance.

List of Tables

List of Figures

Glossary

Term	Definition
abrasion loss value (ALV)	mass loss of asphalt mixture in percentage during abrasion
aggregate gradation	proportionate amount of aggregates by mass passing a series of sieve with consecutive sizes
asphalt binder	an asphaltic binder, which is used to glue the loose aggregates to form an integral mass during compaction. It can be either straight asphalt or modified asphalt; straight asphalt is a kind of brownish or black substance derived from petroleum, characterised by the high viscosity.
asphalt mastic	a viscous mixture composed of asphalt binder and fillers
asphalt mixture	a paving mixture composed of asphalt binder and mineral aggregates, compacted and laid in layer(s), and widely used in flexible pavements
asphalt mixture design	a series of procedures to design proper asphalt mixture for specific application, including material selection, aggregate gradation design, determination of asphalt binder content, and performance tests, etc.
clogging	degradation of air voids content in Porous Asphalt Mixture (PAM), usually caused by the debris and sands on pavement surface and rendering impaired drainage
draindown	the phenomenon that asphalt mastic flows downwards within an asphalt mixture during transporting, mixing, and compacting process

Discrete Element Method (DEM)	a type of numerical simulation method for computing the force and motion within an assembly of discrete particles
fillers	the fraction of aggregates passing 75 μm sieve
mean coordination number (MCN)	mean number of effective contacts around each particle in a model. An effective contact refers to a particle-to-particle contact carrying nonzero normal force
Nominal Maximum Aggregate Size (NMAS)	the size of the first sieve though which at least 90% aggregates of an aggregate gradation pass
packing	stone-on-stone framework formed by coarse aggregates and voids filled by fine aggregates and asphalt mastic completely or partially
permeability	capability of a permeable mixture in transferring water
porosity	ratio of voids within an assembly of particles by volume
Porous Asphalt Mixture (PAM)	a type of asphalt mixture with an open-graded design, rendering permeable structure and possessing high air voids content, e.g. in excess of 18%
ravelling	deficiency in adhesiveness and cohesiveness of asphalt mixtures with some aggregates being torn away from pavement surface
total air voids (TAV) content	air voids content in a compacted asphalt mixture, including both water-accessible air voids (WAAV) content and disconnected air voids content
voids in coarse aggregates (VCA) ratio	ratio of two types of VCA values, voids in coarse aggregates of a compacted asphalt mixture (VCA_{mix}) and that of an coarse aggregate blend under dry-rodded condition (VCA_{DRC}), namely VCA_{mix}/VCA_{DRC}

water-accessible air voids (WAAW) content	content of inter-connective air voids in a compacted asphalt mixture that allows water to pass through

Chapter 1 Introduction

1.1 Background

Asphalt mixture, also called asphalt concrete (AC), is a composite mixture mainly formed by mineral aggregates and asphalt binder. It is widely applied in flexible pavements, being compacted and laid in layer(s). Porous Asphalt Mixture (PAM) is a particular type of asphalt mixture with high content of air voids (i.e. usually in excess of 18%), which is generated by an open-graded design. Namely, coarse aggregates predominate in the aggregate blend to produce the stone-on-stone backbone in PAM, while the fine fraction content is much lower and insufficient to fill up all the air voids created by the coarse fraction. The specific structure of PAM is favourable for pavement application in terms of driving safety and environmental benefits.

Engineering experience and laboratory investigations show that application of PAM in the road pavement can enhance skid resistance between pavement surface and tyres in wet conditions by reducing aquaplaning, and splash and spray, which is attributed to the excellent drainage performance generated by the high content of water-accessible air voids (Khalid and Jimenez 1995; Ferguson 2005). Meanwhile, a lowered noise level is observed on permeable roads since compressed air generated between tyres and pavement, which is the main source of noise, is partially absorbed into the voids distributed on the surface's macro texture. In fact, alleviating noise pollution is the primary objective of utilising PAM in some countries, such as U.K., the Netherlands, and Germany (Fabb 1998). In addition, the operating environment can benefit from the application of PAM as well, as accrued from the functions of PAM in generating cooling effect, mitigating glare, facilitating infiltration, etc.

The intrinsic feature of PAM, namely high air voids content, directly contributes to the essential functions, namely adequate permeability, noise reduction, and cooling effect, while disutility effects on the strength and durability should be taken into consideration in PAM design, among which ravelling and clogging are the critical ones. Ravelling refers to the deficiency in asphalt mixture's cohesiveness with some aggregates being torn away from pavement surface especially under the severe environment (e.g. exposure to moisture, ageing, and oxidation) and/or heavy traffic condition, and consequently the structure of PAM pavement deteriorates gradually. Clogging refers to the degradation of PAM's porosity, which causes the premature loss of PAM's essential functions, such as efficient drainage and noise absorption, thereby decreasing the functional service life of PAM pavement. Hence, the two disutility effects of ravelling and clogging should be carefully dealt with during the procedure of asphalt mixture design as well as on-site application.

As a country located in Southeast Asia and specifically at 1.22 degrees north of the equator, Singapore possesses the typical tropical and equatorial climatic condition, namely experiencing high temperature and rainy weather throughout the year with frequent thunderstorms during monsoons (Fong 2012). Thus it is favourable to apply PAM in Singapore to alleviate the issues of pavement drainage and promoting cooler environment during daytime. Though PAM is generally weaker than conventional dense asphalt mixture in the aspects of strength and durability if no additional modification is applied, it possesses great potential for low-strength pavement application, especially considering the tremendous development in infrastructural networks for pedestrian/cyclist pathways in Singapore (Koh and Wong 2012).

1.2 Problem statement

Various asphalt mixture design methods for PAM have been proposed in different countries over the years. In order to assess PAM's basic functions, several performance tests have been introduced and applied in asphalt mixture design, such as permeability test, abrasion resistance test, moisture susceptibility test, and ageing test (Smith et al. 1974; Nicholls and Carswell 2001; Watson et al. 2003; Zhu 2005).

In terms of volumetric measurement, air voids content is the most critical parameter for permeable mixtures to realise essential functions, including the content of total air voids (TAV) and water-accessible air voids (WAAV). However, most current PAM design methods have been focused on pavement applications in the field of high volume traffic; instead, less emphasis has been put on PAM's high air voids content for the function of storm water management (Putman and Kline 2012). Nowadays PAM has been utilised in various situations, including expressways, arterial roads, collector roads, local access roads, airport pavements, and parking lots etc., and it is important that PAM should be appropriately designed for each specific application, with consideration of climatic and traffic conditions. Herein, the present research is conducted on PAM design for low-strength pavement applications in a tropical environment.

In terms of aggregate packing, PAM's open-graded design generates the distinctive mixture structure, namely the particle-to-particle interlocking is mainly created by coarse aggregates, and high content of air voids is retained due to the low amount of fine fraction. Thereby very little mixture stability is derived from the fine aggregates. PAM's mechanical properties, such as the capability in carrying external loads and resisting deformation, is therefore heavily attributed to the packing condition generated by the coarse aggregates.

Most packing theories and corresponding aggregate gradation design methods are based on dense asphalt mixtures (Fuller and Thompson 1907; Kandhal 2002; Vavrik et al. 2002). Meanwhile, in current packing theories, the evaluation of packing condition in aggregate blends and/or asphalt mixtures is limited to assessing volumetric parameters (e.g. voids content and/or unit weight), due to the ease in laboratory measurement. For example, Kandhal (2002) assessed the stone-on-stone framework in an asphalt mixture through the comparison between two kinds of voids in coarse aggregates (VCA) value, namely voids in coarse aggregates of compacted aggregate mixture (VCA_{mix}) and voids in coarse aggregates of coarse aggregate blend under dry-rodded condition (VCA_{DRC}) with the same material and aggregate gradation, and it was assumed that aggregate interlocking was adequate upon the ratio of VCA_{mix}/VCA_{DRC} being less than 1.0. In Bailey's method, the

factor to evaluate the packing condition was the unit weight of aggregate mixture, and Rodded Unit Weight (RUW) and Loose Unit Weight (LUW) were regarded as the reference values for a specific aggregate blend (Vavrik et al. 2002). In fact, various kinds of voids content value in an aggregate blend and/or a compacted asphalt mixture were utilised to describe the aggregate interaction (Furnas 1931; Al-Jarallah & Tons; Kim et al. 2009).

On the other hand, as compared to volumetric parameters, particle-to-particle contacting mechanism within a compacted mixture is a more direct and meaningful parameter to describe the packing condition among aggregates, which relates strongly to asphalt mixture's behaviour as well. Thus, a desired PAM gradation should be designed involving both volumetric analysis and contacting mechanism. Nonetheless, little research has been conducted on analysing aggregate interlocking in the aspect of contacting mechanism due to the difficulty in measurement by means of conventional methods in the laboratory.

With the development of Discrete Element Method (DEM), a type of numerical simulation method, the particle-to-particle contact within an assembly of particles can be explicitly illustrated by DEM simulation, in which the algorithm is a dynamic process based on the alternate execution of law of motion (Newton's second law) and force-displacement law. Particle Flow Code in 3 Dimensions (PFC3D), an application software based on DEM theory (Itasca 2008), was applied in this research. Simulation parameters generated in PFC3D model, such as porosity and coordination number, are effective in assessing the particle interaction in a mixture (Cundall and Strack 1983). Therefore it is valuable to obtain a better understanding of packing condition in PAM using DEM simulation together with measurements in the laboratory.

1.3 Objectives

The broad objective of this research is to obtain a suitable PAM design for application in pedestrian/cyclist pathways in Singapore. This shall be realised through three aspects: (a) investigating the impacts of design factors on PAM's mechanical and functional properties, (b) evaluating the development of packing

condition in PAM, and (c) assessing the potential of PAMs for the specific application, namely low-strength pavement application in wet environment, by means of a series of appropriate and practical performance tests. The corresponding specific objectives of the research are:

- To investigate the effect of design factors, namely aggregate gradation (G), gyration compaction level (GCL), and asphalt binder type (ABT), on PAM's basic properties, such as air voids content, permeability, strength, resistance to abrasion, resistance to moisture etc.;

- To discern the development of particle-to-particle interlocking in PAMs via laboratory measurements and DEM simulation, and analyse the role of aggregates of different size ranges within the coarse fraction;

- To design appropriate PAMs that are well-fitted for Singapore's low-strength pavement application, through proper determination of the design factors and assessment of the resultant packing condition via DEM simulation; and

- To assess the feasibility of designed PAMs in specific pavement applications (i.e. pedestrian/cyclist pathways in tropical regions), through a series of performance tests, including both standard and modified testing methods.

1.4 Significance

This research introduces a simulation (DEM) approach to explicitly evaluate the establishment and development of packing structure in PAM in terms of particle-to-particle contact, which thus provides a better understanding in contacting mechanism within an assembly of compacted particles and hence be valuable in guiding PAM aggregate gradation design. Moreover, modified performance tests are proposed to measure PAM's resistance to ravelling and clogging, which are useful for assessing PAM's functional attributes.

1.5 Organisation

The flowchart of research overall planning is given in Figure 1.1. This thesis comprises eight chapters. Chapter 1 gives the problem statement together with background knowledge on PAM and relevant packing theories, and describes the objectives to be accomplished. Chapter 2 outlines the literature reviews on the development of PAM, the current mixture design methods, the assessment of various packing theories, and the introduction of numerical simulation methods. Chapter 3 presents the materials and methodologies selected in conducting laboratory measurements and establishing numerical simulation models in this research. Chapters 4-7 are the main body of the thesis, and they are covered as follows:

- Chapter 4 looks into the effect of several critical design factors, namely aggregate gradation (G), gyration compaction level (GCL), and asphalt binder type (ABT), on PAM's basic properties.

- Chapter 5 examines the development of packing condition in PAM by means of both laboratory measurement and DEM simulation, and evaluates the role of the aggregates of different size ranges within the coarse fraction.

- Chapter 6 focuses on the PAM design for the specific applications, namely pedestrian/cyclist pathways in wet environment, based on the findings in Chapters 4 and 5. The basic properties of the designed PAMs, namely mixture strength and permeability, are measured in the laboratory and the packing structures in the PAMs are subsequently analysed through DEM simulation.

- Chapter 7 focuses on the experimental design for measuring PAM's resistance to ravelling and clogging, and the experimental results of the designed PAMs are subsequently evaluated.

The findings of the research are summarised in Chapter 8, and the recommendations for further research are presented as well.

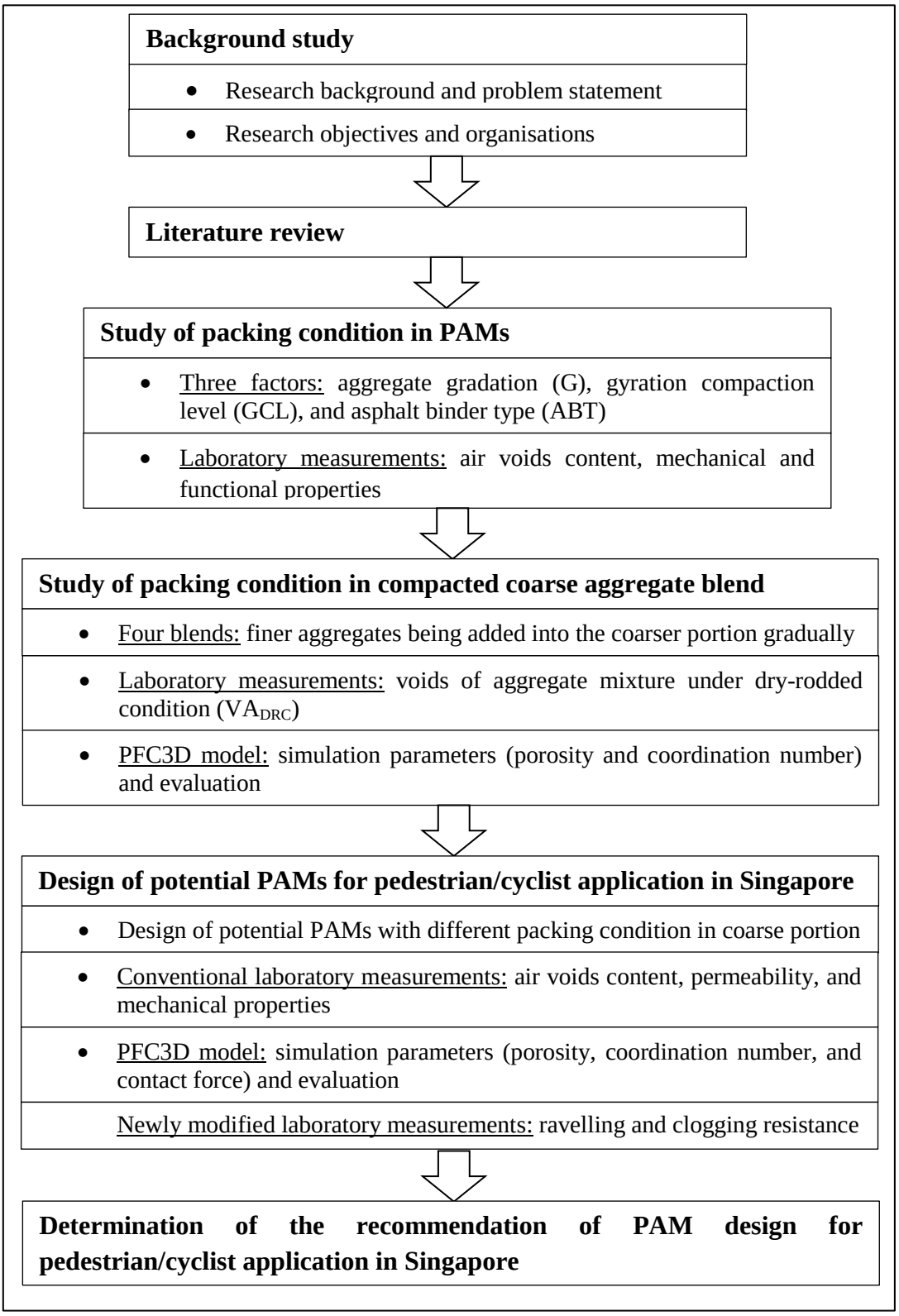

Figure 1.1 Flowchart of research activities

Chapter 2 Literature review

2.1 Introduction

This chapter documents the related research work in the field of Porous Asphalt Mixture (PAM), including PAM's characteristics and practical application. Subsequently, the development of asphalt mixture design method is presented. Especially, current gradation design methods and packing theories are introduced, and related limitations are stated. In addition, numerical simulation methods are introduced, in which Discrete Element Method (DEM) is useful for assessing the packing structure established in PAM, thereby alleviating the excessive trial-and-error laboratory work in conventional methods.

2.2 Porous Asphalt Mixture (PAM)

Asphalt mixture is a type of composite material commonly used in flexible pavements. Asphalt mixture is fabricated by mixing and compacting a designed blend of mineral aggregates, asphalt binder, and additives if necessary, generating the three-phase structure composed of aggregates, asphalt binder, and air voids (Figure 2.1).

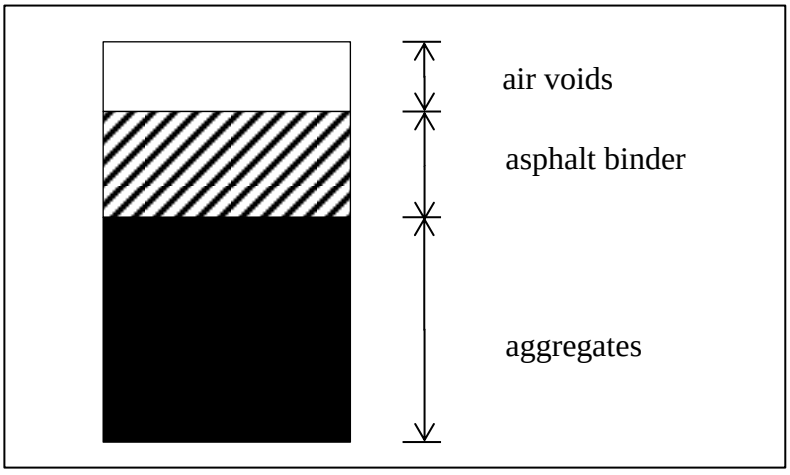

Figure 2.1 Three-phase structure of asphalt mixture

PAM, a kind of asphalt mixture, is characterised by its high content of air voids (i.e. usually greater than 18%), which arises from the open-graded design, namely coarse aggregates account for a dominant proportion in the aggregate blend (i.e. 70~85%), thereby resulting in a less continuous aggregate gradation as compared to dense asphalt mixture. Permeable pavement is usually constructed of PAM in the surface course, rendering benefits in reducing splash and spray, alleviating traffic noise, improving skid resistance, and generating cooling effect etc. On the other hand, ravelling and clogging are the two major problems confronting PAM construction, which should be taken into consideration in PAM mixture design.

2.2.1 Characteristics of PAM material

From the engineering experiences, the benefits arising from the application of PAM material can be categorised into two aspects:

(1) driving safety, namely aquaplaning alleviation, splash and spray mitigation, glare reduction, and skid resistance enhancement; and

(2) environmental benefits, namely noise alleviation, driving comfort, infiltration effect, and cooling effect.

However, mixture strength and durability are jeopardised due to the larger air voids content existing in PAM, resulting in pavement distresses related to ravelling and clogging, and additional maintenance cost is subsequently incurred. The detailed advantages and disadvantages associated with PAM are given as follows.

Advantages

(1) Aquaplaning

For dense asphalt mixtures, rainwater is removed from pavement surface via geometric design (e.g. cross slope) and subsequently be collected in the ditches along the roadsides, since water is prevented from seeping through the pavement structure due to the impervious mixture design. In this case, a thin sheet of water is formed on the pavement surface, i.e. a water film exists between pavement and tyre (Figure 2.2), especially when the cross slope is not adequate for drainage and/or

under the condition of heavy rainstorm. The water film in the tyre-water-pavement interface leads to the loss of traction and makes it hard to control vehicle operation, especially in braking, steering, and accelerating. Instead, the problem of aquaplaning can be efficiently alleviated or even be avoided by applying PAM material, since water can drain away rapidly on both lateral and vertical directions, i.e. across the road surface via cross slope design and downwards through the pervious wearing course.

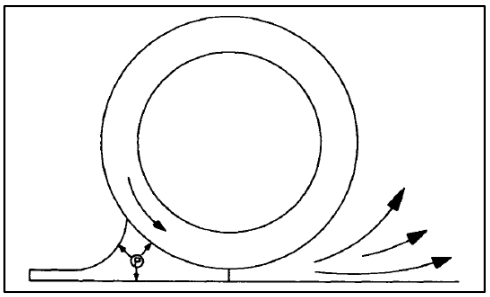

Figure 2.2 Aquaplaning: tyre-water-pavement interface (Khalid and Jimenez, 1995)

(2) Splash and spray

'Splash' is the phenomenon that water is thrown by rolling wheels as a vehicle is running on a wet surface, and is usually followed by 'spray', which refers to mist being formed by numerous minute water droplets (Figure 2.3). Splash and spray jeopardises the visibility and causes serious problems in driving safety (Khalid and Jimenez 1995; Nicholls 1997; Ferguson 2005). For example, visual range can be shortened to below 5~10 m, and windscreens may be misted and dirtied. In the case of PAM, due to the permeable pavement surface, no substantive water source exists for splash and spray since no pool is formed on the road.

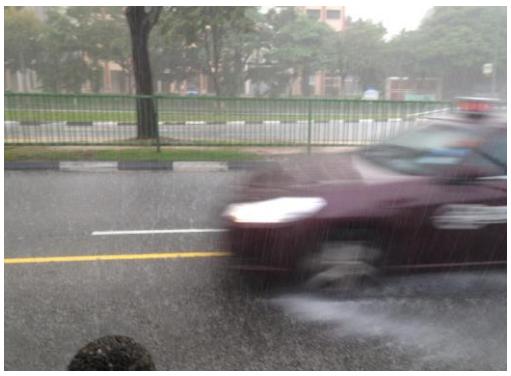

Figure 2.3 Splash and spray

(3) Skid resistance

Rainwater may lubricate both the surfaces of pavement and tyre, reducing the coefficient of friction between them and thereby compromising driving safety. By application of PAM, the loss of skid resistance at wet surface can be mitigated since the water on the road surface can be removed quickly.

(4) Noise reduction

As compared to dense asphalt mixture, PAM reduces noise level by around 3 dB(A) on average, which is caused in two aspects: (a) noise arising from rolling tyres is decreased, and (b) the noise that transmits downwards is greatly absorbed into the air voids in PAM (Nelson and Abbott 1990; Bendtsen and Andersen 2005; Ferguson 2005). The noise generated by the interaction between tyre and surface is directly related to the profile of pavement surface. As wheels roll rapidly, vibration between tyres and surface is generated by air compressing and relaxing, which is the main source of noise. In fact, for conventional pavement of dense asphalt mixture, the surface is smoother than that of PAM in terms of macro-texture, hence resulting in less vibration. However, the air voids in PAM serve to alleviate the degree of compression, leading to lowered traffic noise.

It should be noted that ‘noise reduction’ is a significant trait of PAM, and it is also the major objective of applying PAM in some countries, such as in U.K., Germany, the Netherlands, Denmark, and Belgium etc. (Nelson and Abbott 1990; Khalid and Jimenez 1995; Nicholls 1997). Though PAM may generate in-vehicle noise due to the macro texture, it provides a quieter pavement to inhabitants living along the roadways.

(5) Cooling effect

Cooling resulting from evaporation is effected as water and water vapour pass through permeable pavement, and hence PAM material generates the effect of cooling by imitating the behaviour of unpaved areas. Meanwhile, less heat is stored in permeable pavement due to the less dense structure, thus a lower temperature at

the pavement surface of PAM is observed (Asaeda and Ca 2000; Golden and Kamil 2005; Starke et al. 2010).

(6) Glare reduction

'Glare' describes the difficulty in seeing due to reflection of bright light. Pavement surface looks like a mirror to drivers as the surface is smooth, and this situation can be readily observed on a dense pavement upon a small rain shower. However, due to the surface voids, PAM plays a role of diffusing reflection and hence makes the pavements and markings more visible (Tappeiner 1993; Nicholls 1997). Comparing the light intensity and RGB (red, green and blue) colour value of the pavement surface in both dry and wet situations, Rungruangvirojn and Kanitpong (2010) found the visibility loss caused by water on the pavement surface of PAM was much lower than that of dense asphalt mixture.

(7) Infiltration effect

The high content of air-connected voids in the structure of PAM allows rainwater to pass through, and simultaneously road pollutants can be carried away to a large extent in this process, which creates an infiltration effect (Brattebo and Booth 2003; James 2008). For example, in the Netherlands, about 90% of the Polynuclear Aromatic Hydrocarbons (PAHs) and heavy metals present on the pavement could be removed through PAM pavement (Bohemen and Janssen van de Laak 2003). In Texas, Barrett and Shaw (2007) found reductions in suspended solids, lead, copper, and zinc at 92%, 91%, 47%, and 75%, respectively, on the pavement surface of PAM as compared to that of conventional dense asphalt mixture. Nonetheless, this feature of PAM may be a drawback in the case of Singapore, since pollutants are entering the water streams and becomes a problem for harvesting surface runoff as safe drinking water.

On the aspects of glare reduction and noise reduction, the advantages of PAM are more related to motorised roads. While in the aspects of aquaplaning alleviation, splash and spray mitigation and skid resistance, PAM benefits the cyclists as well. On the other hand, Singapore is a tropical country with rapid urbanisation. Meanwhile, pedestrian/cyclist pathways in Singapore are being substantially

expanded and widened to enhance the off-road cycling network (Koh and Wong 2012). Thus, application of PAM on pedestrian/cyclist pathways can potentially help to mitigate urban heat island (UHI) effect given PAM's cooling effect.

Disadvantages

(1) Ravelling

Since water can pass through and be stored in the water-accessible air voids (WAAW) within the PAM material, undesirable effects are inevitably exerted on the structural layer, especially those related to moisture distresses. Meanwhile, asphalt binder ages and oxidises rapidly due to the larger areas exposed to sunlight and/or heated air in the voids. The combined effects of moisture damage and ageing tend to impair the adhesiveness and cohesiveness of asphaltic materials, resulting in ravelling. Furthermore, PAM strength is weakened, which is partially reflected by decreased Marshall stability, if no additional technical measures (e.g. applying modified asphalt binder) are taken.

(2) Clogging

Clogging, which is referred to as porosity degradation, is another negative issue on PAM. Ineffective drainage caused by gradual clogging may shorten the service life of permeable pavements (Ferguson 2005; Coleri et al. 2013). In order to eradicate the vegetation in the pores of PAM material to prevent clogging, herbicides are commonly used, which however may result in pollutants in the soil. Nowadays, high-pressure water jets and vacuum suction are developed to clean the permeable pavements to mitigate clogging.

Meanwhile, 'double-layer' permeable structure, which is composed of a coarse single-grained PAM as bottom layer and a fine-graded PAM as top layer (Figure 2.4), is developed in the Netherlands, and it is another means to alleviate clogging (van Bochove 1996).

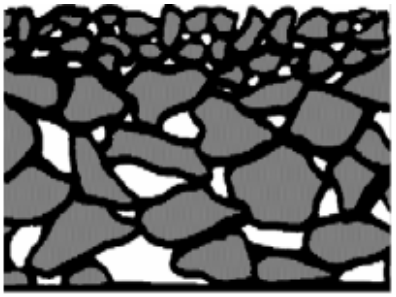

Figure 2.4 Double-layer PAM structure (van Bochove, 1996)

(3) Life cycle cost

Life cycle cost of PAM pavement is generally higher than that of impermeable one, which generally includes three parts: (a) raw materials of higher quality and constructing a water-tight layer underneath the surface layer in some situations; (b) frequent maintenance to achieve comparable service life as conventional impermeable pavements; and (c) economical loss relating to trafficking limitations during maintenance procedures (Kluck et al. 2010). For example, based on Norway's experience (Table 2.1), the unit costs of single-layer PAM and double-layer PAM are about 69% and 161% greater than that of dense asphalt mixture, respectively, and about 52% and 134% greater than that of Stone Mastic Asphalt (SMA), respectively (Knut and Juned 2011).

Table 2.1 Investment costs of various pavement materials (EUR/ m^2)
(Knut and Juned 2011)

Pavement material*	TSF8	SMA11	SPAC11	DPAC8/16	DPAC11/16
cost of paving AC	9.62	10.13	12.85	25.04	25.02
cost of delay and warning**	0.19	0.79	0.33	0.55	0.55
total investment cost	9.81	10.91	16.58	25.59	25.57

*TSF8: thin bituminous surfacing with a maximum aggregate size of 8 mm and a dense-graded design; SMA11: stone mastic asphalt with a maximum aggregate size of 11mm; SPAC11: single-layer porous asphalt concrete with a maximum aggregate size of 11mm; DPAC8/16: double-layer porous asphalt concrete with the maximum aggregate sizes of 8 mm and 16 mm on the top and bottom layers, respectively; DPAC11/16: double-layer porous asphalt concrete with the maximum aggregate sizes of 11 mm and 16 mm on the top and bottom layers, respectively.

** Calculation is based on dual carriageway with traffic condition of Average Annual Daily Traffic (AADT) =20,000

2.2.2 Applications of PAM material

(1) Global application

PAM is referred to in various terms in different countries and areas, such as Open Graded Friction Course (OGFC), Porous or Permeable Friction Course (PFC), drainasphalt, and popcorn mix etc. PAM is referred to as OGFC in most States in the U.S. while termed as PFC according to local specification (Texas Department of Transportation [TxDOT] 2004). In Europe, PAM was originally introduced as 'Friction Course' and subsequently termed as 'Pervious Macadam' in the U.K., and the term 'Porous Asphalt (PA)' has been widely adopted in Europe since 1992.

In Europe, PAM is broadly paved under various climatic conditions, ranging from 'hot and dry' to 'cold and wet' (Fabb 1993). In the U.K. PAM was first introduced by the U.K. Air Ministry in the 1950's and was applied in both civil and military airfield runways in the 1960's (Fabb 1998). In the field of road pavements, PAM did not receive much attention until the 1990's, mostly because of the intrinsic limitations in aspects of strength and durability. Before using PAM on roads, a series of research was conducted by Transport Research Laboratory (TRL), and most of the research was focused on conventional requirements instead of practical site performance. Nevertheless, a new design method for PAMs based on performance was developed in 2001, which was resulted from four laboratory tests implemented on both in-field and laboratory specimens (Nicholls and Carswell 2001).

The first application of PAM in Spain was in 1980 with the target of improving traffic safety in rainy areas. Meanwhile, it is remarkable that Cantabro test, which is currently extensively utilised in the asphalt mixture design of PAM, was initially developed at the University of Cantabria (Ruiz et al. 1990; Khalid and Jimenez 1995). Up to now, PAM has been widely applied in Spain, and relevant performance records have been well established.

In the U.S., PAM has been used in several States since the 1950's in order to enhance the frictional resistance of pavement surface. Some States stopped using PAM subsequently due to the unacceptable durability while many other States'

Department of Transportation (DOT) reported quality performance (Kandhal and Mallick 1998). Federal Highway Administration (FHWA) introduced an asphalt mixture design procedure for OGFC (i.e. PAM) in 1974 (Smith et al. 1974), and National Centre for Asphalt Technology (NCAT) modified the procedure in 2000 and proposed an asphalt mixture design method of new-generation OGFC (Rajib et al. 2000).

In Malaysia, the first permeable pavement was built in 1991 and the project was completed in 1995. As a material offering high skid resistance, PAM has been applied as a safety remedial measure to deal with high traffic fatality in Malaysia.

Although PAM has been applied almost all over the world, ravelling and clogging are still the two severe problems encountered, rendering it unfavourable in some areas. For example, according to the feedbacks from 33 state agencies in the U.S., there were 6, 3, 4, and 1 States reporting bad experience of PAM applications in four zones, respectively, namely wet-freeze, wet-no freeze, dry-freeze, and dry-no freeze (Kandhal and Mallick 1998). In addition, ravelling can develop rapidly and even reach the whole structural layer, consequently lowering the pavement life to 6~8 years (Huber 2000). Hence, issues of ravelling and clogging should be carefully studied and handled in asphalt mixture design of PAM material, and be customised for specific climate and traffic conditions.

(2) Value-add application in Singapore

Singapore is located in Southeast Asia and specifically at 1.22 degrees north of the equator. Due to the special geographical features, Singapore's climate is classified as 'tropical and equatorial', which involves warm and damp situation throughout the year and two monsoon periods, namely the Northeast monsoon (December – March) and the Southwest monsoon (June – September) (Fong 2012). Moreover, in Singapore: average temperature is between 23~32 °C (Figure 2.5), around 50% of the days in the year experience rainfall (Figure 2.6), and thunderstorm occurs frequently (Figure 2.7) (National Environment Agency [NEA] 2015).

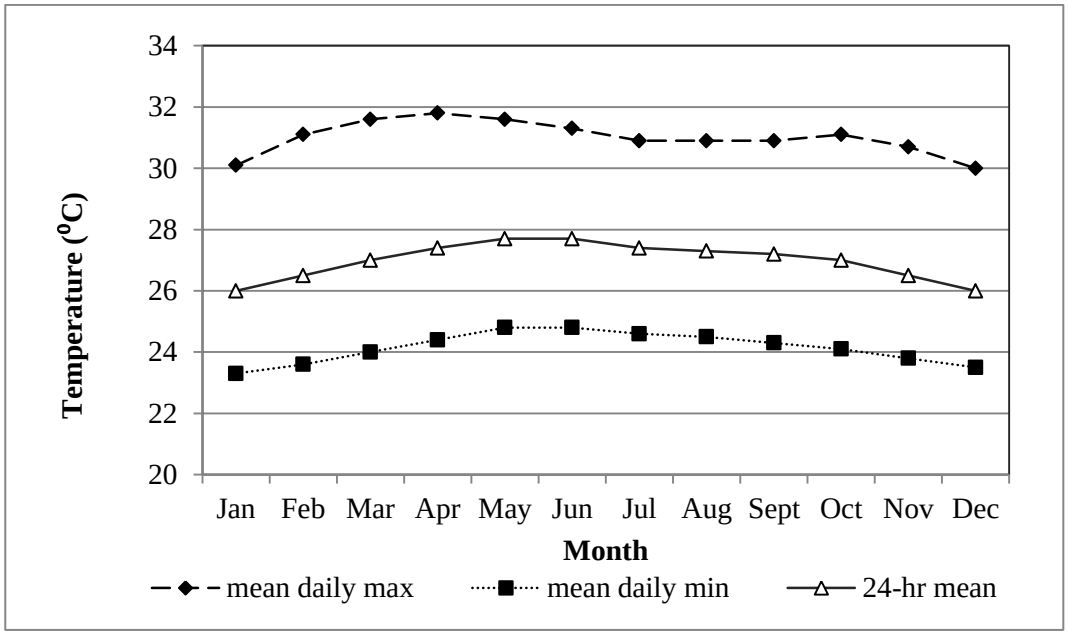

Figure 2.5 Temperature in Singapore

Notes: mean daily min = averaging the daily minimum temperature for each month for the 80-year period (1929-1941 and 1948-2014); 24-hr mean = averaging the daily temperature for each month for the 80-year period (1929-1941 and 1948-2014); mean daily max = averaging the daily maximum temperature for each month for the 80-year period (1929-1941 and 1948-2014).

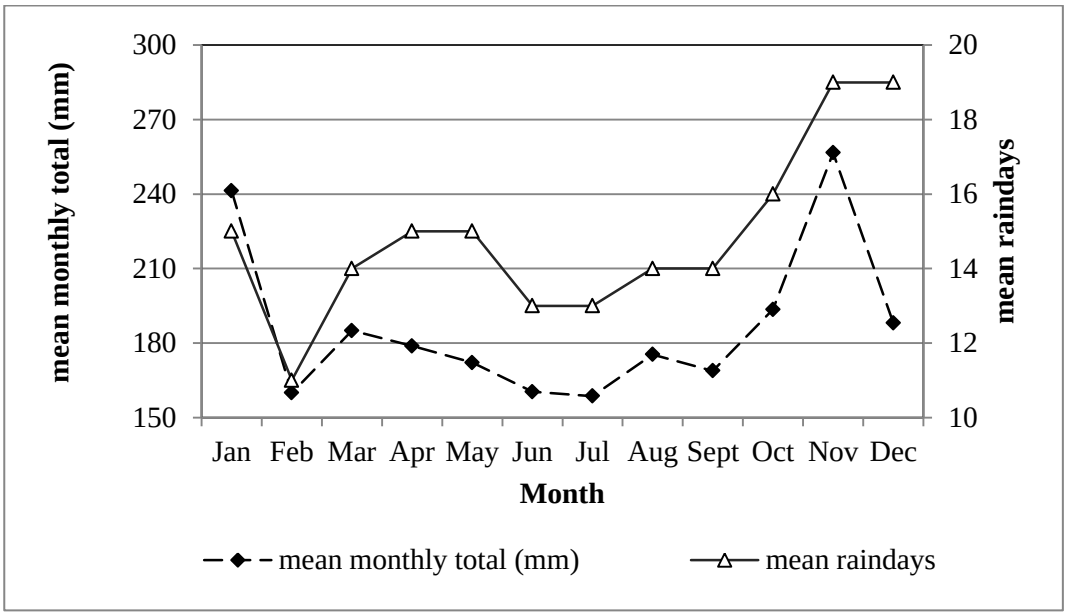

Figure 2.6 Rainfall in Singapore

Notes: mean rainday = averaging the total number of raindays for each month for the 124-year period (1891-2014); mean monthly total = averaging the monthly total rainfall for each month for the 146-year period (1869-2014).

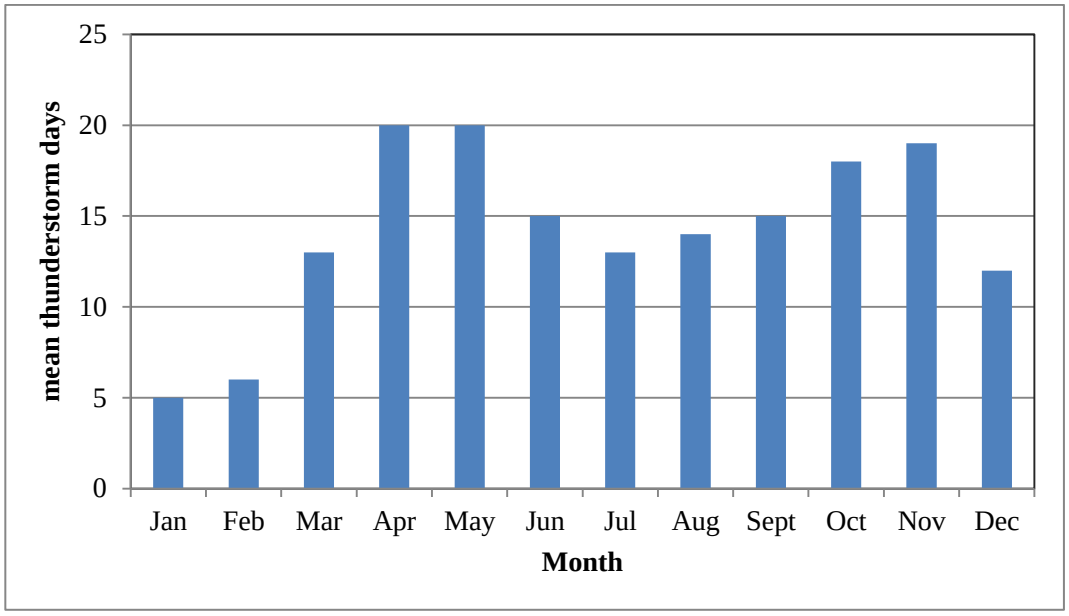

Figure 2.7 Thunderstorms in Singapore

Notes: Mean thunder days = averaging the total number of days thunder is heard for each month for the 33-year period (1982 – 2014).

Given PAM's excellent performance in drainage and effectiveness in cooling effect, it is favourable to apply PAM in Singapore, so as to obtain positive effects in relation to the environment.

In terms of application, it can be divided into two categories, i.e. normal roads and pedestrian/cyclist paths. Normal roads consist of expressways, arterial roads, collector roads, and local access roads, while pedestrian/cyclist pathways include most of the pathways in communities and parks whose users are limited to pedestrians and cyclists rather than motor vehicles. Worldwide, there is a surge in non-motorised transport which leads to expansion and/or rejuvenation of infrastructural networks for pedestrians and/or cyclists. In Singapore, the current off-road cycling network is being expanded from the current 200 km to the 300 km round-island green network (Koh and Wong 2012). Likewise, existing pedestrian footpaths are being widened to allow sharing of pathway between pedestrians and cyclists.

The open-graded aggregate structure for PAM mixtures in highways is designed to accommodate stresses induced from traffic loadings. On the other hand, in terms of application in pedestrian/cyclist pathways, more attention should be placed in

PAM's functional performance (e.g. drainage) in the mixture design in view of the lower strength requirement

2.3 Asphalt mixture design

Asphalt mixture is a composite material, and the main components are mineral aggregates and asphalt binder. Major stone-on-stone skeleton is formed by coarse aggregates, and resultant voids are partially filled by asphalt mastic (mixture of asphalt binder and fillers) and fine aggregates. The basic design procedure of an asphalt mixture is generally as follows:

(a) Select the type of raw materials, including mineral aggregates, asphalt, and additive (if necessary);

(b) Design aggregate gradation;

(c) Determine the Optimal Asphalt Content (OAC); and

(d) Evaluate the properties of asphalt mixture so as to meet the specific requirements (e.g. strength, moisture susceptibility, ageing resistance, etc.).

2.3.1 Materials in asphalt mixtures

(1) Aggregate

Mineral aggregates and asphalt are the two major materials used in fabricating asphalt mixtures, while aggregates account for around 85% and 70% by volume in dense asphalt mixture and PAM, respectively. In fact, a stable skeleton in an asphalt mixture is mainly attributed to well compacted aggregates, which plays an important role in resisting traffic load and external deformation. For PAM material, it is a kind of open-graded asphalt mixture of which mixture strength and durability are relatively weaker than dense asphalt mixtures, hence stiffer aggregates are required. Crushed stones are recommended for PAM, which can provide higher stability in asphalt mixtures and yet render adequate permeability (Foster et al. 1970; Nicholls 1997). On the other hand, recycled materials, such recycled concrete aggregates (RCA) and waste glasses, were suggested for low-strength pavement

application due to the lowered requirement in pavement strength (Chen and Wong 2013, 2015).

(2) Filler

Fillers generally refer to particles finer than 0.075 mm. The performance of asphalt mastic, whose components are fillers and asphalt binder, are heavily dependent on the properties of fillers, such as particle size, particle shape, surface area, surface texture, and chemical composition etc. For example, asphalt binder can be stiffened by fillers, with finer fillers producing more significant stiffening effect (Zulkati et al. 2012a, b). Lime is a type of mineral filler that has been widely used to enhance mixture durability (Lesueur and Little 1999). Given that pure lime (CaO) is not stable and easily reacts with water, hence hydrated lime ($Ca(OH)_2$) are more widely applied due to its chemical stability. For PAM material, lime is commonly used to enhance anti-stripping ability (Shuler and Hanson 1990; Kanitpong et al. 2007).

(3) Asphalt binder

In an asphalt mixture, asphalt binder functions as the gluing agent and bonds loose aggregates into an integrated mass upon compaction and contributing to mixture tensile and shear strength. Straight asphalt is a black (or brownish), viscous (or semi-solid) substance produced from crude petroleum. Chemically the main elements in straight asphalt are carbon (83%~87% around) and hydrogen (10% around), resulting in ageing upon the reaction with oxygen and hence hardening of the asphalt binder (Li and Zhang 2004). Rheological properties of asphalt binder strongly influence asphalt mixture's in-field performance, such as rutting and cracking.

Several methods have been developed to grade asphalt binder, most of which are based on the property of viscosity. For example, in penetration grading method, the viscosity of asphalt binder is described by penetration value, which is the value in unit of 0.1 mm for a standard needle penetrating on asphalt specimen in 5 seconds at 25˚C, and higher viscosity is reflected by a lower penetration value. However, Superpave performance grading is a more competent method for its capability in indicating the applicable temperature range directly. For instance, an asphalt binder

graded as PG 64-22 can be appropriately used in areas in which the average seven-day maximum temperature is no higher than 64˚C and the average seven-day minimum temperature is no lower than -22˚C. The asphalt binder grading in Superpave method is realised through a series of tests, involving rolling thin film oven (RTFO), pressure ageing vessel (PAV), rotational viscometer (RV), dynamic shear rheometer (DSR), bending beam rheometer (BBR), and direct tension tester (DTT) (Asphalt Institute [AI] 1996; Papagiannakis and Masad 2008).

For PAM, an asphalt binder with a high viscosity is required so as to minimise stripping and early ageing. Moreover, modified asphalt binder, e.g. polymer-modified asphalt binder, fibre-modified asphalt binder and asphalt rubber, is broadly used in PAM, due to the improvement on the aspects of abrasion loss, rutting, and moisture susceptibility (Rajib et al. 2000; Tayfur et al. 2007; Hsu et al. 2011; Chen et al. 2013). Also, asphalt binder of high viscosity generally renders better performance in draindown test, which indicates higher adhesiveness between asphalt binder and aggregates.

(4) Additive

To enhance the performance of asphalt mixtures, additives are frequently used in PAM materials, such as Ethylene Vinyl Acetate (EVA), Styrene Butadiene Styrene (SBS), and various fibres. The main role of the additives is to improve the visco-elastic behaviour of asphalt binder, resulting in the decrease in permanent strain in asphalt mixtures especially in the cases of heavy traffic at slow moving rate at high temperature.

Presently, the common fibres used in pavement engineering are cellulose fibre and polymer fibre, e.g. polyster fibre and polyproplylene fibre. Despite the excellent ability of fibre in absorbing asphalt binder, cellulose fibre is not the most desirable since part of the asphalt binder is absorbed inside the fine tubes that are dispersed on the surface of cellulose fibre, which neither increases the thickness of asphalt binder nor enhances the strength of asphalt mixture (Qin 2004). In addition, cellulose fibre is easy to be dampened, which negatively influences the adhesiveness between asphalt binder and aggregates. Contrarily, polymer fibre is

more desired since it offers better performance at both high and low temperatures with less absorbed asphalt binder (Punith et al. 2009; Qian et al. 2014).

2.3.2 Conventional asphalt mixture design methods for dense asphalt mixtures

According to the development of asphalt mixture design methods, there are several well-known and widely adopted methods, e.g. Hveem method, Marshall method, and Superpave method.

(1) Hveem method

Hveem's procedure of designing asphalt mixture was formed in 1959 and adopted by several States in the U.S. (Vallerga and Lovering 1985). A kneading compactor was used in Hveem method, possessing a rotating unit on the base. The properties of compacted asphalt mixtures were assessed through stabilometer, cohesiometer, and swell test. Stabilometer measures the stability of an asphalt mixture through a triaxial test using a specific testing setup, and the result is calculated according to the radial expansion caused by axially applied load. Cohesiometer is utilised to evaluate cohesiveness among asphalt mixture through a bending test as the applied force is controlled and increased steadily. Swell test assesses the susceptibility of the asphalt mixture by measuring the changes in permeability and volume before and after moisture conditioning. In selecting OAC, air voids content and Hveem stability are the two decisive factors, and the content of asphalt binder corresponding to 4% air voids is generally favoured for dense asphalt mixtures.

Kneading method is capable of well compacting the asphalt mixture in the laboratory, and Hveem stability is a proper index to evaluate the internal friction of shear strength and hence appropriately assesses the resistance to rutting. However, testing equipment involved in Hveem procedure is relatively expensive and not portable. Moreover, volumetric parameters related to asphalt mixture's performance (e.g. durability and anti-cracking) are not considered herein.

(2) Marshall method

Prompted by the augmentation in aircraft wheel loads during World War II, the Corps of Engineers Waterways Experiment Station (WES) began research to obtain

proper mixture design method by a simple portable apparatus. Bruce Marshall's apparatus was selected and applied to conduct a series of laboratory experiments along with the field tests. Consequently, based on the compaction efforts and densities both in laboratory and in field, a compaction effort of 50 blows per side of the asphalt mixture specimen was adopted as a standard, and then modified to 75 blows per side along with the increased traffic loading (Foster 1982; White 1985).

Table 2.2 The design criteria of Marshall method for HMA (AI 1997)

traffic condition*	light	medium	heavy
Marshall stability (kN)	≥ 3.3	≥ 5.3	≥ 8.0
flow (0.25mm)	8-18	8-16	8-14
air voids content (%)	3-5	3-5	3-5
VFA (%)	65-75	65-78	70-80

*Light traffic: Equivalent Single Axle Load (ESAL) is less than 10^4; medium traffic: ESAL is between 10^4 and 10^6; Heavy: ESAL is greater than 10^6.

The design criteria of Marshall method for dense Hot Mix Asphalt (HMA) are given in Table 2.2. Marshall stability is the peak load the sample of asphalt mixture can bear at 60 ℃ during testing, and flow value is the corresponding vertical deformation at peak load. Meanwhile, volumetric analysis is involved in Marshall method, including air voids content, Voids in Mineral Aggregates (VMA), and Voids Filled with Asphalt (VFA). To date, Marshall method has been widely used all over the world due to its simplicity. However, the impacting effect of Marshall compactor cannot well simulate aggregate orientation in field construction.

(3) Superpave method

Superpave stands for Superior Performing Asphalt Pavements, and Superpave method was developed in the late 1990's by Strategic Highway Research Program (SHRP). Performance Grading (PG) system was introduced to grade asphalt binder, which can directly indicate the appropriate application region according to the temperature range. Aggregates are assessed in two aspects: consensus properties (i.e. coarse aggregate angularity, fine aggregate angularity, flat and elongated particles, and clay content) and source properties (toughness, soundness, and deleterious

materials). Moreover, Superpave Gyratory Compactor (SGC) was developed as the compaction machine, which can orient the aggregate particles as in-field condition (McGennis et al. 1995; Robert 1996).

Regarding the procedure of asphalt mixture design, volumetric parameters and densification are the two critical factors. Requirements in VFA and Voids in Mineral Aggregate (VMA) for asphalt mixture regarding different Nominal Maximum Aggregate Size (NMAS) (i.e. refers to the first sieve size through which at least 90% of an aggregate blend passes and is also termed Nominal Maximum Particle Size [NMPS]) are given in Table 2.3, and the target air voids content is 4%. Lack of performance related testing is the major drawback in Superpave method, and thereby poor performance may occur in the field despite the asphalt mixture meeting all the design criteria.

Apart from the distinguishing features of the three mixture design methods, they are all limited to dense asphalt mixtures due to the target air voids content being always exactly or around 4%, which is much less than that is required for PAM. Furthermore, no specific test incorporated in the above design methods aims to evaluate and correlate with PAM performance in the field, such as permeability, ravelling, ageing, etc.

Table 2.3 Requirements of VFA and VMA for asphalt mixture in Suprepave method

Traffic condition (10^6 ESALS)	VFA (%)	Minimum VMA (%)				
		NMAS (mm)				
		37.5	25.0	19.0	12.5	9.5
< 0.3	70-80	11.0	12.0	13.0	14.0	15.0
0.3~3	65-78					
≥ 3	65-75					

2.3.3 Specific asphalt mixture design methods for PAM

Asphalt mixture design methods for PAM are broadly based on engineering experience, and several examples are given in the following.

(1) the U.K. method

Before 2001, PAM design in the U.K. followed the requirements in the local specification, possessing no direct relation with PAM performance in the field such as hydraulic conductivity. Therefore, a PAM design method with performance-related criteria was studied and developed, which included four laboratory tests conducted on both site and laboratory samples (Nicholls and Carswell 2001). The initial selected tests were vertical and horizontal permeability, particle loss, scuffing, and affinity. Subsequent performance tests were horizontal permeability test and particles loss test as direct relation to in-site performance.

(2) Japanese and Taiwan method

In Japan, asphalt binder content in PAM is determined by draindown test and Cantabro test, and PAM performance at high temperature is assessed via rutting test. The design procedure is: (a) determining the desired air voids content, (b) selecting materials and designing the primary aggregate gradation, (c) determining the primary asphalt binder content, (d) determining the aggregate gradation that meets the desired air voids content, (e) calculating the air voids in asphalt mixture and determining the optimal asphalt binder content, and (f) conducting performance tests on asphalt mixture. A similar design procedure is also used in Taiwan (Zhu 2005). Meanwhile, in order to gain high strength, desired durability, and adequate resistance to moisture damage, modified asphalt and additives (e.g. fibre and lime) are also recommended.

(3) the U.S. method

Before 2000, OGFC mixture design in the U.S. followed the procedure introduced by the FHWA in 1974, and some States reported unacceptable durability despite satisfactory feedback from others (Smith et al. 1974). To establish a rational design system for new-generation OGFC, NCAT conducted a series of studies on OGFCs with various gradations and different additives. Consequently, it was found that the addition of polymer or fibre could effectively improve the performance of OGFCs. Also, a four-step asphalt mixture design system was introduced to produce high-quality OGFCs (Rajib et al. 2000). For determining OAC value, four criteria were

proposed, which were (a) minimum air voids (18%), (b) maximum abrasion loss of unaged specimens (20%), (c) maximum abrasion loss of aged specimens (30%), and (d) maximum draindown of total asphalt mixture mass (0.3%). Clearly, the balance of asphalt binder content has drawn the researchers' attention. High content of asphalt binder reduces the air voids and further decreases the permeability, leading to distresses such as bleeding in high-temperature conditions. In contrast, low asphalt binder content tends to cause distresses like ravelling and stripping.

Asphalt design method for OGFC was renewed by later researchers, and SGC was found to be superior to Marshall compactor in terms of less aggregate breakdown (Watson et al. 2003). The compacting effort of 50 gyrations was almost the same as that generated by 50 blows of Marshall compactor. Additionally, 2.36 mm wire mesh was recommended to be used in draindown test, instead of the standard 4.75 mm mesh.

2.4 Aggregate gradation and packing theory

Packing condition within an asphalt mixture is an important issue to the performance in the field (e.g. resistance to rutting and cracking etc.), and it is governed by various factors, such as aggregate gradation, aggregate properties (i.e. shape, strength, surface texture), compaction level, asphalt binder content etc. Aggregate gradation, also called particle size distribution, represents the distribution of particles with various sizes in an aggregate blend, and it is expressed by the proportionate amounts of aggregates by weight over a series of consecutive sieves. Among the factors to aggregate packing, aggregate gradation is the most unstructured one, namely it is a relatively independent factor and can be readily modified, and hence it deserves more attention (Roque et al. 1997; Ruth et al. 2002; Vavrik et al. 2002; Suresha et al. 2009; Alvarez et al. 2010a; Mansour and Putman. 2013).

For dense asphalt mixture, a quality mixture packing refers to a strong stone-on-stone backbone formed by coarse aggregates and sufficient asphalt mastic to fill the voids. However, in the case of PAM, the amount of fine aggregates should be

restricted to a low level, e.g. 15~20%, so as to achieve sufficient permeability (Rajib et al. 2000).

2.4.1 Maximum density curve

To maximise density of conventional dense asphalt mixture, studies were conducted to obtain the ideal aggregate gradation, among which Fuller's maximum density curve was a broadly adopted method and it can be described by Equation (2.1) (Fuller and Thompson 1907). The *n* value was initially suggested as 0.5 to obtain the densest mixture and was subsequently modified as 0.45 by Good and Lufsey's research (1965).

$$P = 100(d/D)^n \tag{2.1}$$

d = diameter of sieve size;

P = total percentage passing the sieve;

D = maximum size of the aggregate.

Based on Fuller's maximum density curve, FHWA developed an aggregate grading chart (Figure 2.8) in the early 1960's (McGennis et al. 1995). It is easy to gain the maximum density line on this chart, i.e. connecting the origin at lower left point to the actual percentage point of NMAS.

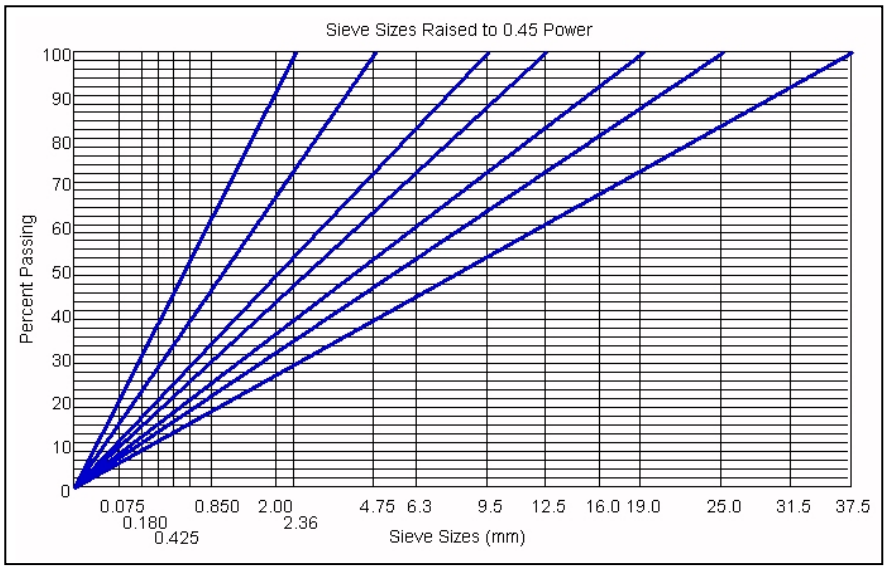

Figure 2.8 FHWA 0.45 power gradation chart (McGennis et al. 1995)

Though dense aggregate mixtures can be readily obtained through this maximum density curve, there should be sufficient air voids content within a mixture to ensure that adequate asphalt binder can fit in. In effect, an aggregate gradation curve that deviated from the maximum density curve was found to be more favourable, thus Bailey method was developed subsequently, whereby aggregates were blended by volume instead of weight.

2.4.2 Bailey method

Based on project experience, Bailey method was initially introduced by Mr. Robert D. Bailey (retired) at the Illinois Department of Transportation in the early 1980's, and was subsequently refined and shaped up into a systematic methodology of asphalt mixture design. Bailey method is a practical tool that leverages on aggregate packing theory and provides a method to adjust the volumetrics and compactability of asphalt mixture, through which aggregate interlocking and balanced continuous gradation can be appropriately created (Vavrik 2000; Vavrik et al. 2002). Thus, Baiely method is widely applied in mixture design of dense asphalt mixture and Stone Mastic Asphalt (SMA) (i.e. with gap-graded design).

The primary theoretical basis of Bailey method is volumetric concerns: for a unit volume, extensive strength could be obtained if it can be filled up with a single stone with the same shape and volume; similarly in the case of asphalt mixture, a high strength structure can be expected if particle-to-particle backbone can be formed by coarse aggregates and the resultant air voids can be exactly filled with fine aggregates and asphalt mastic (Vavrik et al. 2002).

Considering coarse and fine aggregates play different roles in aggregate packing, the primary concern in aggregate gradation is to determine the breaking sieve (BS) size, namely the one to differentiate between coarse and fine fractions in an aggregate blend. Conventionally, a fixed sieve size of 4.75 mm is regarded as the BS size (Rajib et al. 2000). Watson et al. (2004) recommended the BS size as the point in the aggregate gradation curve below which the curve starts to flatten out. In Bailey method, according to 2-dimentional aggregate packing model (Figure 2.9),

breaking sieve is selected as the one closest to 0.22×NMAS, i.e. the average voids size.

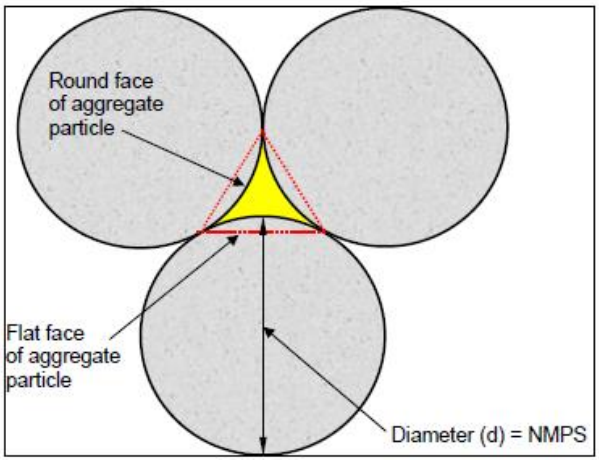

Figure 2.9 2-dimensional aggregate packing model

Note: NMPS=Nominal Maximal Particle Size, and NMPS=NMAS.

In order to obtain the desired volume of air voids within the coarse aggregates, a proper value of Chosen Unit Weight (CUW) should be determined, and the reference parameters are Loose Unit Weight (LUW) and Rodded Unit Weight (RUW), which refer to the unit weight of coarse aggregates with no compaction effort and sufficient compaction, respectively, and correspond to the lower and higher limits to form a particle-to-particle structure, respectively (Figure 2.10).

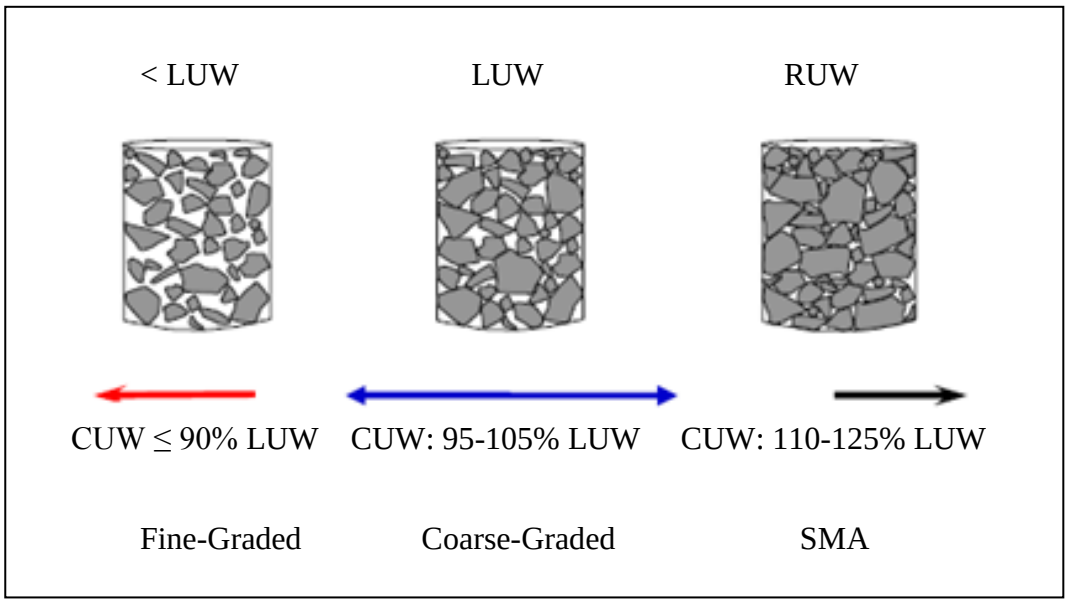

Figure 2.10 Chosen Unit Weight (CUW) ranges by mixture type

Moreover, three additional Bailey ratios, i.e. (a) CA ratio, (b) FA_c ratio, and (c) FA_f ratio, are introduced to produce and evaluate a trial blend. Three parameters to classify the sizes of different aggregates are introduced as well, i.e. Primary Control Sieve (PCS), Secondary Control Sieve (SCS) and Tertiary Control Sieve (TCS). The relevant calculations are given in Equations (2.2) – (2.4).

$$PCS = NMAS \times 0.22 \tag{2.2}$$

$$SCS = PCS \times 0.22 \tag{2.3}$$

$$TCS = SCS \times 0.22 \tag{2.4}$$

- CA ratio

Coarse Aggregate ratio (CA ratio) is applied to evaluate the proportion of coarse aggregates in a blend and analyse the characteristics of the voids within the structure. This parameter can be expressed as Equation (2.5).

$$CA = \frac{P_{HS} - P_{PCS}}{100 - P_{HS}} \tag{2.5}$$

P_{HS} = percentage passing the half sieve, % (half sieve is defined as the sieve closest to the size of NMAS ×0.5);

P_{PCS} = percentage passing PCS, %.

- FA_c ratio

Coarse portion of Fine Aggregate (FA_c ratio) is used to state the compacting and filling condition controlled by the fine part and coarse part within fine aggregates. When the fine aggregates of an aggregate blend are analysed alone, they can be regarded as a combination of coarse part and fine part, and the air voids created by the coarse part in the fine aggregates can be filled by the fine part. FA_c can be calculated by Equation (2.6).

$$FA_c = \frac{P_{SCS}}{P_{PCS}} \tag{2.6}$$

P_{SCS} = percentage passing SCS, %.

- FA_f ratio

Fine portion of Fine Aggregate (FA_f ratio) evaluates the fine aggregates in an aggregate blend, which fill the air voids generated by the coarse part of the fine aggregates. The calculation is given by Equation (2.7).

$$FA_f = \frac{P_{TCS}}{P_{SCS}} \tag{2.7}$$

P_{TCS} = percentage passing TCS, %.

Although Bailey method is a straightforward and practical approach to produce well-compacted asphalt mixtures, it should be recognised that a stipulated CUW does not necessarily lead to a desired coarse aggregate structure (Kim et al. 2009b). It can be attributed to the fact that aggregate interlocking is not dependent on unit weight and/or density of coarse aggregates only, but also on the proportion of coarse particles with different sizes. For example, coarse particles with different sizes may act independently if the coarser aggregates float in the matrix composed of finer coarse particles and fine fraction, thereby resulting in a poorly compacted asphalt mixture. In addition, Bailey method cannot provide a direct and explicit parameter to represent the packing condition of an asphalt mixture in a quantitative manner (Shen and Yu 2011).

2.4.3 Modified Bailey method for PAM

Bailey method was initially limited to dense asphalt mixtures, and a modified Bailey method for PAM was introduced by Zhu (2005) through adding a new volumetric factor, namely reserved porosity, which refers to the expected air voids content to be achieved in PAM design. It was found that reserved porosity is an effective parameter to estimate and control air voids content in PAM material. Through a similar approach, Zhang and Hao (2012) subsequently investigated five parameters in Bailey method for PAM, which were (a) chosen unit weight, (b) desired passing percentage of 0.075 mm sieve size, (c) blend by volume of coarse aggregates, (d) blend by volume of fine aggregates, and (e) reserved porosity. It was shown that adequate air voids content and PAM's performance (e.g. dynamic stability, anti-cracking capability, and moisture susceptibility etc.) can be realised by means of this method. Nevertheless, the inherent drawback in Bailey method still

exists, namely appropriately selected unit weight need not result in adequate aggregate packing in the designed PAMs.

2.4.4 Binary mixture model

Furnas (1931) established a packing theory based on binary mixture mode, in which an ideal packed aggregate mixture was composed by two fractions, namely coarse and fine aggregates, and cavities among big particles were filled by the small fraction. The interfering effect of coarse/fine fraction on the other fraction was defined as (a) wall effect: voids increase around a matrix of fine aggregates due to an isolated coarse particle inside, and (b) loosening effect: interlocking of a matrix of coarse aggregates was disturbed as fine particles are not small enough to fit into the interstices (Figure 2.11) (Mangulkar and Jamkar 2013). Hence aggregate packing is influenced by diameter ratio of coarse and fine particles as well.

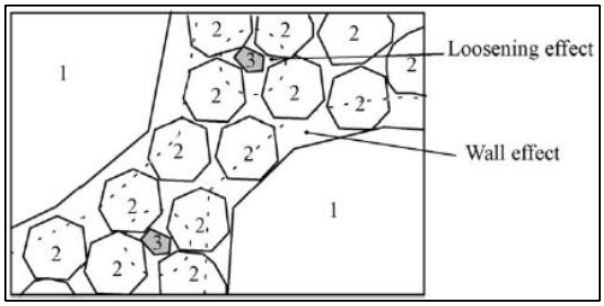

Figure 2.11 Wall effect and loosening effect (Mangulkar and Jamkar 2013)

Based on a binary mixture model, Al-Jarallah and Tons (1981) proposed a graphical and analytical method to predict air voids content in two-size aggregate mixtures, in which size ratio was a critical value that indicated the diameter ratio of the particles retained on two different sieves. It was concluded that aggregate mixtures with the same size ratio should generate the same packing voids contents under the same compaction condition. Hardiman (2004) introduced a procedure for application of binary mixture model in aggregate gradation design. Herein finer aggregates were added into coarser fraction stepwise as minimum porosity was obtained in coarser fraction within various proportions. As shown in Figure 2.12, A~D denoted the coarse aggregates with descending sizes and E was the fine fraction. The relatively densest packing in coarse aggregates was realised by properly determining the

proportions of coarse aggregates within different size ranges stepwise, and the target air voids content was achieved subsequently by selecting appropriate amount of fine fraction.

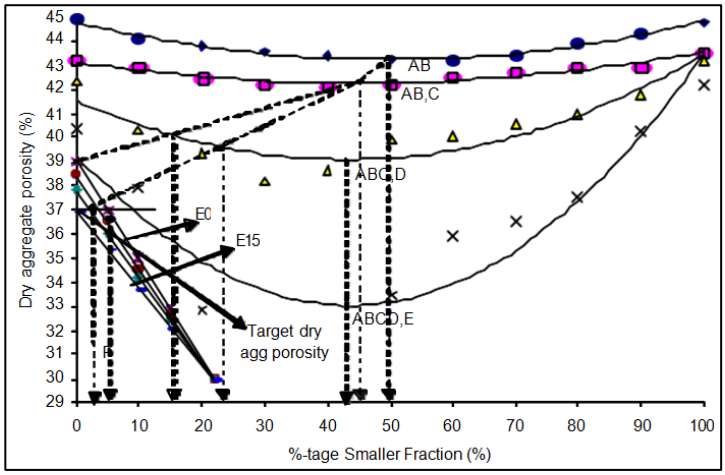

Figure 2.12 Relation between dry aggregate porosity and percentage of aggregate with smaller fraction (Hardiman 2004)

Aggregate gradation design based on binary mixture model was kind of an empirical-mechanistic method, in which porosity was a critical parameter in aggregate gradation design. Considering that porosity could be easily measured in the laboratory, it is simple and straightforward to implement this method in aggregate gradation design without strict requirement in engineering experience. However, the evaluation of asphalt mixtures was completely dependent on porosity without direct and in-depth analysis in terms of skeleton generation and load transmission, thereby rendering the method insufficient on consideration of mechanistic performance.

2.4.5 Dominant Aggregate Size Range (DASR) model

Kim et al. (2006) proposed a model to evaluate packing condition in coarse aggregate structure of asphalt mixtures based on the relationship between mixture porosity and aggregate interlocking. Dominant Aggregate Size Range (DASR) model was introduced and interstitial volume (IV) and interstitial components (IC) were referred to as the volume and components within the interstices of DASR (Figure 2.13). Upon dominant aggregate structure being formed by coarser

aggregates, resultant porosity generated by finer particles retained on next sieve was calculated to assess the interaction between aggregates within contiguous size ranges, which was defined as DASR porosity. It was suggested that DASR porosity be below 50% and relative proportion (%) of aggregates retained on contiguous sieves be within 70/30 so as to obtain quality performance (Kim et al. 2006, 2009a).

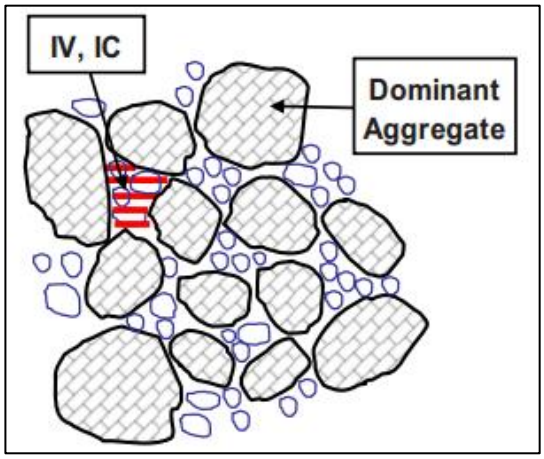

Figure 2.13 Sketch of dominant aggregate (Kim et al. 2009a)

DASR model is a conceptual approach to modify coarse aggregate structure in aggregate gradation design, providing a solid aggregate framework. However, the relevant criteria to estimate aggregate gradation were based on engineering experiences and were lacking in theoretical explanation. Meanwhile, the design factor of aggregate gradation in DASR model was limited to porosity instead of load transfer mechanism.

2.4.6 Voids in Coarse Aggregate (VCA) index method

Kandhal (2002) suggested a pass/fail criterion to stone-on-stone contact based on Voids in Coarse Aggregate (VCA) index. Voids in Coarse Aggregates of a compacted asphalt mixture (VCA_{mix}) and Voids in Coarse Aggregates of a coarse aggregate blend under dry-rodded condition (VCA_{DRC}) were calculated, and the ratio of VCA_{mix}/VCA_{DRC} was recommended to be less than 1.0 to obtain stone-on-stone backbone. It is straightforward to apply VCA index method in describing packing condition in the coarse fraction of an asphalt mixture; however, research has shown that there is no determinant linkage between VCA_{mix}/VCA_{DRC} ratio and

properties of the asphalt mixture (Suresha et al. 2009; Alvarez et al. 2010a; Mansour et al. 2013).

On the whole, most existing aggregate gradation design methods are based on mixture's volumetric properties since they are readily measured in the laboratory, such as CUW in Bailey method, DASR porosity in DASR model, and VCA_{mix}/VCA_{DRC} ratio in VCA index method, and the relevant criteria to evaluate packing condition are based on engineering experiences. Hence, the theoretical basis of packing mechanism in the aggregate mixture is inadequate, such as contact force and contact points, whereby such kind of parameters are more directly related to asphalt mixture's behaviour under external loading/deformation. Thus, it is more meaningful to involve both volumetric and mechanical parameters in aggregate gradation design.

2.5 Numerical simulation of asphalt mixture

It is favourable to apply numerical simulation in asphalt mixture design and aggregate gradation design so as to alleviate the excessive and tedious trial-and-error laboratory work in conventional methods. Meanwhile, mechanical details (e.g. stress/strain distribution, contact force, etc.) can be readily obtained by means of numerical simulation, which is hardly achieved by experiments alone. Generally, current numerical simulation methods regarding asphalt mixture are categorised into two types, namely Finite Element Method (FEM) and Discrete Element Method (DEM). FEM is based on continuum theory and more suitable to solve the problems in relatively homogeneous objects; while DEM model is an assemblage of discrete elements, which is capable of providing a micro-mechanical insight on granular materials.

2.5.1 FEM simulation

FEM is a relatively mature simulation method as compared to DEM, and it can be applied in most types of structural mechanics to solve for deformation and stress in solid bodies. The numerical technique embodied in FEM is to find approximate

solutions of Partial Differential Equations (PDE) as well as of integral equations, and the procedure includes (Cook et al. 2002):

(a) Input geometric and physical parameters according to engineering experience or practical measurement;

(b) Discretise solid body into a mesh;

(d) Generate matrices to describe the behaviour of individual elements;

(d) Combine all the individual elements into a global stiffness matrix; and

(e) Solve the global stiffness matrix to obtain displacement field and stress (or strain) field of the whole structure.

Currently FEM has been widely used in pavement engineering. Cheung and Cebon (1997) studied the behaviour of power-law creep-sensitive materials by means of FEM and laboratory experiments, and it was found that the elastic and viscous behaviour of creep-sensitive materials in the form of thin films could be satisfactorily modelled via FEM. With the objective of investigating strain distribution in asphalt mixtures and the relevant nonlinear behaviour, Bahia et al. (1999) modelled asphalt mixture via FEM with an idealised internal structure, in which the aggregates were assumed as 2D circular objects. Results showed that asphalt binder can undergo strains (in oscillatory shear test) ten times higher than the bulk strains that can be carried by asphalt mixtures. To investigate the early age strength of concrete cracking, Lawrence et al. (2012) conducted stress analysis via FEM in which the temperature distribution was obtained by finite element thermal analysis.

FEM is commonly and broadly used in modelling pavement structure. For example, Kim et al. (2009a) built a model for a three-layer pavement in order to study the viscoelasticity of asphalt pavement and its effect on cracking (Figure 2.14), and a finer mesh was set on the asphalt layer aimed at obtaining more accurate response results in this layer, which was treated as viscoelastic. By means of a User Material Subroutine (UMAT) in ABAQUS, a commercial FEM software, two non-linear modulus models to describe the resilient behaviour of pavement foundation were

established, namely in forms of an axisymmetric and a 3-dimensional stress states, respectively. Results showed that lower tensile strains occurred in the asphalt layer when using a 3-dimensional model as compared with the axisymmetric one.

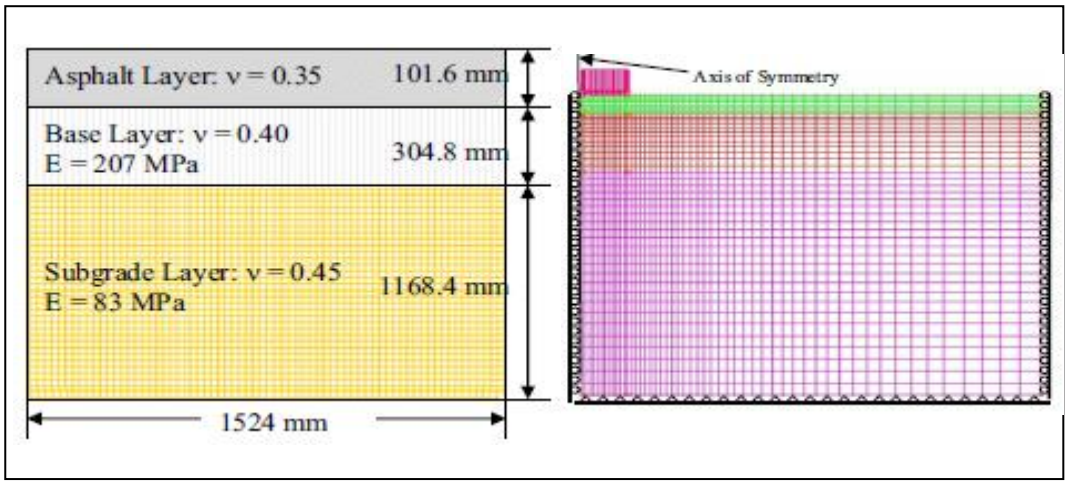

Figure 2.14 The FEM model for an axisymmetric model of a three-layer pavement (Kim et al. 2009a)

Huang et al. (2011) developed a three-layer asphalt pavement to study the pavement response under various loadings and temperatures, and nonlinear viscoelastic-viscoplastic constitutive model was applied. Verified by experiments at different stress levels and temperatures, the model was capable in assessing the effect of temperature on permanent deformation and tensile viscoplastic stress on cracking.

On the whole, it is common and useful to apply FEM to solve the problems in pavement engineering, especially in the aspect of analysing the response of asphalt layer under various traffic loadings, which is attributed to the strong capability in computing displacement and stress/strain distribution in the structure. Nevertheless, very little research has been conducted to model the micro-mechanical behaviours of asphalt mixtures through FEM, due to its deficiency in accounting for the slippage among aggregates, which noting the fact that it is very difficult to simulate the interlocking condition of compacted aggregates by FEM.

2.5.2 DEM simulation

DEM model is an assemblage of discrete particles, which is computed by alternately applying force-displacement law and law of motion (Newton's second

law), through which movements and interactions among particles can be obtained (Itasca 2008). Research shows that asphalt mixture behaves like a granular material, and hence it is more appropriate to analyse the stress pattern in an asphalt mixture using DEM technique instead of continuum models (Shashidhar et al. 2000).

- **Development of DEM**

DEM was initially introduced by Cundall (1971) in the field of rock and soil engineering. It was designed to solve the problems of rigid body motion based on simple assumptions, and normal stiffness and friction were considered to compute the interaction among blocks. Cundall and Strack (1983) collaborated afterwards and developed a 2D-DEM (i.e. Discrete Element Method in 2 Dimensions) computer program BALL and a 3D-DEM (i.e. Discrete Element Method in 3 Dimensions) computer program TRUBALL successively, which treated the block as an assembly of discs and spheres, respectively.

In 1992, Particle Flow Code (PFC), a simplified DEM program, was developed by Cundall and Hart (Itasca 2008). In PFC, an engineering structure can be modelled as an assembly of particles, and the individual particle is a disc in PFC2D (i.e. Particle Flow Code in 2 Dimensions) and a sphere in PFC3D (i.e. Particle Flow Code in 3 Dimensions). In PFC, 'ball' and 'wall' are the two basic elements: balls are used to simulate the small particles, which can be further combined as an assembly, while rigid boundaries are represented by walls. PFC possesses the superiority in modelling and describing the micro-mechanism of granular material with the following traits:

(a) the physical properties of the material can be directly assigned to its basic elements in the model, namely the balls;

(b) the friction of the material can be represented through slip and separation model;

(c) the behaviour of particle-to-particle interaction is described by contact-stiffness model; and

(d) relevant parameters (e.g. porosity, contact force, and coordination number etc.) can be measured and recorded along iterations (Shen and Yu 2011).

Nonetheless, significant constraints are encountered in PFC:

(a) amount of time consumed in the process of iterations (Liu and You 2011); and

(d) poor efficiency in producing elements with irregular shapes (Yu and Shen 2012).

Microfabric Discrete Element Modelling (MDEM) was introduced by Buttlar and You (2001) to simulate the mechanics of asphalt mixtures, through which interactions between different phases (e.g. aggregate-to-aggregate, aggregate-to-mastic, mastic-to-mastic) can be identified separately.

To overcome the weakness with prescribed shape, i.e. disc and sphere, Ghaboussi and Barbosa (1990) developed a computer program BLOCK3D in which particles used in simulation were six-sided solids, which could better model angular materials. Regarding to PFC model, current research has indicated that angularity and relevant interlocking effect can be well modelled by means of 'clump' samples, namely individual particle is created by combining balls of various sizes (Figure 2.15), and combined effect of interlocking and friction can be shown in corresponding model (Matsushima and Saomoto 2002; Lu and McDowell 2007; Chen 2010; McDowell and Ferellec 2010; Yu and Shen 2012).

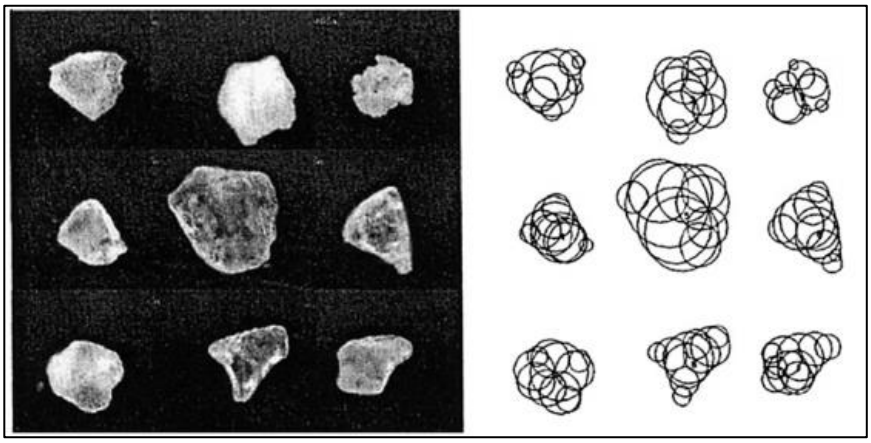

Figure 2.15 Example of clumps in 2-D model (Matsushima and Saomoto 2002)

On the whole, it is more favourable to use DEM, rather than FEM, to study the packing of DEM material due to the strong capability in analysing micro-mechanism, especially regarding particle-to-particle interaction among an assembly of aggregates. Also, considering PAM is mostly composed of coarse aggregates and

asphalt mastic, it is more suitable to be treated as discontinuous object, which fortifies the superiority of DEM in evaluating packing condition in PAM material.

- **Theory of DEM (Itasca 2008)**

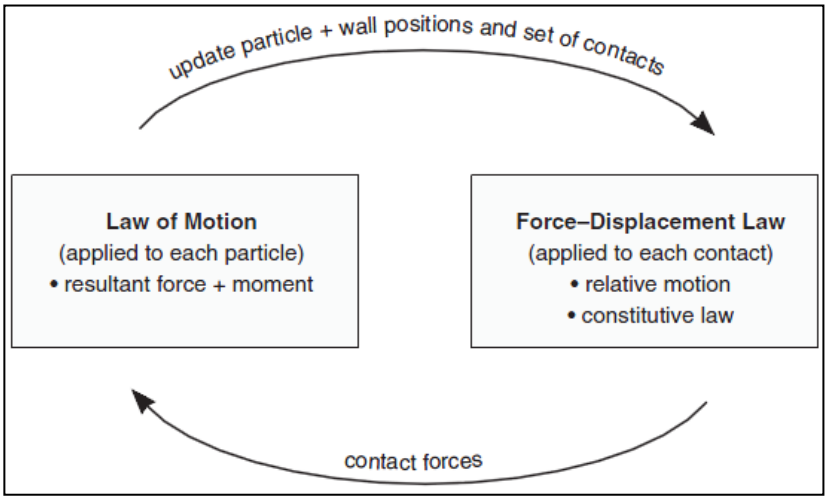

Figure 2.16 Calculation cycle in DEM (Itasca 2008)

The calculation in DEM is a dynamic process performed on an assembly of particles, and law of motion (Newton's second law) and force-displacement law are implemented alternatively through a time-stepping algorithm (Figure 2.16). It is assumed that velocity and acceleration are constant in each step (i.e. cycle).

(1) Force-displacement law

There are two types of contact forces arising from contact points (Equation 2.8), namely normal force and shear force.

$$F_i = F_i^n + F_i^s \tag{2.8}$$

F_i = contact force vector;
F_i^n = normal force;
F_i^s = shear force.

The normal force and shear forces are calculated by Equations (2.9) and (2.10), respectively.

$$F_i^n = k_n u_n \tag{2.9}$$

k_n = normal stiffness;

u_n = overlap, i.e. the relative displacement in the normal direction.

$$\Delta F_i^s = k_s \Delta u_s \tag{2.10}$$

ΔF_i^s = the increment of shear force;

k_s = shear stiffness;

Δu_s = the relative displacement in the tangent direction.

Total normal stress is calculated through normal stiffness k_n, which is a secant modulus. However, since shear stress is path-dependent, it is treated in an incremental fashion. Thus, shear stiffness k_s, a tangent modulus, is used to obtain the increment of shear force.

(2) Law of motion (Newton's second law)

Based on the individual properties and force-displacement law, the resultant force and moment imposed on a rigid particle can be determined in the PFC model. Subsequently, the motion of the particle, named the translational motion and the rotational motion, can be obtained through Newton's second law (Equation 2.11).

$$F_i = m(\ddot{x}_i - g_i) \tag{2.11}$$

m = mass of the particle;

$\ddot{x}_i$ = acceleration of the particle;

g_i = body force acceleration of the particle (e.g. gravitational acceleration).

Upon the determination of acceleration, updated velocity and position of the particle can be determined by Equations (2.12) and (2.13), respectively, which are used to calculate the contact force in the next cycle.

$$\dot{x}_i^{(t+\Delta t)} = \dot{x}_i^t + \ddot{x}_i^{(t+\Delta t/2)} \Delta t \tag{2.12}$$

$\dot{x}_i^{(t+\Delta t)}$ = velocity of the particle at time $(t + \Delta t)$;

$\dot{x}_i^t$ = velocity of the particle at time t;

$\ddot{x}_i^{(t+\Delta t/2)}$ = acceleration of the particle at time $(t + \Delta t/2)$;

Δt = a time step.

$$x_i^{(t+\Delta t)} = x_i^t + \dot{x}_i^{(t+\Delta t/2)} \Delta t \quad (2.13)$$

$x_i^{(t+\Delta t)}$ = position of the particle at time $(t + \Delta t)$;

x_i^t = position of the particle at time t;

$\dot{x}_i^{(t+\Delta t/2)}$ = velocity of the particle at time $(t + \Delta t/2)$.

- **Application of DEM in engineering**

DEM was initially introduced to deal with problems in soil and rock engineering, and relevant experiences have demonstrated that DEM simulation by means of PFC model is well-fitting for evaluation, especially in particle packing (Cundall and Strack 1983). Holt et al. (2005) compared the controlled laboratory experiments and DEM simulation and found DEM simulation was feasible to predict the unconfined strength and Young's modulus of rock-like material while the specimens were made of glass beads and epoxy in the laboratory. To assess the spalling in rock engineering, Cho (2010) conducted axially compression bending test on synthetic rock and used DEM simulation to discern the stress path in the beam; it was found that dilation was a suitable indicator for evaluating the spalling process. Fakhimi and Gharahbagh (2011) researched the impact of pore size and pore distribution on rock's behaviour on uniaxial compression test and tensile strength test by means of DEM, and it was shown that rock's elastic modulus and strength were influenced by the pore size and larger representative elemental volume was required for the model with larger-size pores.

Currently PFC has been applied in pavement engineering as well in order to understand behaviour of asphalt mixture on the aspect of micro-mechanism and build the linkage between macro-behaviour and micro-mechanism (Abbas et al. 2005; Chen 2010; Shen and Yu 2010; Jiang et al. 2011; Micaelo et al. 2011; Wu et al. 2011; Cai et al. 2013).

Wu et al. (2011) modelled compression tests of asphalt mixture at a constant strain rate by PFC3D, and a good agreement in stress-strain relation was obtained between

simulation and laboratory tests across a range of temperatures (0, 10, and 20 °C) and strain rates (0.02, 0.1, and 0.5/s). Softening behaviour was successfully simulated as well to represent bond breakage. Yu and Shen (2013) conducted dynamic creep tests for a dense asphalt mixture in PFC3D, and complex modules, including dynamic modulus and phase angle, were successfully obtained at various temperatures and frequencies, and simulation results showed nonlinear behaviour of phase angle at high temperature as well.

You et al. (2008) modelled asphalt mixture's behaviour via MDEM models. Results showed that 3-D model generated more accurate modulus than 2-D model. Taking models of 4% air voids content as an example, 3-D model and 2-D model deviated by 3.25% and 16.15% as compared with laboratory measurements, respectively. Meanwhile, 3-D models were feasible to estimate mixture moduli at various temperatures (0, -10, and -20 °C) and loading frequencies (0.1, 1, 5, and 10 Hz). Furthermore, four contact models were introduced to represent interactions among elements within the asphalt mixture's MDEM model: within the same piece of aggregate, within mastic, between aggregate and mastic, and between two adjacent aggregate pieces. Simulation results (dynamic modulus and phase angle) showed good agreement with laboratory measurements, indicating MDEM's capability in describing asphalt mixture's viscoelastic behaviour (Liu et al. 2009). To reduce computing time in MDEM in simulating dynamic creep test for asphalt mixture, regular frequency was subsequently replaced by virtual frequency based on time-temperature superposition principle, and similar simulation results were attained as compared to laboratory results (You et al. 2011).

On the aspect of aggregate packing in asphalt mixture, Micaelo et al. (2011) modelled static compaction procedure of three types of asphalt mixtures (i.e. two dense asphalt mixtures and one PAM) via PFC2D, and their results showed good agreement with corresponding laboratory test. Shen and Yu (2011) established a series of PFC3D models to describe aggregate gradation, in which finer particles were added into previous coarser model stepwise, and the role of finer particles in a blend, namely coarse or fine fraction, was evaluated based on the effect on the volumetric property, namely creating or filling voids, respectively.

In terms of asphalt mastic, Abbas et al. (2005) studied dynamic mechanical behaviour of asphalt mastic via PFC2D, which could rationally show the stiffening effect of mineral fillers as a function of volumetric proportion, while predicted dynamic modulus were underestimated.

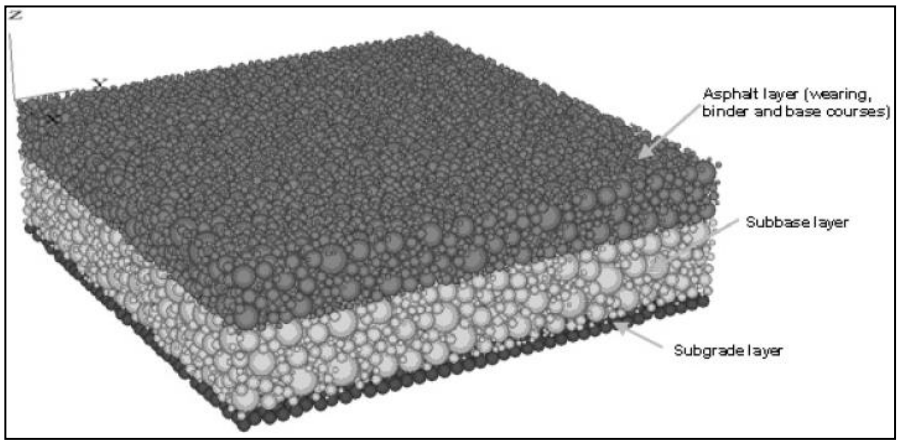

Figure 2.17 Multi-layer pavement model in PFC3D (Dondi et al. 2007)

Regarding pavement structure, Dondi et al. (2007) built a multi-layer pavement model (Figure 2.17) by PFC3D, which was loaded subsequently and strain and displacement developed in the structure were evaluated as well. The results from PFC3D showed a good agreement with that gained from BISAR (Bitumen Stress Analysis in Roads) software.

2.6 Summary

PAM has been widely utilised worldwide due to the outstanding improvement in driving safety and environment, e.g. reduced aquaplaning, mitigated splash and spray, lowered noise level, enhanced skid resistance, and cooling effect etc., while ravelling and clogging are the major problems encountered. For Singapore, PAM is an appropriate choice given the excellent drainage function, which can help in alleviating the flood phenomenon caused by frequent thunderstorms. Furthermore, PAM's cooling effect is also desired considering the constant high temperature throughout the year for a tropical country.

Asphalt mixture design for PAM varies across different countries, and there is a trend that more attention is being paid on performance-based asphalt mixture design according to specific application condition, such as putting concerns into

permeability and abrasion resistance. Considering the great potential in developing off-road cycling network in Singapore, investigation shall be conducted in PAM asphalt mixture design for low-strength pavement application in the tropical area.

PAM's significant trait, high air voids content, is attributed to the open-graded design, in which coarse fraction is dominant in the aggregate blend. Thus aggregate packing, which is mostly generated by interlocked coarse aggregates, is an important factor in PAM's performance. Currently, most aggregate gradation design methods are based on volumetric properties (e.g. CUW, VCA, and porosity) due to the accessibility in laboratory measurement, while more direct and meaningful factor in packing mechanism is inadequate due to the difficulty in obtaining relevant parameters from laboratory testing.

On the other hand, DEM technique is capable of providing in-depth insight in micro-mechanism of an assembly of particles, and particle-to-particle interaction can be well represented though a proper contact model. Regarding the stone-on-stone framework created in an aggregate mixture, it is appropriate to be regarded as discrete object. Therefore, it is appropriate to investigate the packing condition in PAM by means of DEM, and distinctive parameters relating to the interlocking mechanism shall be developed.

Chapter 3 Research methodology

3.1 Introduction

Open-graded design is a remarkable feature in PAM, namely coarse aggregates are the main component in aggregate gradation to create air voids in the stone-on-stone framework and the content of fine fraction is strictly controlled to ensure that sufficient air voids remains in the asphalt mixture so as to achieve adequate drainage capacity. Hence air voids content is an important volumetric parameter in PAM design and a large amount of research has been conducted in the past to investigate the impacts of air voids content on PAM's performance especially in terms of strength and permeability. Nonetheless, less attention has been paid on the packing condition in PAM, including the development of particle-to-particle framework and its role in PAM's performance. Meanwhile, hardly any direct and explicit parameters have been defined that can well indicate the packing condition in an aggregate blend.

In this research, the properties (e.g. air voids content, mixture strength, and permeability) of PAMs with design factors at different levels are investigated. Subsequently potential PAM designs for low-strength pavement application in Singapore shall be proposed, and the resultant properties of designed PAMs shall be evaluated on the aspects of mechanical strength and functional performance as well. In addition, DEM simulation is applied to reveal the development of packing structure in PAM by means of the PFC3D model.

In this chapter, material selection and fabrication method for designed PAM specimens in this research are introduced. Measurement methods in the laboratory to obtain volumetric parameters and performance indices are documented, and the corresponding method that establishes the PFC3D model to simulate the designed PAMs is stated as well.

3.2 Preparation of PAM specimens

3.2.1 Material selection

Crushed granite was selected in this research as the mineral aggregates, which is widely used in pavement construction in Singapore. The basic mechanical properties of mineral aggregates, including Los Angeles (LA) abrasion value, aggregate impact value (AIV), and 10% fines value etc. were characterised and the results are shown in Table 3.1. These properties describe the resistance of aggregates to mechanical degradation.

The requirements for aggregates in PAM in Singapore are relatively lower than that in other countries. Meanwhile, the granite's LA abrasion value exceeded the upper limit. However, they are still potentially usable in this research due to the lowered requirement for pedestrian/cyclist pathways in terms of strength.

Table 3.1 Mechanical properties of crushed granite

property	value	specification requirement (LTA 2010)
LA abrasion value (%, by mass)	37.2 (± 1.2)*	< 20
aggregate impact value (%, by mass)	27.9 (± 1.0)	< 30
10% fines value (kN)	179 (± 2.5)	> 130
flakiness index	8.5 (± 1.2)	< 25
elongation index	27.0 (± 1.9)	< 30

Note: value in parenthesis refers to standard deviation

The bulk specific gravity and water absorption of aggregates within different size ranges were measured and the results are shown in Table 3.2. All the measurements in the characterisation tests were based on three replicates.

Table 3.2 Bulk specific gravity and water absorption of crushed granite

size range (mm)	bulk specific gravity	water absorption (%)
19.0-13.2	2.60 (±0.007)	0.48 (±0.04)
13.2-9.5	2.62 (±0.002)	
9.5-6.3	2.58 (±0.004)	
6.3-4.75	2.60 (±0.008)	
4.75-2.36	2.62 (±0.010)	
< 2.36	2.60 (±0.027)	1.29 (±0.008)

Two types of asphalt binder, Pen 60/70 and PG 76, were utilised in this research, with pertinent properties given in Tables 3.3 and 3.4, respectively. Pen 60/70 is a common kind of straight asphalt binder without modification, and PG 76 asphalt is modified by Styrene Butadiene Styrene (SBS), which possesses lower penetration value and more resistance to the damages caused by high temperature, such as hardening. In additional, 2% hydrated lime (by mass) was applied as fillers in the case of Pen 60/70 asphalt so as to enhance PAM specimen's anti-stripping property.

Table 3.3 Properties of Pen 60/70 asphalt binder

property	Pen 60/70 asphalt
relative density at 25 ^{0}C	1.01
penetration at 25 ^{0}C, 100g, 5s (0.1mm)	62
softening point, ring and ball (^{0}C)	50
flash point, Cleveland open cup (^{0}C)	276
loss on heating (% by mass)	0.2
ductility at 25 ^{0}C at 5cm/min (cm) (after thin-film oven test)	100
retained penetration at 25 ^{0}C (%) of original (after thin-film oven test)	80
mixing temperature (^{0}C)	150-165
compacting temperature (^{0}C)	125-145

Table 3.4 Properties of PG 76 asphalt binder*

Property		Value
Original binder	relative density @ 25/25 ℃	> 1.00
	penetration @ 25 ℃ (0.1 mm)	> 50
	softening point (℃)	> 80
	loss on heating (% wt)	< 1.0
	flash point (Cleveland cup) (℃)	> 230
	toughness @ 25 ℃ (Nm)	>20
	tenacity @ 25 ℃ (Nm)	> 15
	viscosity @ 135 ℃ (Pa s)	1.377
	mixing temperature (℃)	165-175
	compaction temperature (℃)	155-165
	Dynamic shear	
	DSR test temperature @ 10 rad/s	82 ℃
	G*/ sin δ	1.1427 kPa
	DSR test temperature @ 10 rad/s	88 ℃
	G*/ sin δ	0.7669
	Estimated passing temperature	84.0 ℃
RTFO residue	**Dynamic shear**	
	DSR test temperature @ 10 rad/s	76 ℃
	G*/ sin δ	2.6482
	DSR test temperature @ 10 rad/s	82 ℃
	G*/ sin δ	1.810
	Estimated passing temperature	78.9 ℃
PAV + RTFO residue	**Dynamic shear**	
	DSR test temperature @ 10 rad/s	28 ℃
	G*/ sin δ	4101.0
	DSR test temperature @ 10 rad/s	25 ℃
	G*/ sin δ	6086.5
	Estimated passing temperature	26.5 ℃
	Creep stiffness	
	BBR test temperature	-12 ℃
	Stiffness	221 MPa
	m-value	0.310
	BBR test temperature	-18 ℃
	Stiffness	659 MPa
	m-value	0.191
	Estimated passing stiffness, S(t)	-13.1 MPa
	Estimated passing m-value	-12.5
	BBR low PG	-22 ℃

*RTFO= Rolling Thin Film Oven, PAV= Pressure Aging Vessel, m-value= slope of the master stiffness curve at 60 seconds in bending beam rheometer (BBR) test

3.2.2 Compaction method

A gyratory compaction machine was utilised to fabricate cylindrical PAM specimens with diameter of 101.6 mm, which can better orient aggregate particles to simulate in-field compaction condition as compared to conventional Marshall hammer (AI 1996).

3.3 Volumetric properties

3.3.1 Voids in Coarse Aggregate (VCA) ratio

Stone-on-stone framework created by the coarse aggregates is the major factor for packing condition in PAM. Voids content is widely used to assess the degree of packing condition in a compacted aggregate blend or asphalt mixture. Two types of Voids in the Coarse Aggregate (VCA) parameters, namely Voids in Coarse Aggregates of coarse aggregate mixture under dry-rodded condition (VCA_{DRC}) and Voids in Coarse Aggregates of compacted asphalt mixture (VCA_{mix}), are commonly used to assess the packing condition in the aggregate mixtures and asphalt mixtures, while it has been suggested that adequate stone-on-stone backbone is produced when VCA ratio (i.e. the ratio of VCA_{mix}/VCA_{DRC}) is less than 1.0 (Kandhal 2002).

For determining the voids content, aggregates of each blend were poured into a bucket of 2,663 mm^3 volume (i.e. 140 mm in diameter and 173 mm in height) in three equal lifts with 25 rods of compaction per lift by a steel rod of 16 mm diameter. The voids content in the aggregate blend, VA_{DRC}, can be obtained by Equations (3.1) and (3.2) (AI 1996).

$$VA_{DRC} = \left(\frac{G_{BA} \times \gamma_w - \gamma_s}{G_{BA} \times \gamma_w}\right) \times 100 \qquad (3.1)$$

G_{BA} = bulk specific gravity of blended aggregates;

γ_w = unit density of water;

γ_s = unit density of dry-rodded coarse aggregates.

Essentially, VA_{DRC} equals to VCA_{DRC} if the aggregate blend is the coarse fraction in an aggregate gradation.

$$\gamma_s = \frac{\sum P_i}{\sum(P_i/\gamma_{si})} \tag{3.2}$$

P_i = individual percentage by mass of the aggregates retained on the i^{th} sieve;

γ_{si} = bulk specific gravity of the aggregates retained on the i^{th} sieve.

To further assess the packing condition in compacted PAMs, VCA_{mix} can be calculated from Equations (3.3) and (3.4) to obtain VCA ratio.

$$VCA_{mix} = \left(1 - \frac{G_{mb} \times P_{CA}}{G_{CA}}\right) \times 100 \tag{3.3}$$

G_{mb} = bulk specific gravity of compacted specimen;

P_{CA} = percentage of coarse aggregate in compacted specimen by mass;

G_{CA} = bulk specific gravity of coarse aggregates.

$$P_{CA} = \left(\frac{\%R_{BS}}{100}\right) \times \left(1 - \frac{P_b}{100}\right) \tag{3.4}$$

R_{BS} = percentage of aggregate retained on breaking sieve (BS);

P_b = percentage of asphalt binder in compacted specimen.

3.3.2 Air voids content in PAM specimen

High air voids content is the most distinctive volumetric feature for PAM materials, which is generated by the open-graded design and greatly contributes to PAM's principal benefits, e.g. excellent drainage performance, noise reduction and cooling effect etc. The total air voids (TAV) content in PAM comprises both water-accessible air voids (WAAV) content and disconnected air voids content. As compared to TAV content, WAAV content in PAM, namely the inter-connective air voids allowing water to pass through, is regarded more important to permeability performance (Zhu 2005; Alvarez et al. 2008).

The TAV content can be obtained through Equation (3.5) in which theoretical maximum specific gravity of asphalt mixture, G_{mm}, was measured via a vacuum pycnometer (Figure 3.1) (American Society for Testing and Materials [ASTM] 2011a). The WAAV content of a PAM specimen was measured through the buoyancy principle, and the volume of inter-connective air voids in a PAM specimen was obtained through the weight of specimen obtained in air and water, respectively, as given in Equations (3.6) and (3.7). It should be noted that the weight of PAM specimen should not be recorded until the inter-connective air voids in the specimen is sufficiently infused with water, namely the reading on the balance is stable. Volume of the compacted specimen is measured through the dimensional method.

Figure 3.1 Vacuum pycnometer

$$TAV = \left(1 - \frac{G_{mb}}{G_{mm}}\right) \times 100 \tag{3.5}$$

$$WAAV = \frac{V_{WAAV}}{V} \times 100 \tag{3.6}$$

V_{WAAV} = volume of inter-connective air voids;

V = volume of PAM specimen.

$$V_{WAAV} = V - \frac{W_{air} - W_{water}}{\gamma_w} \tag{3.7}$$

W_{air} = weight of compacted specimen in air;

W_{water} = weight of compacted specimen in water.

3.4 Performance tests of PAMs

For each PAM design, three replicated tests were conducted for a series of measurements in the laboratory, including draindown test, Marshall test, moisture-conditioned Marshall test, indirect tensile stiffness modulus (ITSM) test, moisture-conditioned ITSM test, Cantabro abrasion test, and ageing-conditioned Cantabro abrasion test, among which the draindown test was conducted on uncompacted specimens. Compacted specimens were first tested for TAV content, WAAV content and permeability rate followed by application of destructive performance tests except the ones used in Cantabro abrasion test and ageing-conditioned Cantabro abrasion test.

3.4.1 Draindown test

Draindown refers to the phenomenon that asphalt mastic flows downwards within an asphalt mixture during transporting, mixing, and compacting process, which usually occurs in the cases of high proportion of coarse aggregates in the asphalt mixtures, such as PAM and stone mastic asphalt (SMA). Meanwhile, draindown is generally related to a high content of asphalt binder and/or asphalt binder of high penetration value (e.g. lack of fine aggregates and fillers to hold asphalt binder and form stiff asphalt mastic), and superfluous asphalt may thus flow down and causes rutting and ravelling in the field especially under high temperature and/or heavy traffic loading. In the laboratory, draindown test is conducted on loose asphalt mixture samples and draindown value is referred to as the mass loss by percentage in the sample upon being heated in an oven at the mixing temperature for one hour. The recommended upper limit of draindown value is 0.3% by mass (Rajib et al. 2000). According to ASTM D 6390-11 (2011b), the detailed procedure is:

(a) prepare loose asphalt mixture sample at designed asphalt binder content and obtain the initial mass;

(b) pour the sample into a wire basket (Figure 3.2), and place the basket into an oven at the mixing temperature with a plate below; and

(c) remove the basket from the oven after one hour heating conditioning and weigh the asphalt mastic that flowed onto the plate, which is referred to as draindown mass. Draindown value is the proportion of draindown mass to initial mass in percent.

In addition, a wire basket with the mesh size of 2.36 mm was used rather than the standard 4.75 mm so as to improve the repeatability of the testing results, as recommended by Watson et al. (2003).

Figure 3.2 Wire basket used in draindown test

3.4.2 Cantabro abrasion test and ageing-conditioned Cantabro abrasion test

Cantabro abrasion test was originally developed in Spain, aimed at estimating PAM's resistance to abrasion, which is directly related to the in-field performance in ravelling, it being one of the major issues encountered by PAMs. The test procedure is similar to that of Los Angeles (LA) abrasion test except that no steel ball is added into the drum chamber. Compacted PAM specimen undergoes 300 drum revolutions in a LA abrasion machine at 25 °C at a speed of 30-33 rpm, which indirectly simulates the abrasion effect from tyres in the field and impairment of asphalt binder's bonding effect. The abrasion loss value (ALV) is obtained as the weight loss in percent, as shown in Equation (3.8).

$$ALV = \left(\frac{P_1 - P_2}{P_1}\right) \times 100 \quad (3.8)$$

P_1 = initial mass of the sample;

P_2 = finial mass of the sample.

ALV usually decreases with the increase in asphalt binder content due to the stronger adhesiveness. While Cantabro abrasion test is broadly used to assess the resistance to wear or particle loss for PAM material, it was found that this test cannot appropriately reflect the abrasion onto the surface of asphalt mixture in the field (Dong et al. 2013). Instead, damage occurring in Cantabro abrasion test is caused by impact effect between the compacted sample and the rigid inside-wall of the drum, which is more severe than the abrasion effect in the field.

Furthermore, due to the high air voids content, PAM tends to get hardened faster than that occurring in conventional dense asphalt mixtures especially under high temperature condition, rendering weaker adhesiveness of the asphalt binder to resist abrasion (Herrington et al. 2005; Alvarez et al. 2010b). Hence ageing-conditioned Cantabro abrasion test should be conducted and the procedure is similar to that of unconditioned Cantabro abrasion test except the specimen is to be conditioned in an oven at 60 ± 1 ºC for seven days before undergoing abrasion. The upper limits of ALVs for unaged and aged PAM specimens are 20% and 30%, respectively (Rajib et al. 2000). Hence, two types of ALV shall be obtained, namely unconditioned Abrasion Loss Value (UC-ALV) and ageing-conditioned Abrasion Loss Value (AC-ALV).

3.4.3 Permeability test

Permeability, which is referred to as drainage performance or hydraulic conductivity, is the essential trait of PAM, being directly related to the basic function of permeable mixture, namely reducing aquaplaning, mitigating splash and spray, consequently providing a safer driving condition. Hence, studies on PAM's permeability test are carried out by many researchers, and a falling head setup to measure permeability is widely utilised and recommended given its convenience

and accuracy (Charbeneau et al. 2011; Noramuena-Contreras et al. 2014). Permeability testing apparatus introduced by Florida Department of Transportation [Florida DOT] (2004) was applied in this research (Figure 3.3), and the coefficient of permeability, *k*, can be calculated through Equation (3.9).

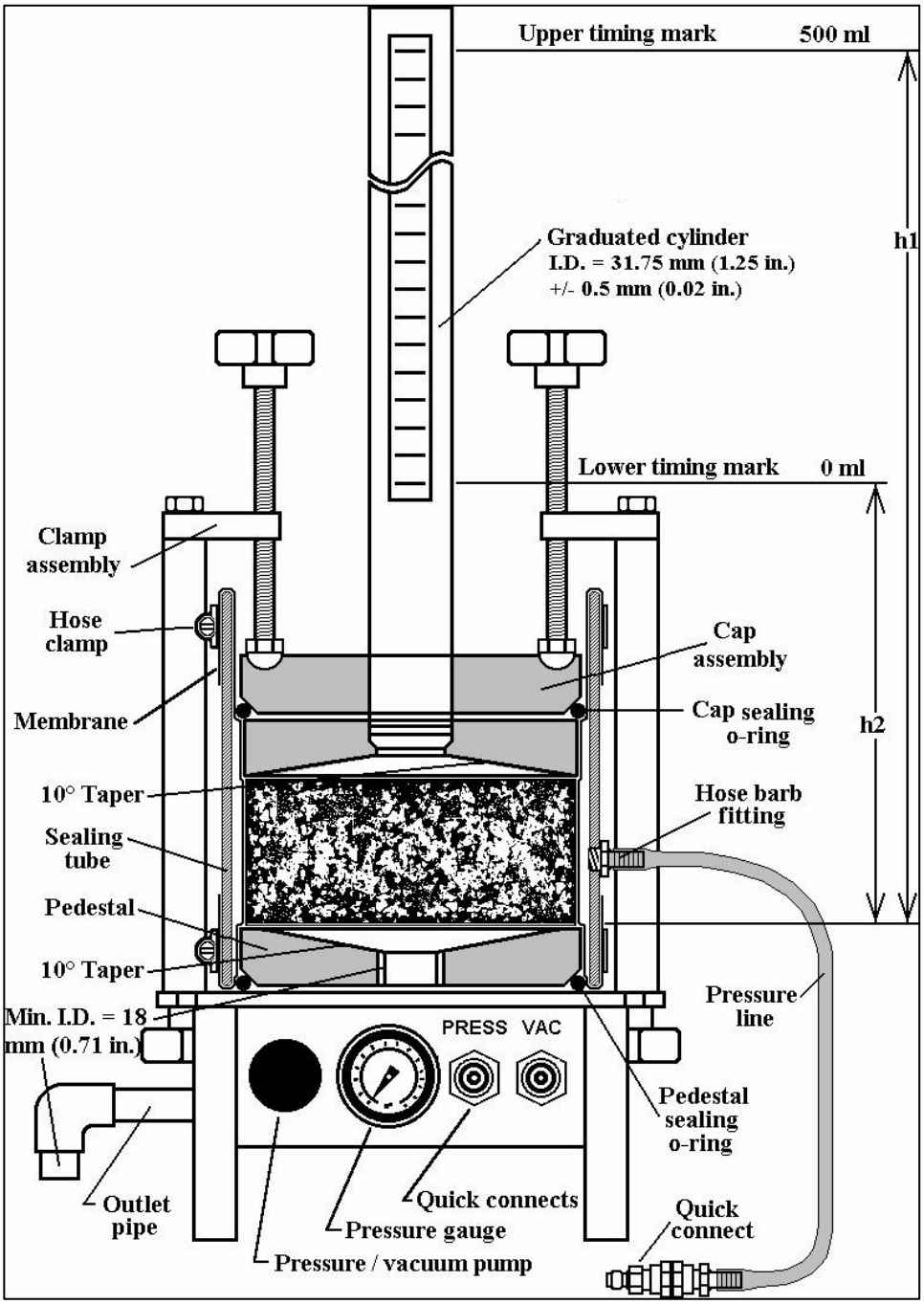

Figure 3.3 Permeability testing apparatus (Florida DOT 2004)

$$k = \left(\frac{aL}{At}\right) \times \ln\frac{h_1}{h_2} \times t_c \quad (3.9)$$

a = internal cross-sectional area of buret, cm^2;

L = mean thickness of PAM specimen, cm;

A = cross-sectional area of PAM specimen, cm^2;

h_1 = initial water head across PAM specimen, cm;

h_2 = final water head across PAM specimen, cm;

t = elapsed time for water passing from h_1 to h_2, s;

t_c = temperature correction coefficient.

Permeability performance is strongly dependent on the water-accessible air voids in PAM material, and it commonly declines along usage due to: (a) clogging and further densification, which reduces voids content in the permeable course, and (b) draindown of asphalt binder in high temperature condition, which makes the bottom of surface layer denser due to the asphalt mastic flown down (Fwa et al. 1999; Alvarez et al. 2008). Thus PAM's permeability after high temperature conditioning and moisture conditioning, which might cause the phenomenon of asphalt draindown, should be examined as well.

3.4.4 Marshall test and moisture-conditioned Marshall test

Marshall test is used to assess the strength of asphalt mixture. Master Loader HM-3000 Humboldt was used to apply a vertical load on the asphalt mixture sample at a constant rate of 50.8 mm/min until failure (Figure 3.4). Before loading, the specimen was soaked in a water bath at 60 ± 1 °C for 30 minutes, and Marshall stability is defined as the peak load the specimen can carry during loading.

Moisture-conditioned Marshall test was conducted to evaluate PAM's susceptibility to moisture damage as well, with the procedure being similar to that of unconditioned Marshall test except that the PAM specimen is conditioned in the water bath at 60 ± 1 °C for 24 hours before loading.

Figure 3.4 Apparatus for Marshall test

Two types of Marshall stability are obtained, namely Unconditioned Marshall stability (UC-MS) (i.e. specimen immersed in the water bath at 60 ± 1 ºC for 30 minutes before testing) and Moisture-Conditioned Marshall stability (MC-MS) (i.e. specimen immersed in the water bath at 60 ± 1 ºC for 24 hours before testing). Retained MS ratio is defined as the ratio of two types of Marshall stability in percentage, shown by Equation (3.10).

$$retained\ MS\ ratio = \frac{\text{MC-MS}}{\text{UC-MS}} \times 100\% \tag{3.10}$$

3.4.5 Indirect tensile stiffness modulus (ITSM) test

Indirect tensile stiffness modulus (ITSM) test was conducted to obtain asphalt mixture's ITSM value. The Material Testing Apparatus (MATTA) was utilised to apply a compression load in the vertical diametric plane of PAM sample (Figure 3.5) with a haversine loading waveshape. The procedure and input parameters were according to the Australian Standard Method 13.1 (Australian Standard [AS] 1995) (Table 3.5). Dynamic load and recoverable deformation were measured during test, and ITSM (MPa) was calculated through Equation (3.11).

$$ITSM = \frac{P(\upsilon + 0.2734)}{\delta t} \tag{3.11}$$

P = magnitude of dynamic load, N;

υ = Poisson's ratio;

δ = total recoverable deformation, mm;

t = thickness of specimen, mm.

Table 3.5 Input parameters for ITSM test

parameter	values
test temperature (^{0}c)	25 ±0.5
loading waveshape	haversine
loading pulse width (ms)	100
pulse repetition period, 10% to 90% (ms)	3000 ±5seconds
target peak strain (με)	50 ±20

Figure 3.5 Apparatus for ITSM test

3.5 DEM simulation via PFC3D model

PFC3D, an application software based on DEM theory (Itasca 2008), was utilised in this research to better understand the establishment of stone-on-stone backbone within compacted mixtures. The basic procedures of DEM simulation via PFC3D consist of:

(1) generate particles with specific size distribution to represent designed aggregate gradation, and assign proper physical and mechanical properties;

(2) set simulation parameters (e.g. porosity, coordination number, and contact force) that can effectively show the contacting mechanism among particles;

(3) compact particle assembly via a servo-mechanism process; and

(4) export the assigned simulation parameters and conduct analysis.

Meanwhile, verification can be conducted on the aspect of voids content, which is readily measured in the laboratory.

3.5.1 Model generation

A container, representing the mould used in the laboratory for measuring the VA_{DRC} value, was first generated in the PFC3D model. It is composed of three parts, namely a cylinder, a bottom plate, and a top plate, and the size was according to that of the mould, namely being 140 mm in diameter and 173 mm in height, while the cylinder was extended 20% in both top and bottom directions for further compaction procedure. The particles that constituted the aggregate blend were generated in the following steps.

<u>Step 1:</u> generating particles to describe aggregate gradation

In this step, the proper amounts of particles in each size were created in PFC3D to represent the designed aggregate gradation, and the detailed procedures are given as follows.

(a) estimate the number of particles in each size range

For an aggregate blend with specific aggregate gradation, around n_i pieces of particles exist in the i^{th} size range, which can be obtained through Equation (3.12).

$$n_i = \frac{M_i}{m_{i\_per}} = \frac{M_{tot} \cdot P_i}{m_{i\_per}} \tag{3.12}$$

M_i = mass of aggregates in the i^{th} size range;

M_{tot} = total mass of the aggregate blend;

P_i = individual percentage of the aggregates in the i^{th} size range by mass;

m_{i_per} = mean mass of per aggregate in the i^{th} size range.

The value of m_{i_per} was obtained through sampling the mass of 100 random pieces of aggregates, and six replicated trials were conducted for each size range. Meanwhile, the mean volume per piece of the aggregates in the ith size range, v_{i_per}, can be obtained as well (Table 3.6).

Table 3.6 Values of m_{i_per} and v_{i_per} for each size range

size range (mm)	m_{i_per} (g)	v_{i_per} (mm^3)
19.0-13.2	6.463 (±0.178)	2485.71 (±68.49)
13.2-9.5	2.474 (±0.123)	944.40 (±47.12)
9.5-6.3	0.752 (±0.045)	291.47 (±17.36)
6.3-4.75	0.230 (±0.016)	88.56 (±6.02)
4.75-2.36	0.069 (±0.008)	26.18 (±2.92)

(b) generate particles of reduced radii

An assembly of particles in PFC3D is required to be initially generated in a loose condition. The radii of particles were consistently reduced to ensure all the generated particles can be contained in the container and be sufficiently re-oriented during compaction cycling as well. The radius of each particle in the ith size range was randomly selected in which the size range was reduced by a Multiplication Factor (MF), which would later be recovered by an expanding process. A MF value of 1.6 was found proper and was thus used (Itasca 2008). For example, for the first size range, 19.0-13.2 mm, the radii of the particles were randomly selected in the range of 5.9375-4.125 mm initially.

(c) eliminate the error in particles amount

Since the radius of each particle was randomly selected in a specific size range in the PFC3D model, some errors would be introduced in the total particle amount for each size range. Thereby, to compensate for such error, the radius of each particle in the ith size range was multiplied by a radius adjustment factor (rf_i) so as to compensate for such kind of error, which was gained by Equation (3.13) and turned out to be quite close to 1.0. In this way, an accurate amount of the particles can be obtained for each size range.

$$rf_i = \sqrt[3]{\frac{V_i/MF^3}{V_{i\_ini}}} = \sqrt[3]{\frac{(M_i/den_i)/MF^3}{V_{i\_ini}}} \quad (3.13)$$

V_i = required volume of the aggregates in the ith size range according to aggregate gradation;

V_{i_ini} = initial volume of the particles in the ith size range, with the radii being reduced by a multiplication factor MF;

den_i = relative density of the aggregates in the ith size range.

(d) assign properties to the model

The density of the particles in each size range was assigned according to the corresponding bulk density values determined in the laboratory (Table 3.2). Aggregate elastic modulus of 40 GPa and Poisson ratio of 0.2 were used, as measured by axial compression test on granite rock in the laboratory. The modulus of the walls in the PFC3D model (i.e. the container) was set as ten times as that of the particles to provide sufficient stiffness. The coefficient of friction strongly influences the packing condition for a compacted assembly of particles. In this research, the coefficient of friction was selected as 0.5 based on the successful experiences of previous research (You et al. 2008; Shen and Yu 2011). The coefficient of friction between particles and walls was set as 0.0, considering the surface of the mould in the laboratory is very smooth.

<u>Step 2:</u> using 'Clump' to represent irregular particle shape

'Clump' as a function provided by PFC3D was utilised to reshape the default spherical particles in the model into irregular shape of the aggregates. In a clumped particle, several spherical balls were combined to behave as an entity. Lu and McDowell (2007) proposed a clumping technique to represent the shapes of fully crushed granites and it showed realistic interlocking among clumps as compared to the laboratory measurement. Hence, this method was applied in this research to generate clumps and the detailed procedure is given in the following.

(1) Determine the shape of the clump

(1.a) Determine the directions to generate balls in a clump

A ball was generated at the centre as a core part of a clump with the radius of *R*. The following balls were possibly generated in 6 orthogonal directions (e.g. ±x axis, ±y axis, and ±z axis). The possibility each direction to be used was set as *p*.

(1.b) Determine the number of balls in each direction

For a selected direction, the maximum number of successive balls to be generated was set directly, which was 2 in this research.

(1.c) Generate balls in each determined direction

Figure 3.6 gives the sketch of clumped geometry with the second Ball B being generated following the central Ball A along x direction.

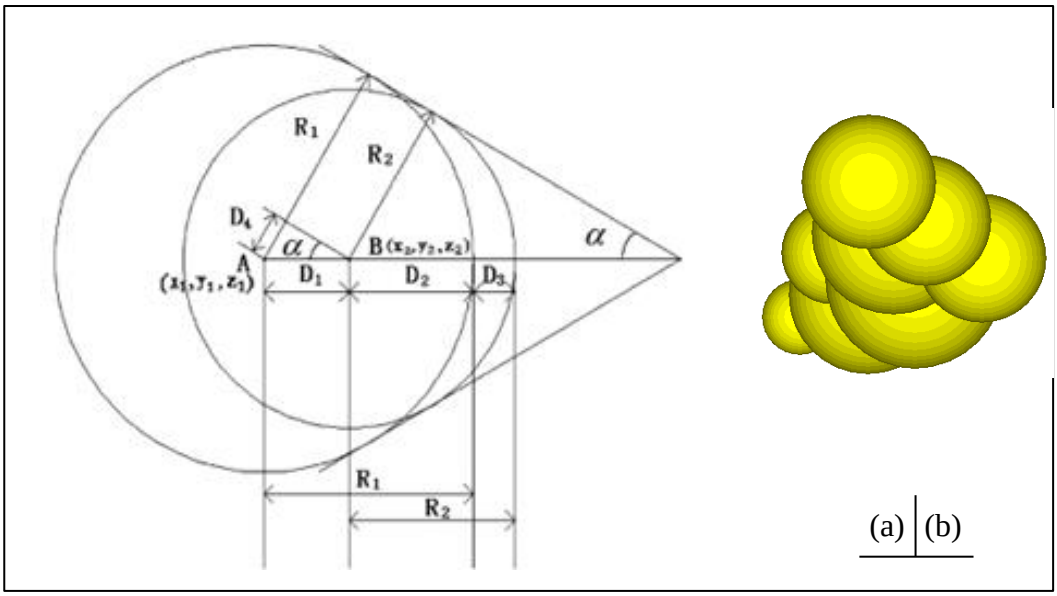

Figure 3.6 Clump generated in PFC3D: (a) geometrical definition (Lu and McDowell 2007), and (b) a resultant example

Here, the centres for Ball A and Ball B are (x_1, y_1, z_1) and (x_2, y_2, z_2), respectively (obviously, $y_1 = y_2$, $z_1 = z_2$); the radii for Ball A and Ball B are R_1 (which equals to *R*) and R_2; D_1 is the distance between the two centres of the balls; D_2 is the distance between the centre of Ball B and the extension of Ball A in x direction; D_3 is the distance between the outermost locations of Ball A and Ball B in +x direction

(namely the direction to produce the successive ball), which is also called as clump extension, and it is selected as $0.2R$; D_4 is the difference in radius between two successive balls, which is randomly selected in the range [0.0, c], and c is selected as $0.2R$. The centre of Ball B can be subsequently obtained, namely $D_1 = D_3 + D_4$.

(1.d) Generate linked balls

If two consecutive balls were both generated in two orthogonal directions, a middle ball was generated, with the average geometric parameters (i.e. radius and position) of the two outermost balls to produce a less jagged surface morphology.

(2) Determine the size of the clump

As the relative centres and radii of the following balls were determined, which were expressed as the function of R (the radius of the central ball), the volume of the clump can be determined as a function of R as well, denoted as $V_{cl}(R)$. The clump particle replaces the initial spherical particle based on the same volume. Hence R can be obtained through Equation (3.14), as an inverse function of $V_{cl}(R)$.

$$R = {V_{cl}}^{-1}[V_{sp}(r)] \tag{3.14}$$

$V_{sp}(r)$ = volume of the initial spherical particle with the radius of r.

Scale factor α to adjust clump particle's volume was obtained through Equation (3.15).

$$\propto = \frac{r}{R} \tag{3.15}$$

The radius of each ball in the clump is scaled by the scale factor α through Equation (3.16).

$$r_s^b = \propto r_i^b \tag{3.16}$$

r_s^b = radius of the b^{th} ball in the clump particle after scaling;

r_i^b = initial radius of the b^{th} ball in the clump particle (the superscript b denotes the b^{th} ball constituting the clump).

In the clump, the relative location of each successive ball to the central ball was gained through Equation (3.17).

$$\boldsymbol{x_s^b} = \boldsymbol{x_c} + \propto (\boldsymbol{x_i^b} - \boldsymbol{x_c}) \tag{3.17}$$

$\boldsymbol{x_s^b}$ = location of the b^{th} ball in the clump particle after scaling;

$\boldsymbol{x_i^b}$ = initial relative location of the b^{th} ball in the clump particle;

$\boldsymbol{x_c}$ = centroid location of the central ball.

(Note: a symbol in bold represents a vector.)

(3) Determine the centroid location of the clump

The centroid location of the clump particle, $\boldsymbol{x^{cl}}$, was placed on the centre of the initial spherical particle, $\boldsymbol{x^{sp}}$ upon replacement (Equation 3.18).

$$\boldsymbol{x^{cl}} = \frac{1}{m}\sum_{b=1}^{N_b} m^b \boldsymbol{x^b} \tag{3.18}$$

N_b = number of balls to constitute the clump;

m^b = mass of the b^{th} ball;

$\boldsymbol{x^b}$ = centroid location of the b^{th} ball.

m = mass of the clump, which equals to $\sum_{b=1}^{N_b} m^b$.

Consequently, the resultant volume of the clump particle equalled to that of the initial spherical particle, and the centroid location of the clump particle was the same as that of the initial spherical particle.

Step 3: expanding the particles to achieve real sizes

Upon the spherical particles being replaced by clumped particles, the initial size of each particle was expanded to the practical size by 10 steps, namely the radius of each spherical ball in a clump was enlarged by $MF^{0.1}$ (i.e. scale factor $\alpha = 1.6^{0.1} \approx 1.048$) at each step. The expanding process was similar to the relevant steps of replacing initial spherical particles with clump particles: the radius of each ball in the clump was scaled through Equation (3.16), the centroid location of the central

ball in the clump, $\boldsymbol{x_c}$, was fixed, and the position of each ball in the clump can be gained through Equation (3.17). Upon each expanding, 5,000 computation cycles were conducted so as to ensure each clump was capable of being completely re-oriented. Figure 3.7 shows an example of the procedure of generating particles for a blend in a PFC3D model, in which the particle blend is composed of 50% 19.0-13.2 mm particles and 50% 13.2-9.5 mm particles by mass as indicated by the different colours.

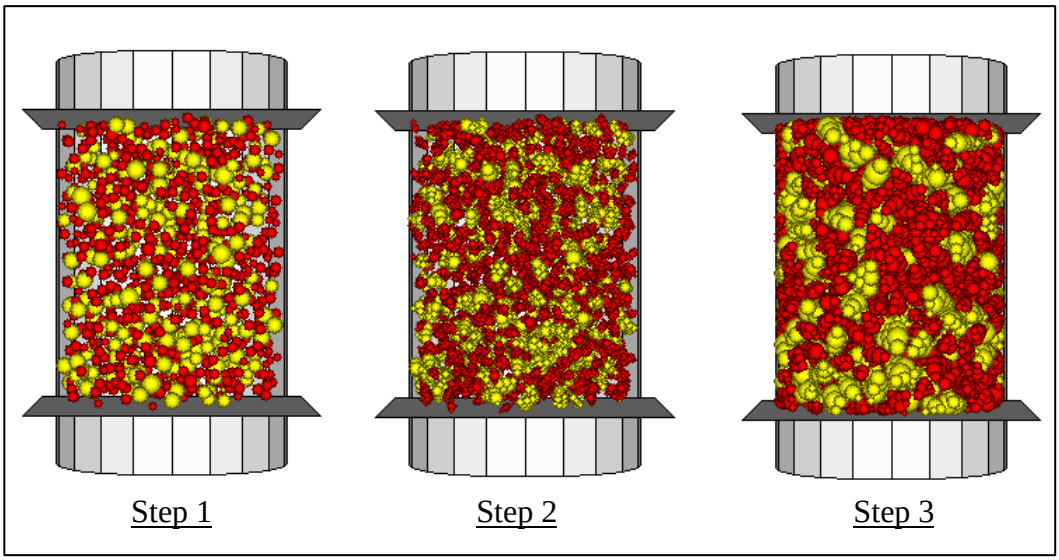

Figure 3.7 The procedure of particle generation in a PFC3D model

3.5.2 Model compaction

Calculation in DEM simulation is a dynamic process, and law of motion (Newton's second law) and force-displacement law are implemented alternately through a time-stepping algorithm. A numerical 'servo-control' mechanism, which is capable of producing a desired stress state in an assembly via adjusting the movement of bottom and top plates, was utilised in this research to obtain a compacted assembly of particles. The servo-control algorithm is given in Equations (3.19) and (3.20), which was compiled via FISH function provided by PFC3D (Itasca 2008). The compaction in the simulation was regarded adequate as the assigned gravitational force was stably applied on the bottom plate.

The stress on the top/bottom plate was detected along the cycling, and the equation for plate movement in each step was obtained through Equation (3.19).

$$\dot{u}^{(w)} = G\left(\sigma^{measured} - \sigma^{required}\right) \tag{3.19}$$

$\dot{u}^{(w)}$ = wall velocity;

$\sigma^{measured}$ = measured stresses on the wall;

$\sigma^{required}$ = required stresses on the wall;

G = 'gain' parameter in servo-control process.

The maximum change in stress on the wall arising from plate movement, $\Delta\sigma^{(w)}$, in one time-step was obtained through Equation (3.20).

$$\Delta\sigma^{(w)} = \frac{k_n^{(w)} N_c \dot{u}^{(w)} \Delta t}{A} \tag{3.20}$$

$k_n^{(w)}$ = average stiffness of the contacts between particles and top/bottom plate;

N_c = number of contacts;

Δt = one time-step;

A = area of top/bottom plate.

The absolute changing value in plate stress was lowered through a relaxation factor, α, for the concern in stability, which is shown in Equation (3.21).

$$\left|\Delta\sigma^{(w)}\right| < \alpha|\Delta\sigma| \tag{3.21}$$

Substituting Equations (3.19) and (3.20) into Equation (3.21) yields Equation (3.22).

$$\frac{k_n^{(w)} N_c G|\Delta\sigma|\Delta t}{A} < \alpha|\Delta\sigma| \tag{3.22}$$

Meanwhile, the 'gain' parameter, *G*, can be determined through Equation (3.23).

$$G = \frac{\alpha A}{k_n^{(w)} N_c \Delta t} \tag{3.23}$$

Hence, in each cycle, top and bottom plates were moved by applying the velocity gained in Equation (3.19), in which *G* was determined through Equation (3.23). Consequently, the assigned gravitational force was applied on the particles in a stable manner via the 'servo-control' mechanism. Thereby, this 'servo-control' procedure allows particles in the PFC3D model to achieve a stable particle-to-particle framework with complete re-orientation.

A linear model was applied as contact model, simulating the behaviour at a contact. Subsequently, the contact stiffness of two entities, including normal stiffness, k^n, and shear stiffness, k^s, can be described by Equations (3.24) and (3.25), respectively (Itasca 2008). In this research, two types of contacts were involved, namely clump-to-clump and clump-to-wall. Figures 3.8 and 3.9 show the sketches of ball-to-ball contact and ball-to-wall contact, respectively.

$$k^n = \frac{k_n^{[A]} \times k_n^{[B]}}{k_n^{[A]} + k_n^{[B]}} \tag{3.24}$$

k^n = normal stiffness;
$k_n^{[A]}$ = normal stiffness of entity *A*;
$k_n^{[B]}$ = normal stiffness of entity *B*.

$$k^s = \frac{k_s^{[A]} \times k_s^{[B]}}{k_s^{[A]} + k_s^{[B]}} \tag{3.25}$$

k^s = shear stiffness;
$k_s^{[A]}$ = shear stiffness of entity *A*;
$k_s^{[B]}$ = shear stiffness of entity *B*.

In addition, the stiffness at contact in PFC3D can be obtained from the linkage with aggregate's physical properties. Two contacting balls are assumed as an elastic beam, and contact stiffness can be derived from Equations (3.26) ~ (3.28).

$$L = 2\tilde{R} = R^{[A]} + R^{[B]} \tag{3.26}$$

L = length of the assumed beam composed by two contacted balls, *A* and *B*;

$\tilde{R}$ = average radius of the two balls;

$R^{[A]}$, $R^{[B]}$ = radius of ball *A* and ball *B*, respectively.

$$k_n^{[p]} = \frac{ES}{L} = EL \tag{3.27}$$

$k_n^{[p]}$ = normal stiffness at contact;

E = material's Young's modulus;

S = cross-sectional area of the assumed beam, which equals to L^2.

$$k_s^{[p]} = \frac{12IG}{L^3} = GL \tag{3.28}$$

$k_s^{[p]}$ = shear stiffness at contact;

G = material's shear modulus;

I = cross-sectional inertia of the assumed beam, which equals to $L^4/12$.

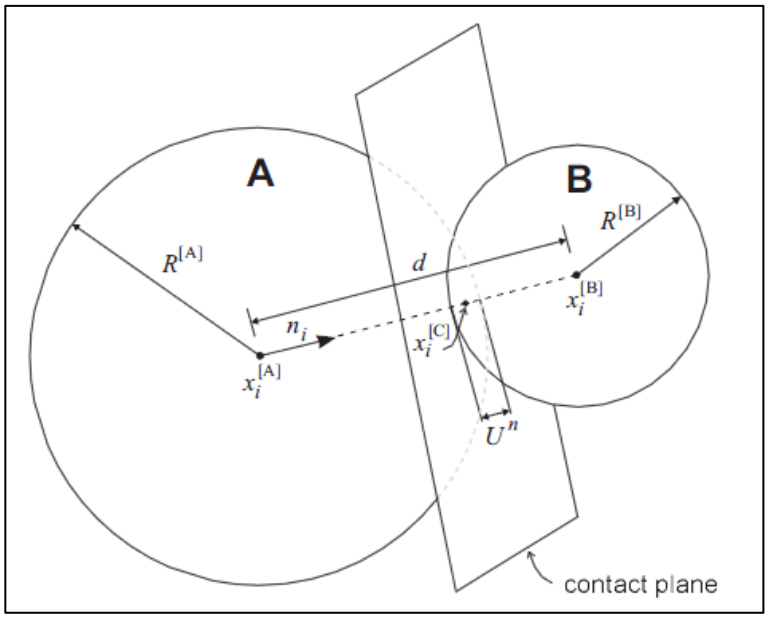

Figure 3.8 Sketch of ball-to-ball contact in PFC3D (Itasca 2008)

Note: $R^{[A]}$ and $R^{[B]}$ denote the radii of entity *A* and entity *B*, respectively; $x_i^{[A]}$ and $x_i^{[B]}$ denote the position vectors of centres of entity *A* and entity *B*, respectively; $x_i^{[C]}$ denotes the position vector of

contact point; d denotes the distance between the centres of entity *A* and entity *B*; $U^{[n]}$ denotes the overlap between entity *A* and entity *B*, and n_i denotes the unit normal of the contact plane.

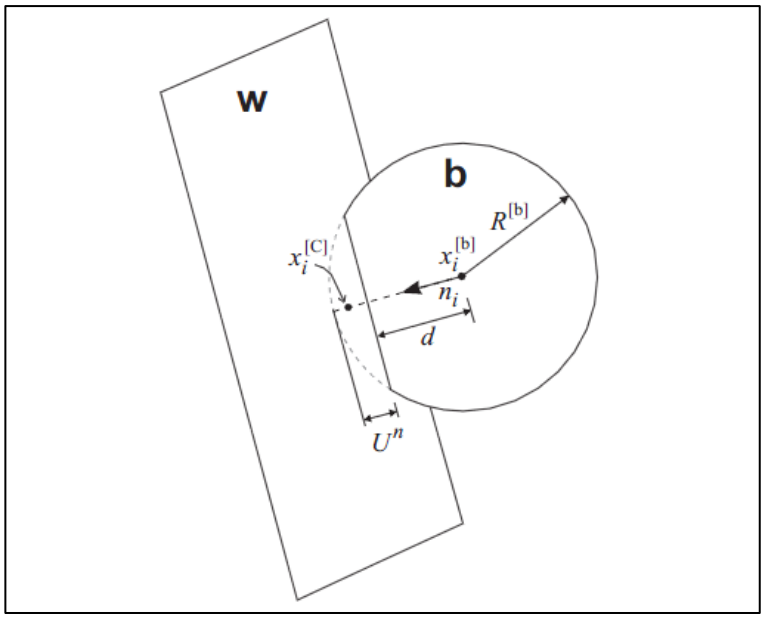

Figure 3.9 Sketch of ball-to-wall contact in PFC3D (Itasca 2008)

Note: $R^{[b]}$ denotes the radius of ball; d denotes the vertical distance between the wall and the centre of ball; and the remaining symbols possess the similar meanings as that shown in Figure 3.8.

Slip behaviour was described through the coefficient of friction, μ. Slip is allowed to occur upon shear force at a contact, F_i^s, being larger than the maximum allowable shear contact force, F_{max}^s, and subsequently F_i^s is set as F_{max}^s in next calculation cycle, as given in Equations (3.29) and (3.30).

$$F_{max}^s = \mu \times F_i^n \tag{3.29}$$

F_i^n = normal force at the contact.

$$F_i^s \leftarrow F_{max}^s \tag{3.30}$$

3.5.3 Simulation parameters

Simulation parameters, which were set to assess the state of compacted assembly of particles in PFC3D model, were traced and recorded along iterations.

(a) Porosity (*n*)

Porosity, denoted as *n*, is defined as the ratio of voids within an assembly of particles by volume, and it can be obtained through Equation (3.31). It should be noted that porosity is a direct simulation parameter to relate to the voids content that was measured in the laboratory.

$$n = \frac{V_{void}}{V_{con}} = 1 - \frac{V_{mat}}{V_{con}} \tag{3.31}$$

V_{void} = volume of the voids in the container;

V_{con} = volume of the container;

V_{mat} = volume of the materials in the container.

(b) Mean coordination number (MCN)

Mean coordination number (MCN) is the mean number of effective contacts around each particle, which can be gained through Equation (3.32), and an effective contact means a particle-to-particle contact carrying nonzero normal force.

$$MCN = \frac{1}{N_p}\left(\sum_{Np} n_c^{(p)}\right) \tag{3.32}$$

N_p = number of the particles in the container;

$n_c^{(p)}$ = number of efficient contacts around each particle.

3.6 Summary

In this chapter, the raw materials (i.e. mineral aggregates and asphalt binder) used in this research and relevant properties are introduced. Compaction method is stated as well. Laboratory tests for PAM's volumetric parameters and performance properties are introduced, while the details related to particular research issues are given in the corresponding chapter later on. On the other hand, the numerical simulation method, DEM, was selected to evaluate the packing condition in PAM, which was achieved

by an application software, PFC3D. The detailed procedures to establish PFC3D are presented.

The experiment design and relevant results from laboratory measurements and DEM simulation shall be discussed in the following chapters. Chapter 4 covers the impacts of design factors, including aggregate gradation (G), gyration compaction level (GCL), and asphalt binder type (ABT), on PAM's fundamental properties. The development of packing structure in PAMs shall be examined by means of both laboratory measurement and DEM simulation in Chapter 5. Based on the findings in earlier chapters, potential PAMs for the specific application, namely low-strength pavement application (i.e. pedestrian/cyclist paths) in Singapore, are designed in Chapter 6, and resultant properties of designed PAMs are evaluated, including volumetric parameters, permeability, mixture strength and aggregate interlocking. In terms of the two major issues in PAM, namely ravelling and clogging, specific experiments were designed and relevant results are analysed in Chapter 7.

Chapter 4 Impacts of design factors on PAM's properties

4.1 Introduction

PAMs' fundamental properties, including air voids content, permeability, strength, resistance to abrasion, moisture susceptibility, and ageing susceptibility etc., are attributed to many factors, such as material selection, aggregate gradation design, and compaction method etc. Thereby proper asphalt mixture design should be carried out so as to achieve the expected functions of PAM for the specific application.

The impact of three critical design factors, namely aggregate gradation (G), gyration compaction level (GCL), and asphalt binder type (ABT), on PAM's properties are investigated as reported in this chapter. Open-graded design is a distinctive feature for PAM, resulting in extraordinarily high air voids content in PAM and contributing to the excellent performance in drainage. Packing condition in PAM is influenced by the gyration compaction level as well, which is controlled by the compaction parameters (gyration compaction in this case), such as compaction pressure and gyration count. In terms of asphalt binder, it affects asphalt mixture's properties in many aspects, such as mixture strength and durability. Meanwhile, asphalt binder plays a role of lubrication in mixture compaction and hence affects the packing condition in the PAM as well.

On the whole, 8 aggregate gradations, 3 gyration compaction levels, and 2 asphalt binders, were selected, resulting in a total of 48 PAM designs. A series of basic experiments, as described in Chapter 3, have been conducted to evaluate the properties of PAMs with design factors at different levels.

4.2 Design factors in PAMs

4.2.1 Aggregate gradation

Aggregate gradation is extremely important to the PAM's properties, given that PAM's functional performance in drainage is directly related to the distinctive open-graded design. In fact, aggregate packing in PAM is mostly established by the stone-on-stone framework by coarse aggregates with the fine fraction in limited amount to fill the air voids created by the coarse ones.

Most design methods of aggregate gradation, such as Fuller's maximum density curve and Bailey method, are based on dense asphalt mixtures, aimed at obtaining the ideal aggregate gradation for maximising density (Fuller and Thompson 1907; Vavrik et al. 2002), and they would not be suitable for open-graded design like PAMs.

In terms of breaking sieve (BS), which distinguishes the coarse and fine aggregates in an aggregate blend, it is a significant construct in aggregate gradation design. The BS of 4.75 mm is conventionally applied, and various methods to determine BS have been proposed in the development of packing theories. For example, in the Bailey method, BS is the sieve closest to the value of Nominal Maximum Aggregate Size (NAMS) multiplying 0.22, wherein 0.22 was generally regarded as the radius ratio of the coarse aggregates and the fine aggregates that can fit into the voids (Vavrik et al. 2002). Shen and Yu (2011) studied the role of particles with various sizes in a mixture via Discrete Element Method (DEM), and particles were categorised into fine fraction if functioning as reducing voids content in the model during the procedure of sequentially adding finer particles into the coarser model. Additionally, Waterson et al. (2004) suggested BS as the one below which the gradation curve started to flatten out based on slope. On the whole, 2.36 mm and 4.75 mm are the two common BSs among the different packing theories.

In order to design a series of representative aggregate gradations for PAM, uniform design method was applied herein, which was developed based on the theories of 'number-theoretical method' and 'quasi Monte-Carlo method', it being able to substantially reduce the required number of experiments (Fang and Ma 2001).

Table 4.1 PAM gradations in several countries

sieve size (mm)	countries and terminologies for PAM									
	U.S.	Japan		Spain		Switzerland	New Zealand		Australia	Singapore
	NCAT	NMAS-13 mm	NMAS-20 mm	P-12	PA-12	DRA11	PA 10	PA 14	OGA	LTA-PA
25.4			100							
19	100	100	95-100	100	100			100	100	100
16						100	100	85-100		
13.2		92-100	53-78						85-100	79-89
12.5	85-100			75-100	70-100					
11.2						90-100				
9.5	55-75	62-81	35-62	60-90	50-80		85-100	35-50	45-70	67-77
6.7									25-45	
5.6						15-40				
4.75	10-25	10-31	10-31	32-50	15-30		20-40	12-22	10-25	17-26
2.8						8-20				
2.36	5-10	10-21	10-21	10-18	10-22		5-15	5-15	7-15	13-23
1.18									6-12	
0.6		4-17	4-17	6-12	6-13				5-10	8-18
0.5						4-10				
0.3		3-12	3-12						4-8	6-12
0.15		3-8	3-8						3-7	4-10
0.09						3-5				
0.075	2-4	2-7	2-7	3-6	3-6		2-5	2-5	2-5	4-8

Table 4.1 shows the PAM gradations prescribed in several counties (Ruiz et al. 1990; Japan Highway Public Corporation 1994; Rajib et al. 2000; Drainasphaltschichten 2001; Australian Asphalt Pavement Association [AAPA] 2004; Transit New Zealand 2007; LTA 2010). The factors and corresponding levels selected in the uniform design method are given in Table 4.2. The fillers content was selected as 5% and the fines within the size range of 2.36-0.075 mm were uniformly distributed. The resultant eight PAM aggregate gradation designs, denoted as G1~G8, were arranged in ascending order by the content of passing 2.36 mm sieve aggregates and thence passing 4.75 mm sieve aggregates, as given in Table 4.3. Additionally, it should be noted that there was no fines of 2.36-0.075 mm in G1 and G2 PAM groups given that the percentage of aggregates passing 2.36 mm sieve equalled to that passing 0.075 mm.

Table 4.2 Factors and levels in uniform design for PAM gradations

factor	level
passing 13.2 mm (%)	80, 85, 90, 95
passing 6.3 mm (%)	30, 40, 50, 60
passing 2.36 mm (%)	5, 10, 15, 20
ratio (9.5 mm-6.3 mm)/(13.2 mm-6.3 mm)	0.2, 0.4, 0.6, 0.8
ratio (4.75 mm-2.36 mm)/(6.3 mm-2.36 mm)	0.2, 0.4, 0.6, 0.8

Table 4.3 PAM gradations by uniform design method

sieve size, mm	passing, % by mass							
	G1	G2	G3	G4	G5	G6	G7	G8
19.0	100	100	100	100	100	100	100	100
13.2	80	90	85	95	90	80	95	85
9.5	74	54	70	59	66	72	51	75
6.3	50	30	60	50	30	40	40	60
4.75	14	20	30	42	21	35	24	44
2.36	5	5	10	10	15	15	20	20
1.18	5	5	9	9	13	13	17	17
0.6	5	5	8	8	11	11	14	14
0.3	5	5	7	7	9	9	11	11
0.15	5	5	6	6	7	7	8	8
0.075	5	5	5	5	5	5	5	5

Upon the determination of aggregate gradation, asphalt binder content for each PAM was determined based on aggregate surface area according to AI method (AI 1997). The empirical formula to estimate the surface area (SA) of aggregates in a blend (m^2/kg) and estimated binder content (EBC) are given in Equations (4.1) and (4.2), and the selected thickness of asphalt binder film (t) is 10 μm. EBC values were used with the underlying assumption of the same asphalt film thickness, so as to avoid the effect of different asphalt film thickness. The resultant EBC values for designed aggregate gradations are given in Table 4.4.

$$SA = 0.41 + 0.41a + 0.82b + 1.64c + 2.87d + 6.14e + 12.29f + 32.77g \quad (4.1)$$

$a, b, c \sim g$ = percentages by mass of aggregates passing 4.75 mm, 2.36 mm, 1.18 mm, 0.6 mm, 0.3 mm, 0.15 mm, and 0.075 mm sieves, respectively.

$$EBC = SA \times t \quad (4.2)$$

Table 4.4 EBC values for designed aggregate gradations

G	EBC (%)
G1	3.3
G2	3.4
G3	3.8
G4	3.9
G5	4.2
G6	4.3
G7	4.7
G8	4.8

4.2.2 Gyration compaction level

Packing condition in PAM is affected by compaction method as well. Higher air voids content in PAM can be obtained by reduced compaction level, which can be achieved by decreased compaction pressure or lower gyration count, albeit at the expense of weaker mixture structure (Suresha 2009).

Three gyration compaction levels were applied to achieve different packing conditions in this research, denoted as P600_N50, P300_N100, and P300_N50,

respectively (Table 4.5), while P600_N50 is a standard configuration according to Superpave design method with compaction pressure of 600 kPa and 50 gyration counts (AI 1996). Considering the low-strength pavement application in view and PAM's core function of drainage, a compaction pressure of 300 kPa was applied in order to increase the air voids content and enhance drainage function, and two gyration counts of 100 and 50 were selected for P300_N100 and P300_N50, respectively.

Table 4.5 Compaction parameters for three gyration levels

gyration level	compaction pressure (kPa)	gyration count	gyratory angle (^{0})	gyration rate (rpm)
P600_N50	600	50	1.25	30
P300_N100	300	100		
P300_N50	300	50		

4.2.3 Asphalt binder type

Asphalt binder type can heavily influence asphalt mixture's properties, such as on the aspects of mechanical performance, anti-ageing performance, and anti-moisture performance. Moreover, it relates to the lubrication effect among mixed aggregates in the process of compaction, thereby affecting the packing in compacted asphalt mixture (Zulkati et al. 2012a). Two types of asphalt binder, namely neat asphalt binder (Pen 60/70) and modified asphalt binder (PG 76) with Styrene Butadiene Styrene (SBS), were applied to assess the effect on PAM's performance. In addition, 2% hydrated lime was added into Pen 60/70 asphalt to improve stripping resistance.

Table 4.6 Design factors for PAMs

design factor	aggregate gradation	gyration compaction level	asphalt binder type
abbreviation	G	GCL	ABT
level	G1~G8	P600_N50 P300_N100 P300_N50	Pen 60/70 PG 76

Altogether eight aggregate gradations, three gyration compaction levels, and two asphalt binder types were selected (Table 4.6). Subsequently a total of 48 PAM designs were studied. The three design factors of aggregate gradation, gyration compaction level, and asphalt binder type were denoted as G, GCL, and ABT, respectively.

4.3 Volumetric properties

A total of 3 uncompacted specimens and 15 compacted specimens were fabricated for each of the 48 PAM designs at selected asphalt binder content. For each PAM design, volumetric properties were measured based on nine replicated PAM specimens, which were subsequently used for permeability test, unconditioned and moisture-conditioned Marshall tests, and ITSM test. In addition, given that ITSM test is non-destructive, the specimens used in unconditioned ITSM test were subsequently applied in moisture-conditioned ITSM test. The average values of bulk gravity, G_{mb}, total air voids (TAV) content, and water-accessible air voids (WAAV) content, are given in Tables 4.7 and 4.8.

Table 4.7 Bulk gravity of the PAMs

G	ABT	GCL		
		P600_N50	P300_N100	P300_N50
G1	Pen 60/70	1.846	1.778	1.743
	PG 76	1.872	1.817	1.784
G2	Pen 60/70	1.890	1.815	1.800
	PG 76	1.888	1.835	1.791
G3	Pen 60/70	1.944	1.897	1.869
	PG 76	1.988	1.930	1.880
G4	Pen 60/70	1.975	1.924	1.872
	PG 76	2.003	1.954	1.926
G5	Pen 60/70	2.028	1.953	1.910
	PG 76	2.047	1.999	1.958
G6	Pen 60/70	2.062	2.010	1.971
	PG 76	2.079	2.034	1.993
G7	Pen 60/70	2.108	2.065	2.023
	PG 76	2.153	2.107	2.042
G8	Pen 60/70	2.134	2.092	2.049
	PG 76	2.146	2.127	2.071

It can be seen that air voids content, both TAV and WAAV, can be affected by any of the three design factors, namely aggregate gradation (G), gyration compaction level (GCL), and asphalt binder type (ABT). Regarding aggregate gradation, air voids content approximately linearly increased with the reduction in passing 2.36 mm aggregates content for each combination of the three gyration compaction levels and the two asphalt binder types (Figures 4.1~4.4). For example, G1 and G2 PAMs, which possessed the lowest content of passing 2.36 mm aggregates among the eight aggregate gradations, namely 5% fillers and no 2.36-0.075 mm aggregates, showed the highest TAV and WAAV contents, whilst the highest content of passing 2.36 mm aggregates in G7 and G8 PAMs (i.e. 20%) contributed to the relatively densest mixture structure, being reflected in the highest G_{mb} values, and the lowest TAV and WAAV contents.

Table 4.8 Air voids content of the PAMs

G	ABT	TAV (%)			WAAV (%)		
		P600_ N50	P300_ N100	P300_ N50	P600_ N50	P300_ N100	P300_ N50
G1	Pen 60/70	26.2	28.7	30.3	20.2	24.3	24.8
	PG 76	25.0	27.0	28.3	18.8	21.4	23.3
G2	Pen 60/70	24.3	27.4	28.0	18.2	22.4	22.7
	PG 76	24.3	26.2	28.0	18.1	21.0	23.2
G3	Pen 60/70	21.5	23.4	24.6	14.9	17.3	18.3
	PG 76	19.1	21.5	23.9	12.4	14.7	17.5
G4	Pen 60/70	20.2	22.2	24.4	13.4	16.0	18.1
	PG 76	18.6	20.5	21.7	12.3	13.9	15.4
G5	Pen 60/70	18.5	21.0	22.6	12.6	16.0	17.3
	PG 76	16.0	18.2	19.5	11.3	12.4	14.3
G6	Pen 60/70	16.0	18.0	19.6	10.5	12.4	14.0
	PG 76	14.1	16.2	18.7	9.7	11.4	12.9
G7	Pen 60/70	13.6	15.4	17.1	9.6	11.1	12.2
	PG 76	11.6	13.0	16.4	8.1	9.0	11.1
G8	Pen 60/70	12.6	14.3	16.1	7.9	8.9	10.4
	PG 76	11.7	12.3	14.9	7.2	7.9	8.9

Meanwhile, it should be noted that asphalt binder content increased with the content of passing 2.36 mm aggregate, since it was determined based on the same thickness of asphalt film. Hence, voids content created by open-gradations in the PAMs could

be further occupied by the higher asphalt mastic content as well as the higher fine aggregate content. On the other hand, both TAV and WAAV contents in designed PAMs appeared to decrease as the content of passing 4.75 mm aggregates increased in some cases (Figures 4.5~4.8), indicating the effect of passing 4.75 mm aggregates in partially separating the stone-on-stone backbone of coarser aggregates and rearranging the voids structure. Notably, in G4 and G8 PAMs, in which the content of passing 4.75 mm aggregates were similar, namely 42% and 44%, respectively, the differences in TAV and WAAV contents were relatively large, which were in the ranges of 6.8-8.3%, and 5.1-7.7%, respectively. This can be attributed to the differences in 4.75-2.36 mm aggregates contents, which were 32% and 24% in G4 and G8 PAMs, respectively, indicating the air voids generated by aggregates larger than 4.75 mm can be fitted in better by passing 2.36 mm aggregates than 4.75-2.36 mm aggregates. This also partially explains the differences in air voids contents between G2 and G5, in which the contents of passing 4.75 mm aggregates were similar as well, namely 20% and 21%, respectively, while the differences in TAV and WAAV contents were in the ranges of 5.4%-8.5% and 5.4%-8.9%, respectively.

Among the three gyration compaction levels, at each aggregate gradation and asphalt binder type, P600_N50 had the most harsh gyration level which also produced the most compact mixture given the highest G_{mb} value (Table 4.7), followed by P300_N100, and P300_N50. Hence, as compared to fabricating PAM at lower compaction pressure (i.e. P=300 kPa) and reference gyration count (i.e. N=50), a denser specimen was achieved from applying higher pressure (i.e. P=600 kPa) or increased gyration count (i.e. N=100), and the effect of increased pressure was more prominent than having half compaction pressure but double the compaction counts. On the aspect of asphalt binder type, it showed that denser specimens were obtained in the case of PG 76 asphalt binder as compared to Pen 60/70 asphalt binder, with PG 76 asphalt binder giving higher bulk densities of compacted specimens and lower air voids contents (i.e. both TAV and WAAV contents). For the two kinds of air voids content, an approximately linear relationship was observed between TAV and WAAV contents (Figure 4.9).

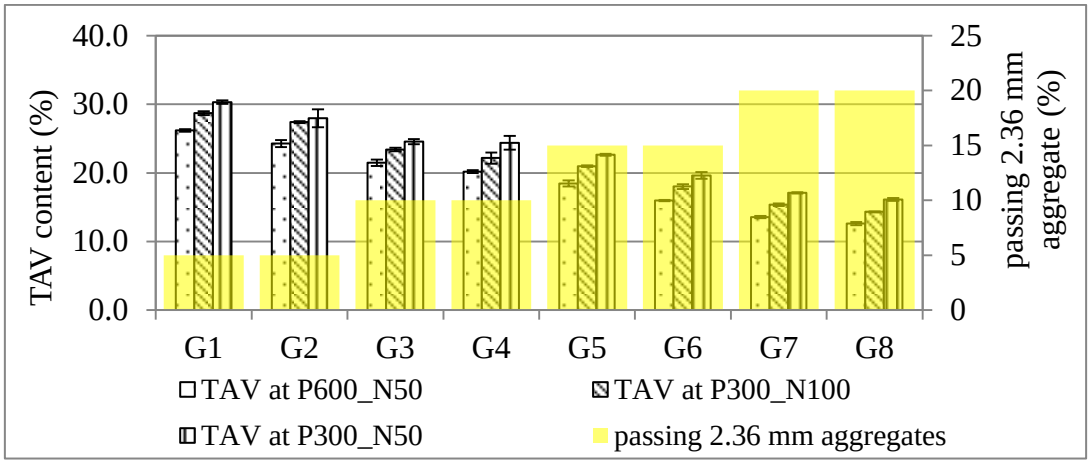

Note: the bar on each column refers to standard deviation

Figure 4.1 Relationship between TAV content and passing 2.36 mm aggregates content among PAM designs of Pen 60/70 asphalt binder

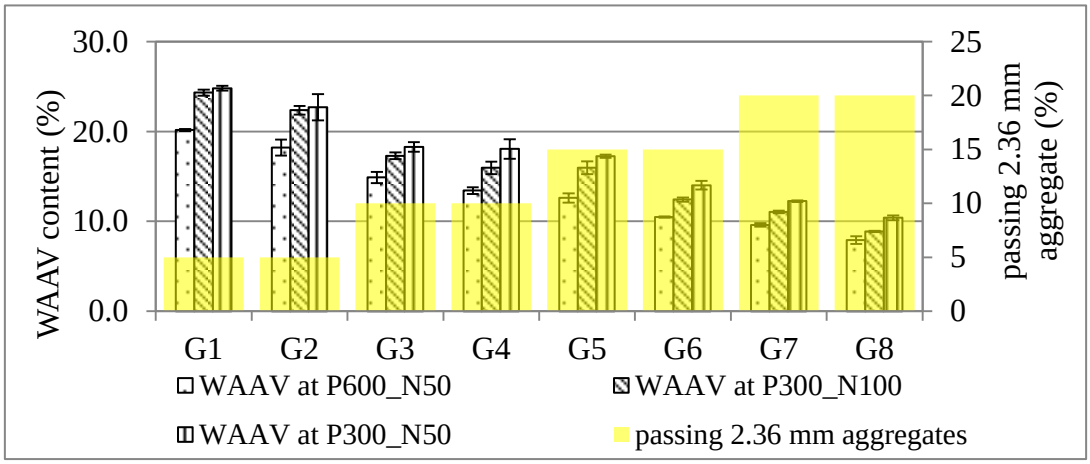

Figure 4.2 Relationship between WAAV content and passing 2.36 mm aggregates content among PAM designs of Pen 60/70 asphalt binder

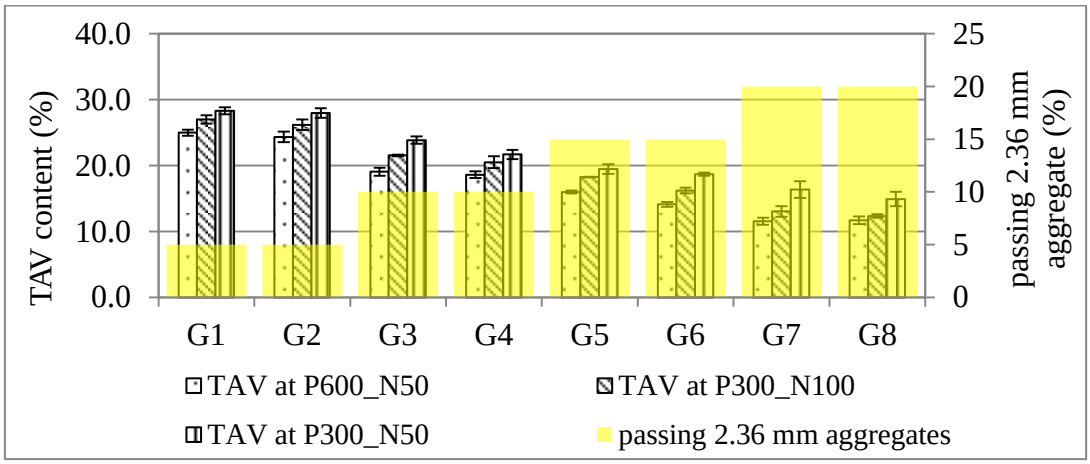

Figure 4.3 Relationship between TAV content and passing 2.36 mm aggregates content among PAM designs of PG 76 asphalt binder

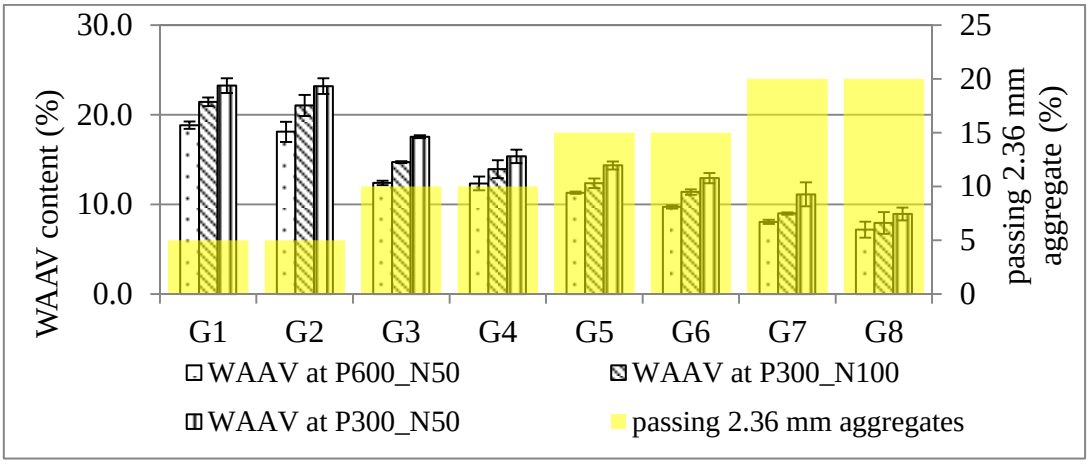

Figure 4.4 Relationship between WAAV content and passing 2.36 mm aggregates content among PAM designs of PG 76 asphalt binder

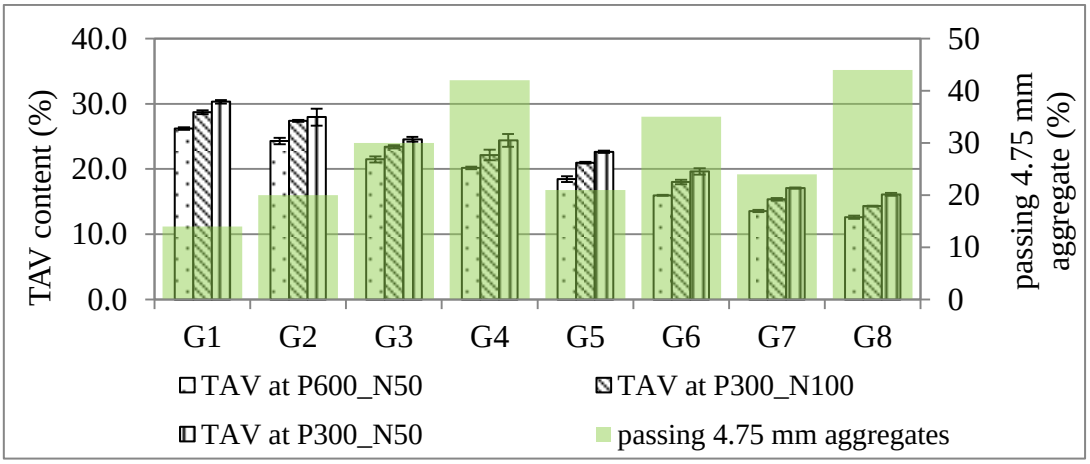

Figure 4.5 Relationship between TAV content and passing 4.75 mm aggregates content among PAM designs of Pen 60/70 asphalt binder

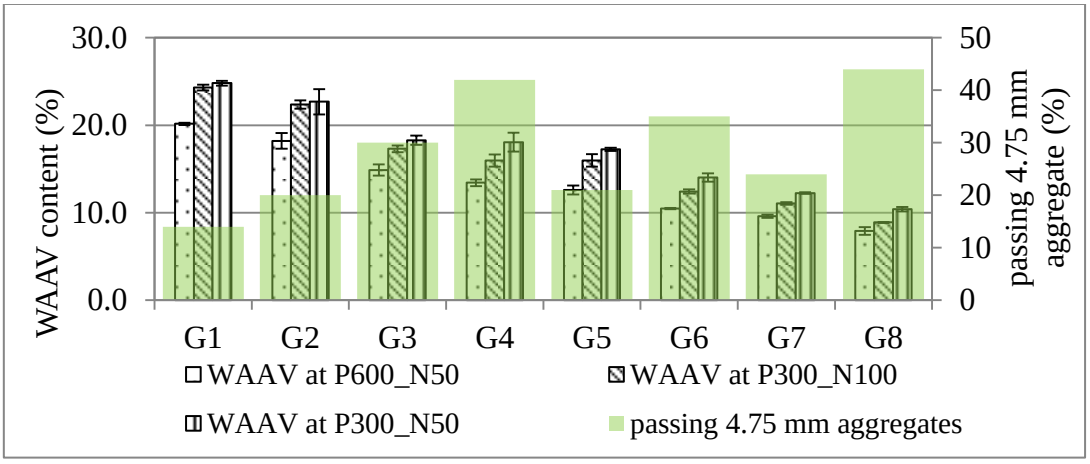

Figure 4.6 Relationship between WAAV content and passing 4.75 mm aggregates content among PAM designs of Pen 60/70 asphalt binder

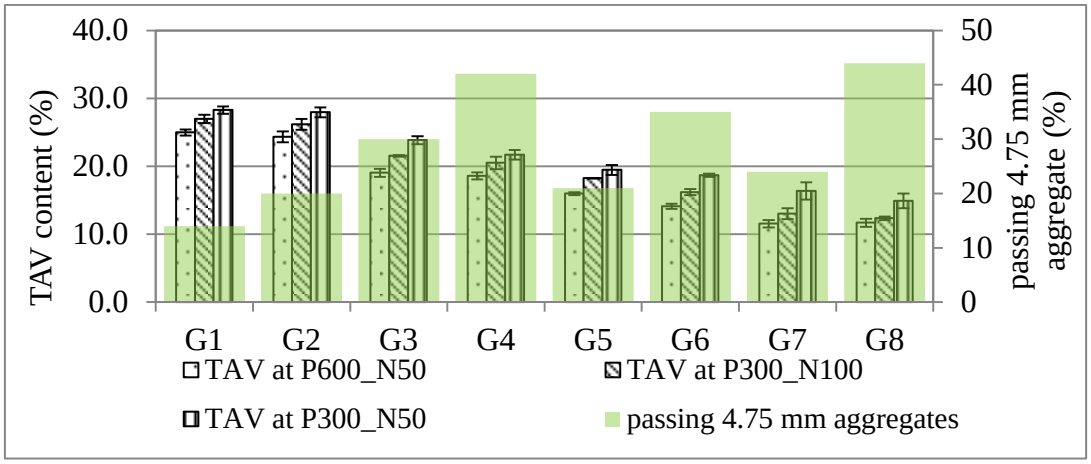

Figure 4.7 Relationship between TAV content and passing 4.75 mm aggregates content among PAM designs of PG 76 asphalt binder

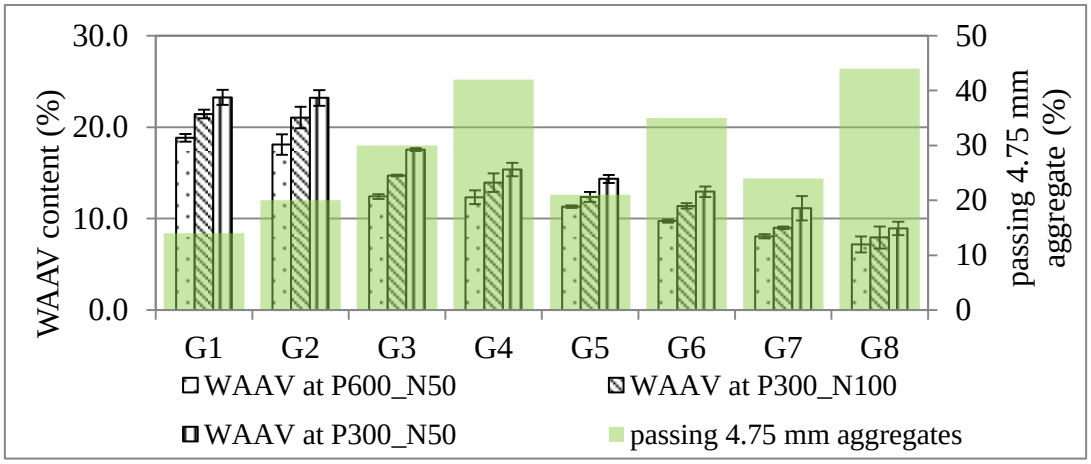

Figure 4.8 Relationship between WAAV content and passing 4.75 mm aggregates content among PAM designs of PG 76 asphalt binder

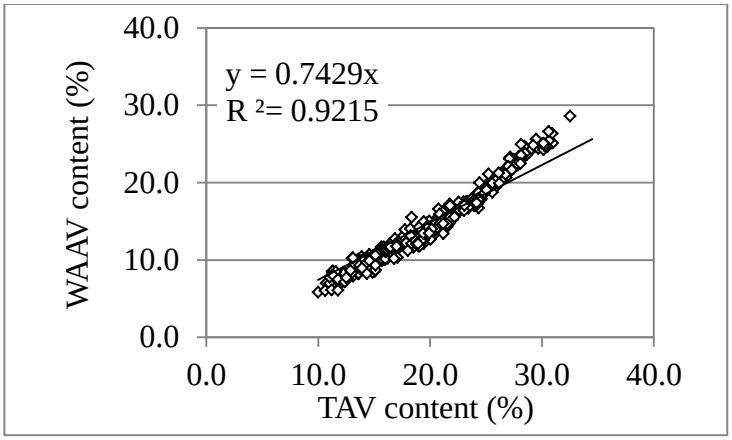

Figure 4.9 Relationship between WAAV and TAV contents

4.4 Draindown test

In draindown test, there was no obvious asphalt mastic drained down for the eight aggregate gradations with designated asphalt binder contents using either of the two types of asphalt binder. It was probably due to the relatively low asphalt binder contents, and hence draindown was not an issue herein.

4.5 Cantabro abrasion test

To assess PAMs' capability in resisting abrasion, Cantabro abrasion test was conducted, and ageing-conditioned Cantabro abrasion test was carried out to estimate the retained abrasion resistance after high-temperature conditioning (Figures 4.10 and 4.11). The results corresponding to the two kinds of Cantabro abrasion tests are shown as unconditioned Abrasion Loss Value (UC-ALV) and ageing-conditioned Abrasion Loss Value (AC-ALV). It was found that Cantabro abrasion loss was dependent on aggregate gradation, gyration compaction level, and asphalt binder type.

PAMs possessing lower content of passing 2.36 mm aggregates showed weaker resistance to abrasion in Cantabro abrasion test. Especially, for G1 and G2 PAMs, whose contents of passing 2.36 mm aggregates were lowest in the eight gradation designs (i.e. 5%), specimens fabricated at low gyration compaction level were severely disintegrated after experiencing 300 gyrations in LA abrasion machine, and hence the relevant ALVs are vacant in Figures 4.10 and 4.11, including UC-ALV and AC-ALV values for G1 of Pen 60/70 asphalt binder at P300_N100 and P300_N50, UC-ALV and AC-ALV values for G2 of Pen 60/70 asphalt binder at P300_N50, UC-ALV value for G1 of PG 76 asphalt binder at P300_N50 , and UC-ALV value for G2 of PG 76 asphalt binder at P300_N50.

Moreover, for each aggregate gradation, higher resistance to abrasion in Cantabro abrasion test was obtained for applying higher gyration compaction level, which was probably due to the resultant better compacted condition. On the whole, in both cases of Pen 60/70 and PG76 asphalt binders, G7 and G8 PAMs at P600_N50 showed lowest UC-ALV and AC-ALV values, which was strongly attributed to the

relatively highest compacted mixture, namely with the highest content of passing 2.36 mm aggregates (i.e. 20%) and highest gyration compaction level.

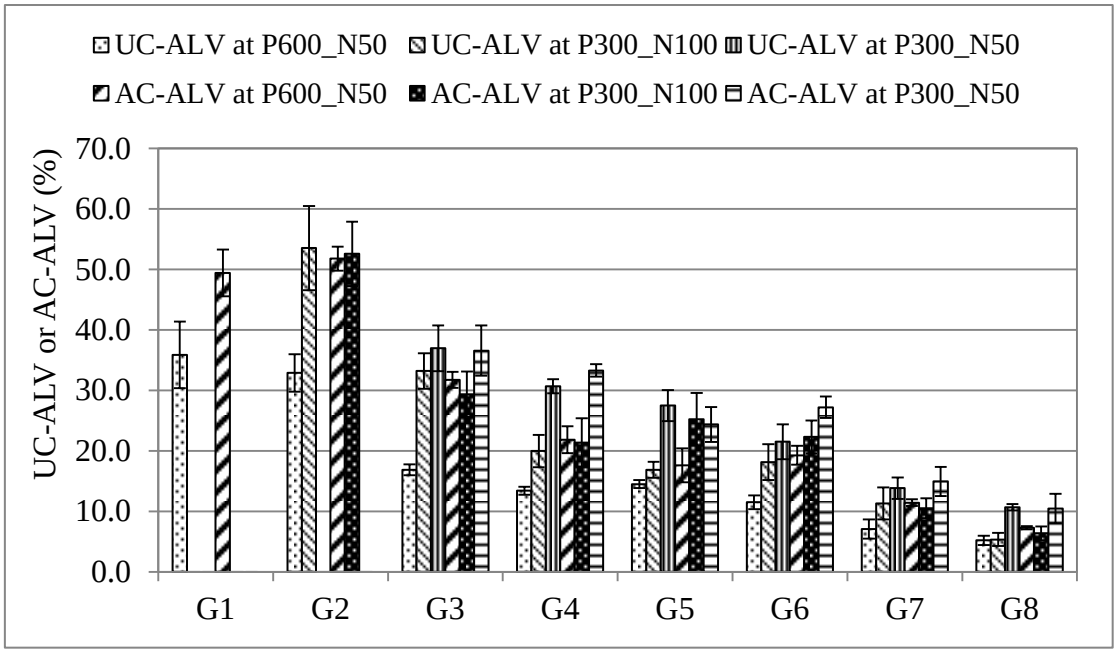

Figure 4.10 Results of Cantabro abrasion test for PAM designs with Pen 60/70 asphalt binder

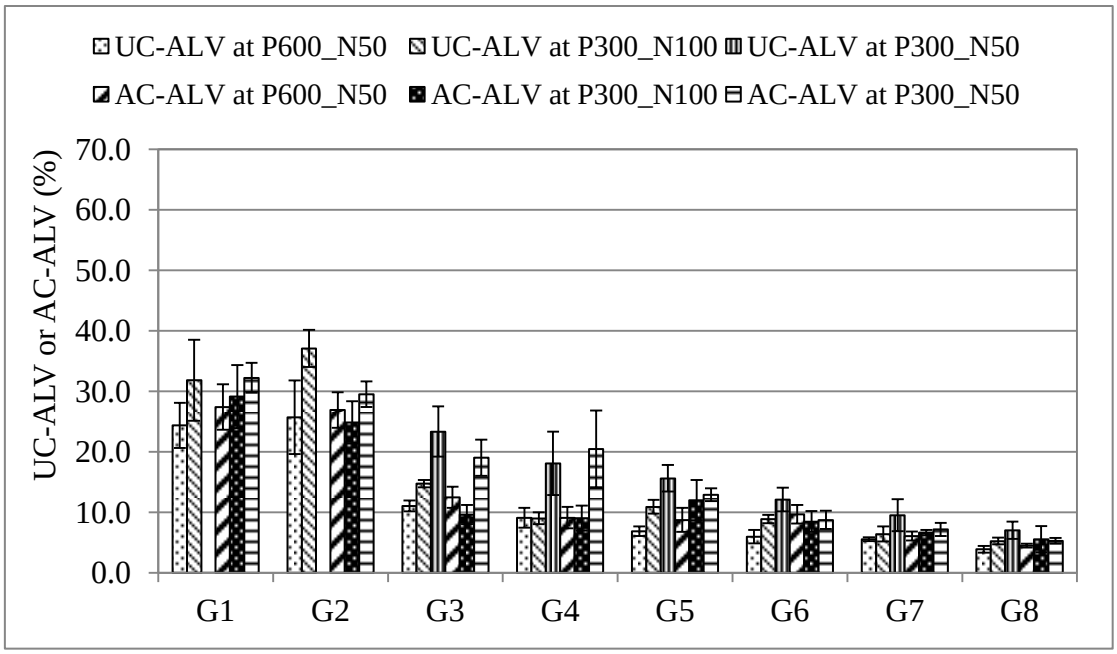

Figure 4.11 Results of Cantabro abrasion test for PAM designs with PG76 asphalt binder

Regarding asphalt binder type, utilising PG 76 asphalt binder can obviously enhance PAMs' resistance in both unconditioned and ageing-conditioned Cantabro

abrasion tests. In the case of Pen 60/70 asphalt binder, only G7 and G8 PAMs at various gyration levels could meet the common requirement in ALV, namely ALVs of less than 20% and 30% for unconditioned and ageing-conditioned tests, respectively. On the other hand, for PAMs with PG 76 asphalt, the corresponding UC-ALV and AC-ALV values to each gradation design and gyration compaction level were largely reduced.

Furthermore, in the case of PAMs with Pen 60/70 asphalt binder at P600_N50 gyration compaction level, AC-ALV was clearly larger than UC-ALV for each gradation design, and the increase was in the range of 120-190%. It could be attributed to the weakened cohesiveness of Pen 60/70 asphalt binder under high temperature condition and the relatively stronger mixture generated by higher gyration compaction level was harshly impaired due to the cohesiveness loss. However, a similar phenomenon did not occur in the case of PG 76 asphalt binder, and the two kinds of Cantabro losses, namely UC-AVL and AC-ALV, were comparable for each aggregate gradation design at various gyration compaction levels. It indicated PG 76 asphalt binder's capability in rendering better resistance against ageing degradation under high-temperature condition.

Given that ravelling is a critical issue for PAM, Cantabro abrasion test is widely used to assess PAMs' durability. However, it was found that this test cannot appropriately well reflect abrasion loss on the surface of asphalt mixture as in the field condition, since damage in the Cantabro abrasion test is caused by impact effect between compacted specimen and the rigid inside-wall of the LA abrasion machine, which is much more severe than abrasion effect in the field (Dong et al. 2013). Thus, for low-strength pavement application, Pen 60/70 asphalt binder is acceptable, and PAMs of relatively lower packing levels, such as G3 and G4 PAMs at P300_N50, are recommended so as to obtain relatively higher air voids contents while the Cantabro abrasion losses would not be extremely large as that found in G1 and G2 PAMs with Pen 60/70 asphalt binder. In motorways, conventional requirements in Cantabro abrasion tests must be met for adequate quality, thus PG 76 asphalt binder is recommended and aggregate gradations generating large air voids contents (e.g. G1 and G2 PAMs) are not appropriate. In addition, a higher

content of asphalt binder can also be used to enhance PAM's performance under Cantabro abrasion test.

4.6 Permeability test

PAMs' performance in permeability was measured through coefficient of permeability, *k* (Tables 4.9 and 4.10). Clearly, less well compacted specimens, which could be achieved by lower gyration compaction level and/or less content of passing 2.36 mm aggregates, showed higher *k* value. Moreover, for each aggregate gradation at each gyration compaction level, PAM with PG 76 asphalt possessed slightly lower *k* value as compared to the one with Pen 60/70 asphalt, which agreed with the volumetric measurements (Table 4.8), namely PG 76 asphalt binder produced denser PAMs than Pen 60/70 asphalt binder.

Table 4.9 Coefficients of permeability for PAMs with Pen 60/70 asphalt binber

G	gyration level		
	P600_N50	P300_N100	P300_N50
G1	198.8 (±5.6)	266.1 (±8.6)	280.7 (±14.6)
G2	130.2 (±9.8)	244.5 (±17.5)	238.1 (±58.0)
G3	87.1 (±9.1)	153.9 (±8.5)	179.7 (±4.8)
G4	64.6 (±5.0)	121.2 (±2.8)	141.4 (±18.0)
G5	35.2 (±1.9)	92.1 (±9.3)	110.6 (±1.9)
G6	21.6 (±4.2)	48.9 (±6.4)	61.9 (±12.6)
G7	7.2 (±0.2)	21.5 (±5.9)	34.0 (±4.5)
G8	5.3 (±0.2)	13.3 (±2.3)	28.4 (±5.5)

Table 4.10 Coefficients of permeability for PAMs with PG 76 asphalt binder

G	gyration level		
	P600_N50	P300_N100	P300_N50
G1	169.0 (±2.3)	253.6 (±11.4)	264.6 (±14.6)
G2	150.8 (±9.8)	214.4 (±8.0)	253.9 (±28.6)
G3	70.0 (±3.7)	122.5 (±5.2)	166.7 (±2.0)
G4	62.8 (±31.6)	105.7 (±21.9)	132.5 (±22.0)
G5	34.6 (±4.9)	77.8 (±23.4)	116.1 (±4.1)
G6	19.3 (±1.7)	46.0 (±9.3)	77.1 (±10.7)
G7	3.6 (±2.3)	15.4 (±2.0)	44.8 (±8.4)
G8	4.8 (±1.2)	7.5 (±0.4)	20.1 (±0.5)

PAM's permeability performance increased with both kinds of air voids contents, namely TAV and WAAV contents (Figures 4.12 and 4.13). There was no obvious trend that WAAV content showed stronger correlation with permeability than TAV content as stated by some research (Mansour and Putman 2013), which was probably due to WAAV content being approximately linearly related with TAV content (Figure 4.9).

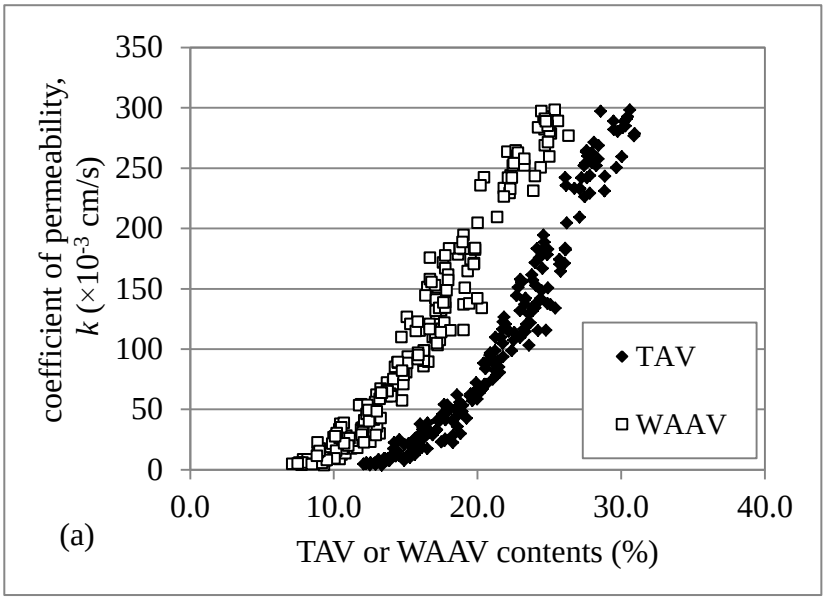

Figure 4.12 Relationship between permeability and air voids content for PAM designs with Pen 60/70 asphalt binder

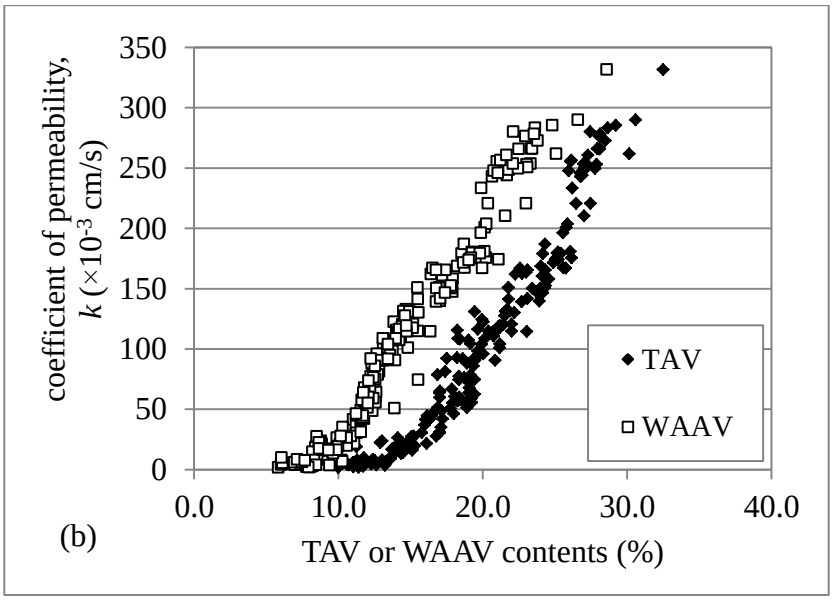

Figure 4.13 Relationship between permeability and air voids content for PAM designs with PG 76 asphalt binder

According to ASTM (2008), coefficient of permeability, *k*, greater than 116 ($\times 10^{-3}$ cm/s) is recommended for PAMs. As a tropical country, the required permeability is raised to be 130 ($\times 10^{-3}$ cm/s) to comparably counter the extremely high rainfall intensity in Singapore (NEA 2014). Hence, a higher limit in permeability performance should be better suited for Singapore's situation, and *k* value greater than 130 ($\times 10^{-3}$ cm/s) is suggested herein to assist in storm water management.

Based on the regression equations between TAV content and coefficient of permeability, *k*, as shown in Equations (4.3) and (4.4) for PAMs with Pen 60/70 asphalt and PG 76 asphalt, respectively, it was found that TAV contents greater than 23.3% and 22.0% for PAMs using Pen 60/70 asphalt and PG 76 asphalt, respectively, are required to achieve adequate permeability (i.e. higher than 130 $\times 10^{-3}$ cm/s). Therefore, in terms of permeability, G1~G4 PAMs are potentially suitable designs for Singapore's application, and a lower gyration compaction level (i.e. P300_N50) are required in G3 and G4 PAMs.

$$y = 0.6911x^2 - 12.597x + 49.147 \quad \text{(Pen 60/70)} \tag{4.3}$$

$$y = 0.5165x^2 - 5.0111x - 10.436 \quad \text{(PG 76)} \tag{4.4}$$

y = cofficient of permeability, *k*, 10^{-3} cm/s;

x = TAV content, %.

4.7 Marshall test

Two kinds of Marshall tests were conducted on designed PAMs, namely unconditioned and moisture-conditioned Marshall tests, and the results are given as unconditioned Marshall stability (UC-MS) and moisture-conditioned Marshall stability (MC-MS), respectively (Figures 4.14 and 4.15). It was found that MS was strongly related to aggregate gradation design for PAMs, and it increased with the augmentation in passing 2.36 mm aggregates content for all gyration compaction levels and both asphalt binder types. For example, G7 and G8 PAMs possessed relatively highest MS values at various gyration compaction levels, while G1 and G2 specimens with Pen 60/70 asphalt binder fabricated at lower gyration

compaction levels (i.e. P300_N50 and P300_N100) were broken during water bath conditioning before loading.

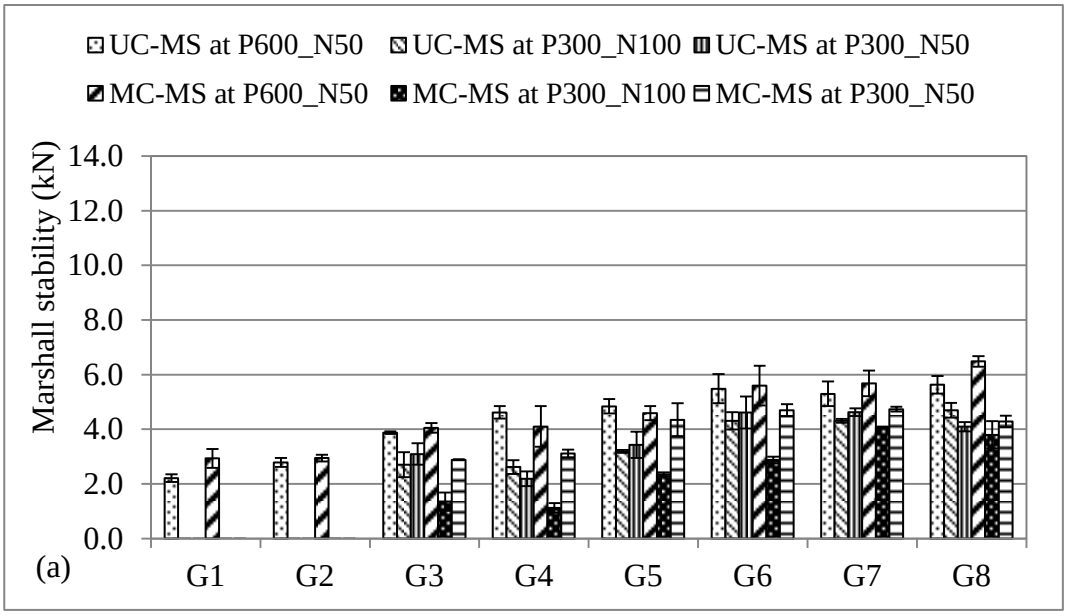

Figure 4.14 Results of Marshall test PAMs with Pen 60/70 asphalt binder

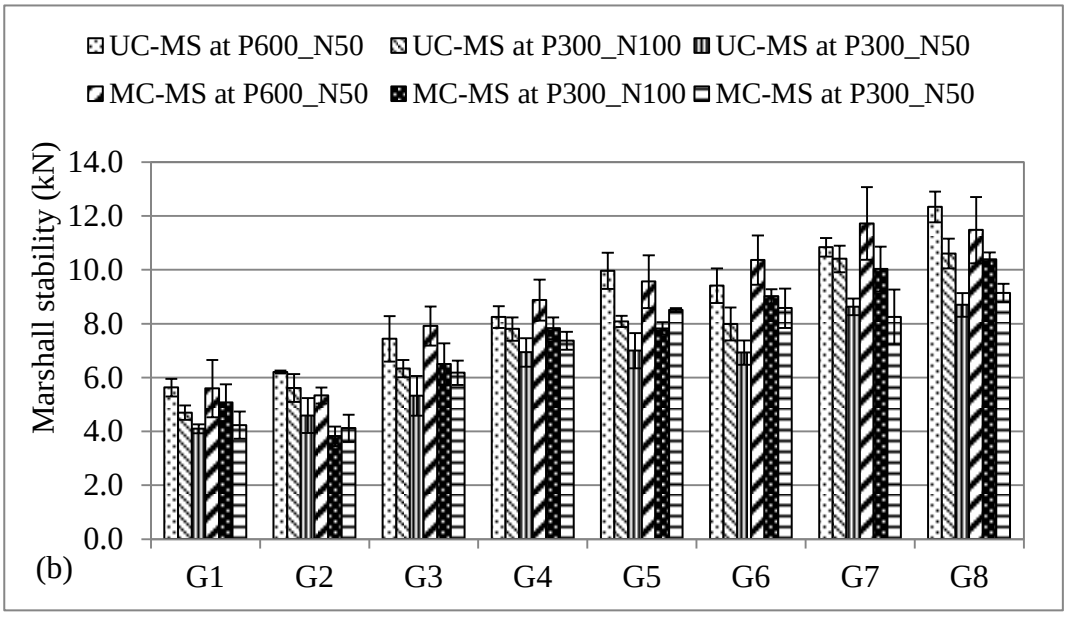

Figure 4.15 Results of Marshall test PAMs with PG 76 asphalt binder

Regarding gyration compaction level, in the cases of PG 76 asphalt binder, for most aggregate gradation designs (except G2 and G5 PAMs in moisture-conditioned cases), a higher gyration compaction level generated higher MS values, which can be attributed to the better compacted structure. However, in the cases of Pen 60/70 asphalt binder, specimens fabricated at gyration compaction level of P300_N100

generally showed lower MS than the ones at gyration level of P300_N50 (except G4 and G8 PAMs in unconditioned cases). This suggests that breakage might occur in PAM specimens during the compaction after 50 gyration counts at the compaction pressure of 300 kN. Moreover, PAMs' strength was greatly enhanced when using PG 76 asphalt binder for all the eight aggregate gradations at various gyration compaction levels, as compared to Pen 60/70 asphalt binder, even when 2% hydrated lime was used for anti-stripping function in the latter case.

For the different packing conditions that resulted from the various combinations of aggregate gradations, gyration compaction levels and asphalt binder types, UC-MS values were generally reduced with the increase in TAV contents (Figure 4.16). The regression equations between TAV content and UC-MS are given in Equations (4.5) and (4.6), corresponding to PAMs with Pen 60/70 asphalt and PG76 asphalt, respectively.

$$y = -0.2349x + 8.5417 \text{ (Pen 60/70)} \quad (4.5)$$

$$y = -0.3912x + 15.365 \text{ (PG 76)} \quad (4.6)$$

y = UC-MS, kN;

x = TAV content, %.

For application in motorways, asphalt mixture possessing a UC-MS value that is no lower than 9.0 kN is required in Singapore (LTA 2010). Thus, modified asphalt binder such as PG 76 asphalt binder is necessary. Meanwhile, according to Equation (4.6), PAMs with TAV content lower than 16.3% is suggested to ensure adequate mixture strength. Herein, G5~G8 PAMs had potential application on motorways while lower gyration compaction levels were not sufficient for some cases, including P300_N100 and P300_N50 for G5 and G6 PAMs, and P300_N50 for G7 and G8 PAMs.

For low-strength pavement application, the lower limit in UC-MS can be decreased to 4.0 kN (AAPA 2002), which enables the utilisation of Pen 60/70 asphalt binder in PAMs for the cases of TAV content less than 19.3%, such as G5 and G6 PAMs at reference gyration compaction level (i.e. P600_N50). On the other hand, in using

PG 76 asphalt, almost all the designed PAMs can meet the requirement in UC-MS for low-strength pavement application and a higher TAV content is allowed to achieve higher permeability, such as G1 and G2 PAMs at lower gyration level, e.g. P300_N50.

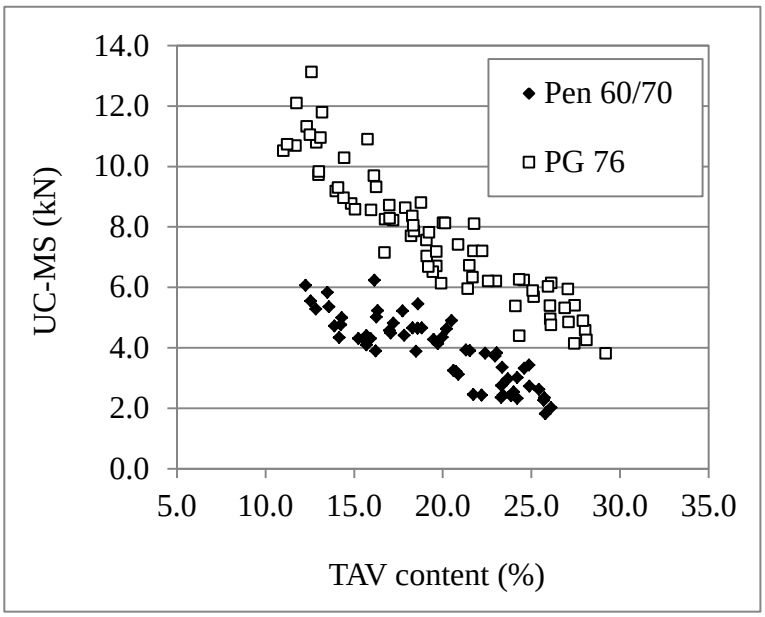

Figure 4.16 Relationship between UC-MS and TAV content

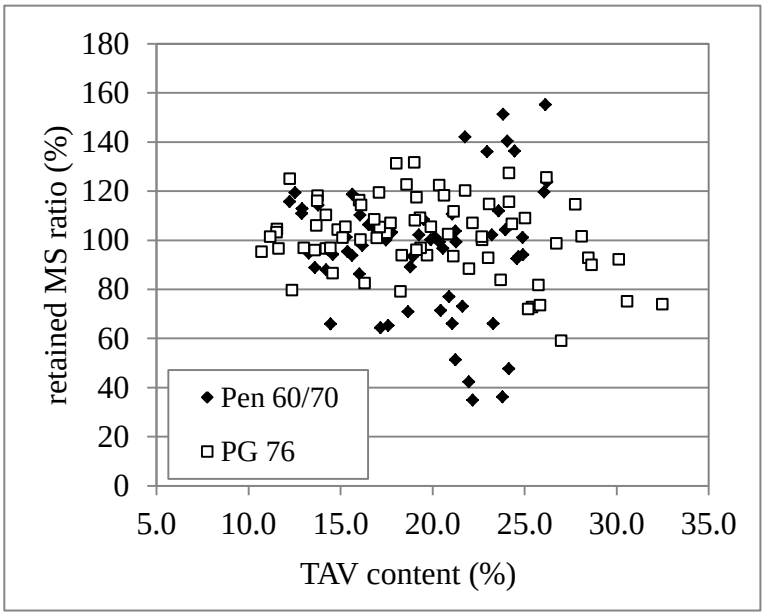

Figure 4.17 Relationship between retained MS ratio and TAV content

On the aspects of retained MS ratio (namely the ratio of MC-MS and UC-MS by percentage), for PAMs of Pen 60/70 asphalt binder, retained MS ratios were greater

than 60% for TAV content less than 20%; while for PAMs of PG 76 asphalt binder, retained MS ratios of greater than 80% were generally found for TAV content less than 25% (Figure 4.17), which indicated PG 76 asphalt binder's stronger resistance to moisture degradation than Pen 60/70 asphalt binder.

4.8 ITSM test

Unconditioned and moisture-conditioned ITSM tests were conducted to obtain unconditioned ITSM (UC-ITSM) and moisture-conditioned ITSM (MC-ITSM) values for designed PAMs (Figures 4.18 and 4.19). The differences in the UC-ITSM and MC-ITSM values among the various PAMs, which were of various aggregate gradations and gyration compaction levels, were similar to that for UC-MS and MC-MS values, namely they increased with higher amount of 2.36 mm aggregates and higher gyration compaction level (e.g. P600_N50) which led to the highest ITSM values for each aggregate gradation design.

ITSM values of the PAMs with PG 76 asphalt binder were not distinctly improved, and were even reduced instead. Nevertheless, PG 76 asphalt binder did show strong adhesiveness and the PAMs did not break during 24-hour moisture-conditioning, which occurred in the PAMs with large voids content (i.e. G1 and G2 PAMs) that used Pen 60/70 asphalt binder.

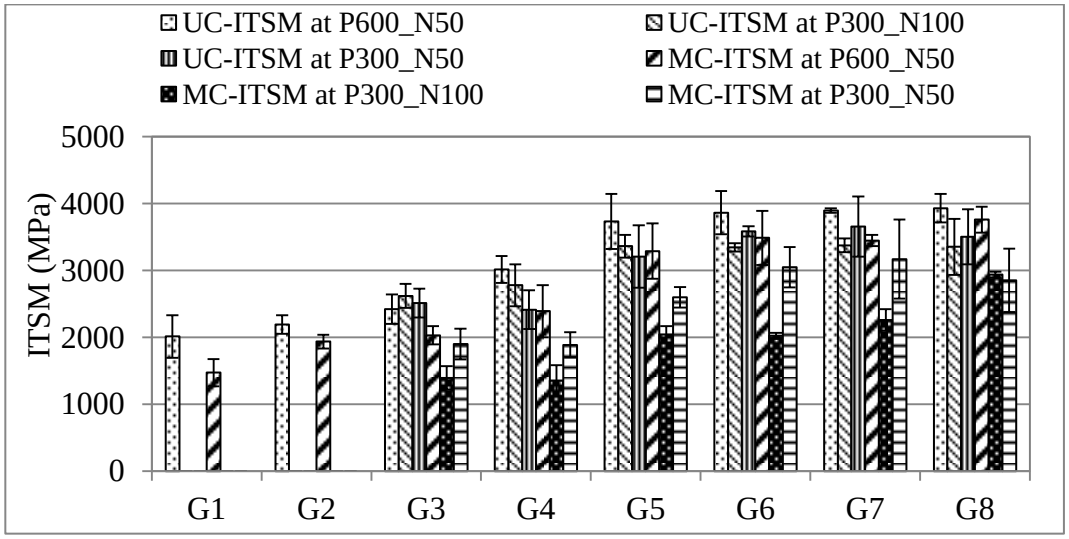

Figure 4.18 Results of ITSM test PAMs with Pen 60/70 asphalt binder

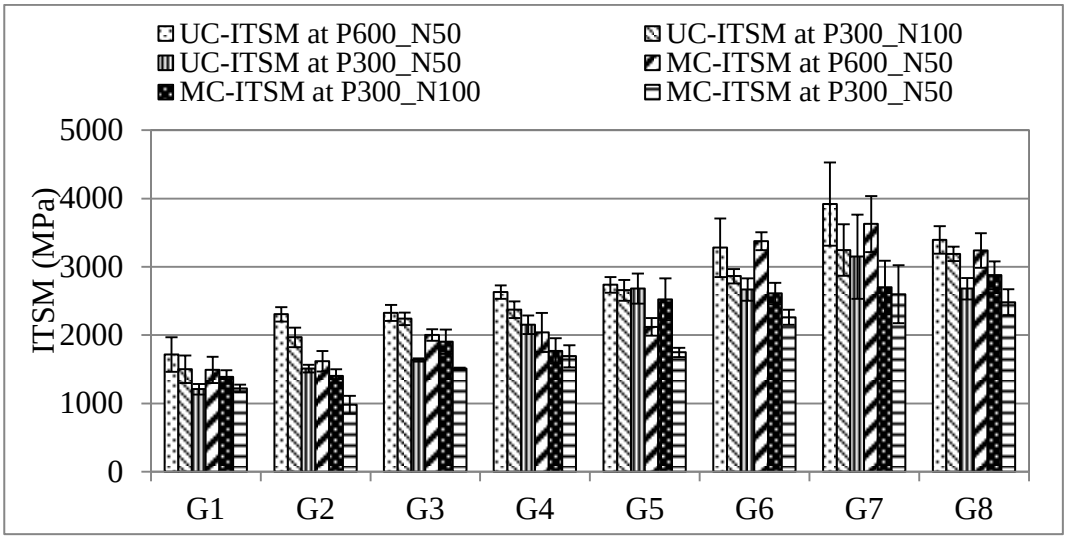

Figure 4.19 Results of ITSM test PAMs with PG 76 asphalt binder

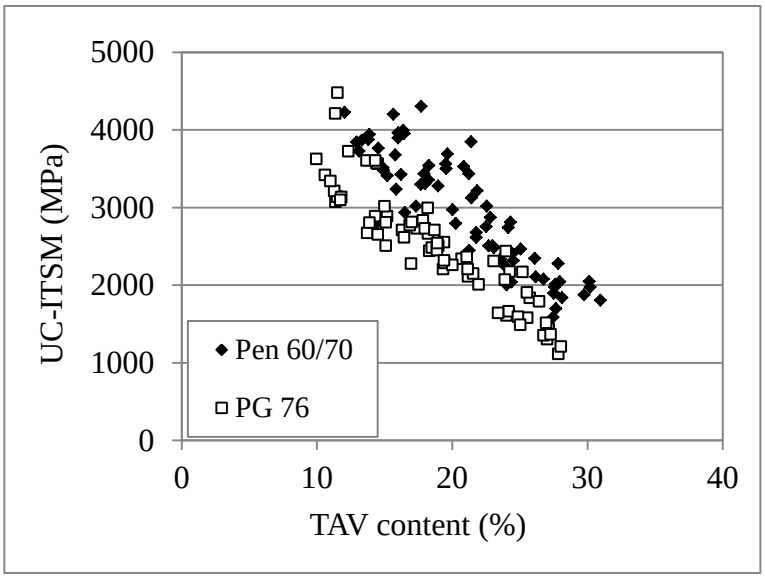

Figure 4.20 Relationship between UC-ITSM and TAV content

In term of air voids content, UC-ITSM decreased with TAV content (Figure 4.20), and there is no distinct relationship between TAV content and retained ITSM ratio (e.g. the ratio between MC-ITSM and UC-ITSM in percentage) (Figure 4.21). In both cases of Pen 60/70 and PG 76 asphalt binders, retained ITSM ratios were generally greater than 80% when TAV content was less than 15%. For PAMs of PG 76 asphalt binder, almost all the specimens possessed retained ITSM ratios higher than 60%, while in the case of Pen 60/70 asphalt binder, retained ITSM ratios lower than 60% occurred when TAV content was larger than 20%.

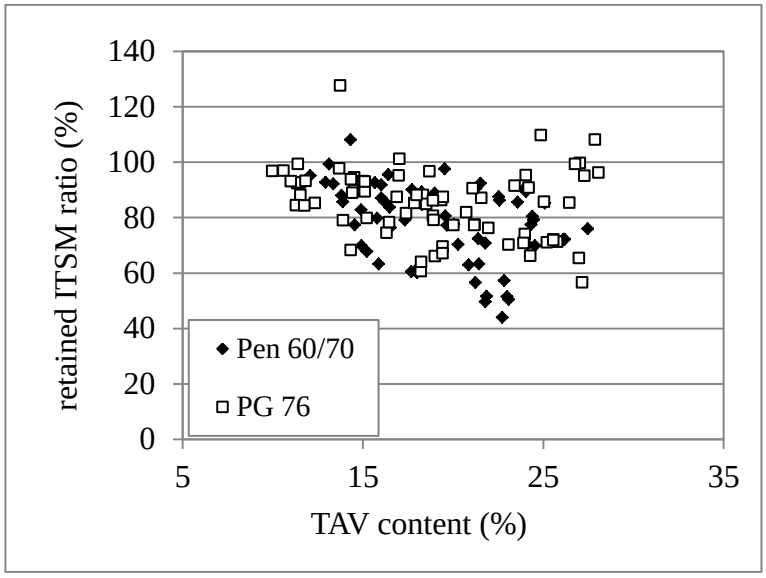

Figure 4.21 Relationship between retained ITSM ratio and TAV content

4.9 Discussion on the factors to PAM's properties

Based on the performance tests, it was found that both PAMs' essential function (e.g. permeability) and mechanical performance (e.g. Marshall stability and ITSM) were dependent on the air voids content. Furthermore, air voids content in PAM was strongly affected by the various packing conditions resulting from the design factors, namely aggregate gradation (G), gyration compaction level (GCL), and asphalt binder type (ABT). In addition, there was an approximately linear relationship between TAV and WAAV contents.

Thereby, the effects of the main design factors and the interactions (i.e. three two-factor interactions and one three-factor interaction) on the response variable (TAV) were evaluated by means of Analysis of Variance (ANOVA) test (Walpole et al. 1998). A three-factor model with full interaction was calculated, and the basic formula is given in Equation (4.7).

$$y_{ijkm} = \mu + \alpha_i + \beta_j + \gamma_k + (\alpha\beta)_{ij} + (\alpha\gamma)_{ik} + (\beta\gamma)_{jk} + (\alpha\beta\gamma)_{ijk} + \varepsilon_{ijk} \quad (4.7)$$

y_{ijkm} = the m^{th} observation of response variable in the case of the i^{th} α, j^{th} β, and k^{th} γ, and α, β, *and* γ represent the three main factors, namely G, GCL, and ABT, respectively;

μ = mean value of response;

α_i = variation caused by the i^{th} α;

β_j = variation caused by the j^{th} β;

γ_k = variation caused by the k^{th} γ;

$(\alpha\beta)_{ij}$ = variations caused by the interactions between α and β;

$(\alpha\gamma)_{ik}$ = variations caused by the interactions between α and γ;

$(\beta\gamma)_{jk}$ = variations caused by the interactions between β and γ;

$(\alpha\beta\gamma)_{ijk}$ = variations caused by the interactions between α, β and γ;

ε_{ijk} = error term.

Herein, the null hypothesis (H_0) was that the mean value of the response variable (i.e. TAV content) remained the same despite the specific combination of three factors, and a confidence level of 95% was selected. H_0 should be accepted if resultant *F*-static (*F*) value was no greater than a threshold value of *F*-critical (F_c), which is corresponding to a *P* value larger than 0.05.

The results from ANOVA test indicated that the TAV content of designed PAMs was significantly affected by the three design factors, namely aggregate gradation (G), gradation compaction level (GCL), and asphalt binder type (ABT), and the interactions among the three factors or between any of the two factors could significantly influence TAV content as well (Table 4.11). Meanwhile, mean square (MS) value of aggregate gradation was the largest among the three main factors, followed by gyration compaction level and asphalt binder type, indicating that adjusting aggregate gradation was the most efficient way to realising required TAV value.

On the other hand, though MS value of asphalt binder type was the lowest among the three factors, indicating the relatively least effect on PAM's packing condition, using PG 76 asphalt can significantly enhance PAM's mechanical properties, such as achieving higher values of UC-MS, MC-MS, UC-ITSM, and MC_ITSM. Hence, it is feasible to achieve a PAM with specific performance (e.g. permeability and/or strength) through adjusting the packing factor(s) or selecting a proper combination of them.

Table 4.11 Results of ANOVA test for designed PAMs regarding TAV*

source of variation		df	MS	*F*	*P*
main factor	G	7	1415.32	2223.25	0.0000
	GCL	2	521.21	818.75	0.0000
	ABT	1	287.55	451.69	0.0000
two-factor interaction	G & GCL	14	1.36	2.13	0.0098
	G & ABT	7	5.99	9.4	0.0000
	GCL & ABT	2	2.22	3.49	0.0314
three-factor interaction	G & GCL & ABT	14	1.78	2.8	0.0005
residual		384	0.637	/	/

*df=degree of freedom, MS=mean square, and *F*= *F*-static value.

4.10 Summary

This chapter assessed the fundamental properties of PAM with three design factors. A total of 48 PAMs were designed at eight aggregate gradations, three gyration compaction levels, and two types of asphalt binder. The findings include:

- As a critical volumetric parameter in PAM, air voids content (both TAV and WAAV contents) was dependent on aggregate gradation, gyration compaction level, and asphalt binder type, generating different packing condition as well. Air voids content increased with the reduction in the amount of passing 2.36 mm aggregates. A constant relationship was not found between air voids content and the amount of passing 4.75 mm aggregates, which could be attributed to the effect of high content of 4.75-2.36 mm aggregates shoving apart the stone-on-stone backbone established by coarser aggregates. Meanwhile, a less dense structure in PAM can be gained by lower gyration compaction level or using Pen 60/70 asphalt binder instead of PG 76 asphalt binder.

- PAMs' performance in permeability was enhanced with the increase in air voids content, and there was no obvious trend that WAAV content possessed a stronger relationship with the coefficient of permeability, *k*, as compared to TAV content, since WAAV content was approximately linearly related to TAV content.

- PAMs containing lower content of passing 2.36 mm aggregates or compacted at lower gyration compaction level showed poorer resistance to Cantabro abrasion. Similar phenomenon occurred in Marshall test and ITSM test, except that PAMs fabricated at P300_N100 gyration compaction level might performed poorer as compared to P300_N50 (namely the even lower gyration level) for the same aggregate gradation.

- PAMs with extremely large air voids content, such as possessing TAV content greater than 25% as in G1 and G2 PAMs at low gyration compaction levels, were hardly capable in withstanding moisture-conditioning or age-conditioning, and likewise for Pen 60/70 asphalt binder, which can be improved by applying modified asphalt binder as PG 76 asphalt binder. Also, PAMs with PG 76 asphalt binder showed stronger resistance to Cantabro abrasion, higher UC-MS and MC-MS values, and higher UC-ITSM and MC-ITSM values, as compared to the PAMs with Pen 60/70 asphalt binder at the same aggregate gradation and gyration compaction level.

- PAM's properties (e.g. permeability and mechanical performance) were influenced by air voids content, and TAV content was statistically dependent on aggregate gradation, gyration compaction level, and asphalt binder type, and their interactions (i.e. the interaction among the three factors or any two of them) as well.

In terms of application, a PAM with specific properties should be designed for the particular situation. In the case of Singapore, the requirement in coefficient of permeability, *k*, is raised up to 130 ($\times 10^{-3}$ cm/s) to counter the higher rainfall. In terms of the performance in Cantabro test, ageing-conditioned Cantabro test, and Marshall test etc., different requirements should be prescribed for different traffic conditions, such as normal application (i.e. motorways) and low-strength pavement application (i.e. pedestrian and cyclist paths).

In the case of pedestrian and cyclist paths which are prospective application in this research, conventional stringent requirements in resisting Cantabro abrasion are not critical since the conventional test is much more severe than actual abrasion in the field. Given the requirement in UC-MS value and permeability performance, modified asphalt binder was suggested, and PAM's TAV content should fall in the range of 22.0-29.1% when PG76 asphalt binder was utilised. A higher air voids content can be achieved by less content of fine aggregates (e.g. G1 and G2 PAMs, which contained no 2.36-0.075 mm aggregates) and/or lower gyration compaction level. Meanwhile, modified asphalt binder was also recommended due to the desired performance of PAM specimens being capable to maintain structural integrity in the face of ageing-conditioning or moisture-conditioning.

Chapter 5 Development of packing structure in PAMs

5.1 Introduction

PAM's properties, such as voids content, strength and durability, is strongly dependent on aggregate packing. Various factors, such as aggregate gradation, gyration compaction level, and asphalt binder, can strongly influence the packing condition in PAM, among which the effect of aggregate gradation is relatively more significant based on previous investigations. Moreover, aggregate gradation is an unstructured control factor, namely it is relatively independent and can be readily modified.

Thereby, the developments of packing structure in the PAMs described in Chapter 4 are evaluated in this chapter. Coarse fraction in the aggregates is the main source in creating the skeletal backbone; on the other hand, fine aggregates are strictly controlled in PAM and their effect is filling the voids within the coarse fraction. Hence the aggregate structure generated by coarse aggregates deserves more attention. For the coarse fraction in each of the eight aggregate gradation designs, four types of aggregate blends (Blend-1~Blend-4) were prepared with the finer portion being added into the coarser aggregates stepwise. Based on the measurements in the laboratory, the interaction between finer and coarser fractions in each type of aggregate blend was evaluated.

On the other hand, DEM simulation is a potential tool which serves to analyse the particle-to-particle interaction within a compacted aggregate assembly, especially in terms of describing micro-mechanism in granular materials. Hence four types of PFC3D models (Model-1~Model-4) corresponding to the compacted aggregate blends in the laboratory were established, and the packing structure in each aggregate gradation design was further evaluated through the simulation parameter, namely coordination number.

5.2 Packing condition in unbound aggregate blends

Packing structure created by coarse aggregates is the major source for aggregate interlocking, especially with respect to PAMs in which fine aggregates account much less than coarse fraction in the aggregate gradation. Breaking sieve (BS), the sieve to differentiate coarse and fine fractions for an aggregate gradation, is commonly selected as 4.75 mm or 2.36 mm based on most packing theories. Based on the experimental results in Chapter 4, air voids content in a PAM specimen possesses a stronger correlation with the content of passing 2.36 mm aggregates as compared to that of passing 4.75 mm aggregates, being mostly due to the fact that the size of aggregates finer than 2.36 mm can fit better the voids created by the coarser fraction in the designed PAMs. Therefore it is more appropriate to regard 2.36 mm as the size of BS, and thereby the development of packing structure generated by aggregates larger than 2.36 mm, namely the coarse aggregates, was evaluated.

5.2.1 Measurement of aggregate packing in the laboratory

In the laboratory, four types of compacted aggregate blends, namely Blend-1~Blend-4 were prepared for each of the eight aggregate gradations, i.e. G1~G8, with finer fraction being added into the coarser aggregate blend consecutively (Table 5.1). The subsequent aggregate blend was finer than the previous aggregate blend due to the addition of finer aggregates, which was regarded as the finer fraction in the subsequent aggregate blend. For example, in Blend-2, finer aggregates (9.5-6.3 mm) were added into the previous Blend-1 proportionally and hereby newly added finer aggregates (9.5-6.3 mm) were regarded as finer fraction. In Blend-1, finer fraction was regarded as 13.2-9.5 mm aggregates.

Table 5.1 Four types of aggregate blend

aggregate blend	particle size range (mm)	coarser fraction (mm)	finer fraction (mm)
Blend-1	19.0-9.5	19.0-13.2	13.2-9.5
Blend-2	19.0-6.3	19.0-9.5	9.5-6.3
Blend-3	19.0-4.75	19.0-6.3	6.3-4.75
Blend-4	19.0-2.36	19.0-4.75	4.75-2.36

For each aggregate gradation design, the voids content in aggregate blend (VA_{DRC}) of the compacted aggregate blend (Blend-1~Blend-4) was measured, and four replicated trials were conducted (Table 5.2). In addition, VA_{DRC} value in the largest size range, 19.0-13.2 mm, was measured as well and it was 43.4% approximately. It can be found that VA_{DRC} value in each aggregate blend was generally reduced with finer fraction being added, meaning that finer fraction possessed the effect of reducing voids content in the coarser blend.

Table 5.2 VA_{DRC} values for the eight aggregate gradations

G	VA_{DRC} value (%)			
	Blend-1	Blend-2	Blend-3	Blend-4
G1	42.5 (±0.2)	40.9 (±0.1)	40.6 (±0.2)	40.5 (±0.1)
G2	42.8 (±0.2)	41.9 (±0.2)	41.5 (±0.3)	40.2 (±0.3)
G3	41.8 (±0.2)	41.6 (±0.2)	40.4 (±0.1)	40.0 (±0.1)
G4	43.4 (±0.1)	42.5 (±0.1)	40.7 (±0.1)	39.8 (±0.2)
G5	42.7 (±0.1)	42.2 (±0.2)	41.6 (±0.3)	41.4 (±0.3)
G6	41.9 (±0.2)	41.4 (±0.1)	40.6 (±0.1)	39.5 (±0.3)
G7	43.1 (±0.2)	42.7 (±0.4)	41.8 (±0.1)	41.1 (±0.3)
G8	42.0 (±0.3)	41.0 (±0.2)	40.4 (±0.2)	40.0 (±0.4)

There are two processes for finer fraction in an aggregate gradation to reduce the voids content: (1) interacting with coarser fraction to rearrange the stone-on-stone skeleton, and (2) filling the voids created by coarser fraction. It is commonly regarded that only fine aggregates, namely the ones passing BS (2.36 mm), can be adequately small to fill the voids in the coarser aggregate blend, hence reducing voids content by the second process.

The relationship between the amount of finer fraction and VA_{DRC} value among the four kinds of aggregate blends is shown in series of profiles in Figures 5.1~5.4 (plotted to different scales).

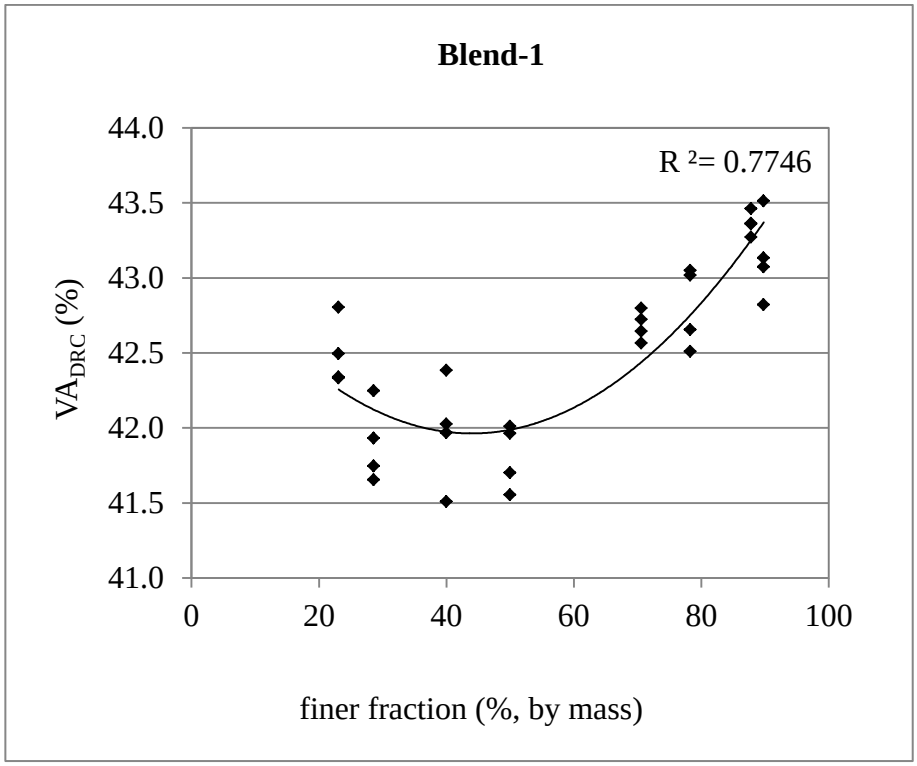

Figure 5.1 Relationship between the amount of finer fraction and VA_{DRC} value in Blend-1

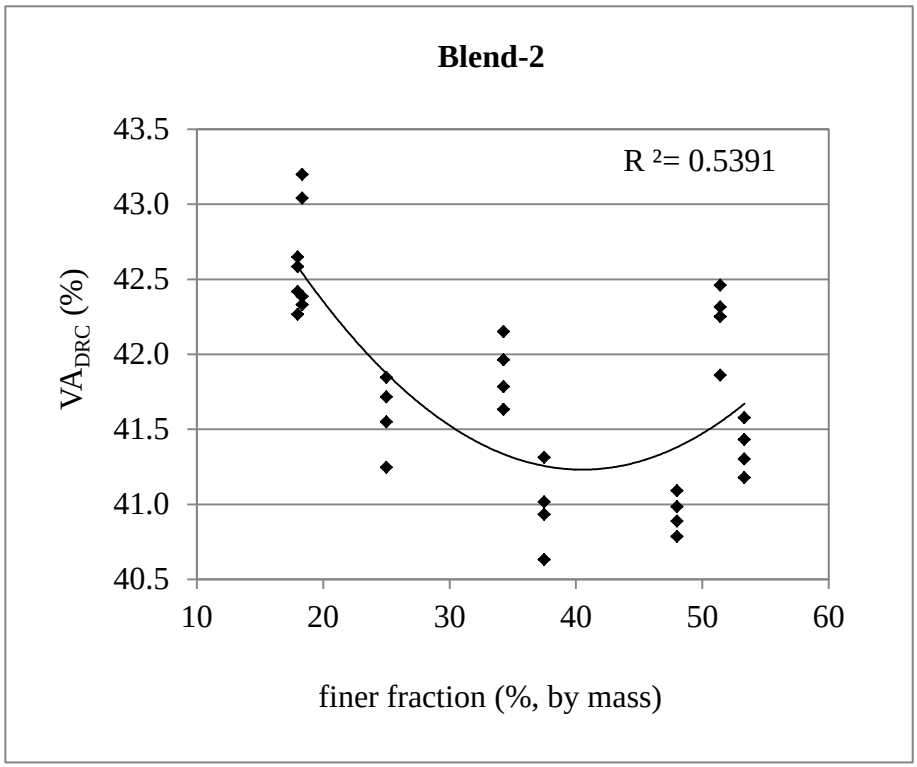

Figure 5.2 Relationship between the amount of finer fraction and VA_{DRC} value in Blend-2

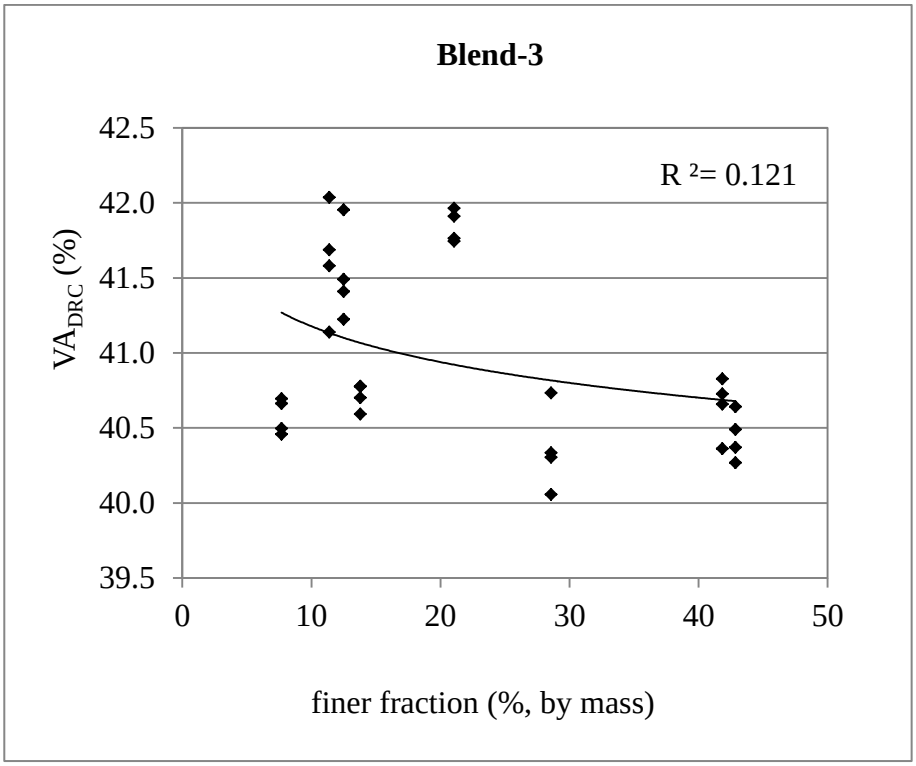

Figure 5.3Relationship between the amount of finer fraction and VA_{DRC} value in Blend-3

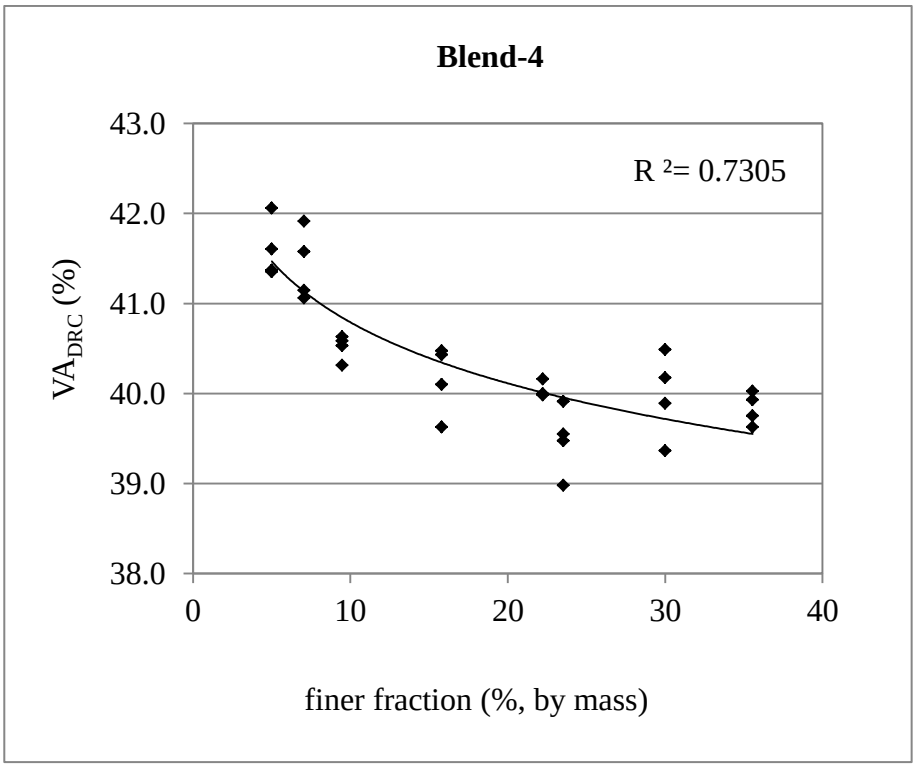

Figure 5.4Relationship between the amount of finer fraction and VA_{DRC} value in Blend-4

- In Blend-1 and Blend-2, there was an approximate quadratic polynomial relationship between the two parameters, namely as finer fraction in an aggregate blend accounted for around 42% and 40% in Blend-1 and Blend-2, respectively, the densest aggregate framework in dry-rodded condition can be realised. Meanwhile, the coefficient of regression (i.e R^2 value) in Blend-2 was much lower as compared to that for Blend-1.

- In Blend-3, the relationship between the amount of finer fraction and VA_{DRC} value was very weak, probably due to the finer fraction in this aggregate blend (i.e. 6.3-4.75 mm aggregates) functioning as 'interceptor', namely intercepting the aggregate blend from achieving the optimal framework (Vavrik et al. 2002), thereby making the effect of 6.3-4.75 mm aggregates on VA_{DRC} value uncertain.

- In Blend-4, VA_{DRC} value decreased with the increase in amount of finer fraction (i.e. 4.75-2.36 mm aggregates) until 25%, and with less distinct reduction in VA_{DRC} value with further increase in the finer fraction. This is likely due to the high amount of finer fraction partially shoving apart the stone framework established by the coarser fraction, leading to rearrangement of the stone-on-stone skeleton.

Based on most packing theories, the packing structure in a compacted aggregate blend is strongly dependent on the particles size distribution. Regarding the size of finer fraction, the diameter ratio of the finer and coarser fractions, *d_ratio*, was estimated using Equation (5.1).

$$d_{\_ratio} = \frac{d_{avg\_fr}}{d_{avg\_cr}} \tag{5.1}$$

d_{avg_fr} = the average diameter of particles in finer fraction;

d_{avg_cr} = the average diameter of particles in coarser fraction.

Additionally, the average diameter of the aggregate in an aggregate blend, d_{avg}, was estimated based on equivalent sphere, as given in Equations (5.2) and (5.3).

Herein the d_{avg} value of the aggregate within a single size range (e.g. the ith size range) can be directly obtained through v_{i_per} value (i.e. the mean volume of per aggregate in the ith size range) in Table 3.5.

$$d_{avg} = 2 \cdot \sqrt[3]{\left(\frac{3}{4} \cdot V_{avg}\right)/\pi} \tag{5.2}$$

$$V_{avg} = \frac{V}{N} = \frac{\sum V_i}{\sum n_i} = \frac{\sum M_i/den_i}{\sum M_i/m_{i\_per}} = \frac{\sum (P_i/den_i)}{\sum (P_i/m_{i\_per})} \tag{5.3}$$

V_{avg} = the average volume of one piece of aggregate in a blend;

V = the total volume of the aggregates in a blend;

N = the estimated number of aggregate pieces in a blend.

The remaining parameters possessed the similar meanings as that in Equations (3.12) and (3.13).

For each of the eight aggregate gradations, the *d_ratio* values in the four types of aggregate blends consecutively decreased with the finer fraction being added (Table 5.3). The size of fine aggregates that can fit in the voids created by coarse aggregates is directly related to the void size, which is further dependent on the size and packing manner of the coarse aggregates.

Table 5.3 Resultant *d_ratio* values in each aggregate blend

G	*d_ratio* value			
	Blend-1	Blend-2	Blend-3	Blend-4
G1	0.724	0.544	0.556	0.535
G2		0.644	0.541	0.427
G3		0.597	0.500	0.529
G4		0.658	0.502	0.418
G5		0.632	0.579	0.439
G6		0.556	0.572	0.419
G7		0.661	0.504	0.452
G8		0.578	0.533	0.488
mean value	/	0.609	0.536	0.463

Generally, the two packing manners, namely hexagon and simple cubic, are regarded as the densest and loosest packing manners respectively, for single-size

spheres to achieve a stable framework, and either of the two extreme conditions is hardly occurring in practical aggregate packing (Smith et al. 1929). In Bailey method, BS sieve is selected as the one closest to 0.22 ×NMAS which was based on the packing manner close to hexagon (Vavrik et al. 2002), namely in which *d_ratio* is 0.22. Through a simple cubic packing manner, Yideti et al. (2013) found that finer particles with diameter of 0.732 multiplying that of the coarser particles can exactly fit in the voids. Hence the resultant voids size varied greatly with respect to different packing manner.

Herein the finer fraction in Blend-4 possessed the average *d_ratio* value of 0.46, which was around the middle value between that resultant *d_ratio* value in hexagon and simple cubic packing manners, indicating its potential effect in filling the voids created by coarser fraction. On the other hand, upon *d_ratio* value being increased up to 0.50 around, finer fraction begun to function as interceptor, such as 6.3-4.75 mm aggregates in Blend-3.

Through the evaluation on VA_{DRC} value and diameter ratio in the aggregate blends, it can be found that aggregates in various size ranges (i.e. 19.0-2.36 mm) can be divided into the following three types.

(a) main-coarse (i.e. aggregate coarser than 6.3 mm): the relatively densest aggregate structure can be achieved by proper selection of the proportion of each fraction (e.g. 19.0-13.2 mm, 13.2-9.5 mm. and 9.5-6.3 mm), and reduced voids content was realised through rearrangement of the stone-on-stone contact as finer fraction was added, while *d_ratio* value was around 0.61.

(b) interceptor (i.e. aggregate of 6.3-4.75 mm): there is no clear relationship between the voids content in aggregate blend and the amount of interceptor, corresponding to a *d_ratio* value greater than 0.50.

(c) quasi-fine (i.e. aggregate of 4.75-2.36 mm): VA_{DRC} value decreased with the content of quasi-fine aggregate, and high quasi-fine content (e.g. larger than 25%) might shove apart the packing structure established by coarser aggregates, while *d_ratio* value was around 0.46.

5.2.2 Evaluation of aggregate packing via DEM simulation

Corresponding to the four types of compacted aggregate blend (Blend-1~Blend-4), four types of PFC3D model were established for each gradation design, denoted as Model-1, Model-2, Model-3, and Model-4, respectively (Figure 5.5).

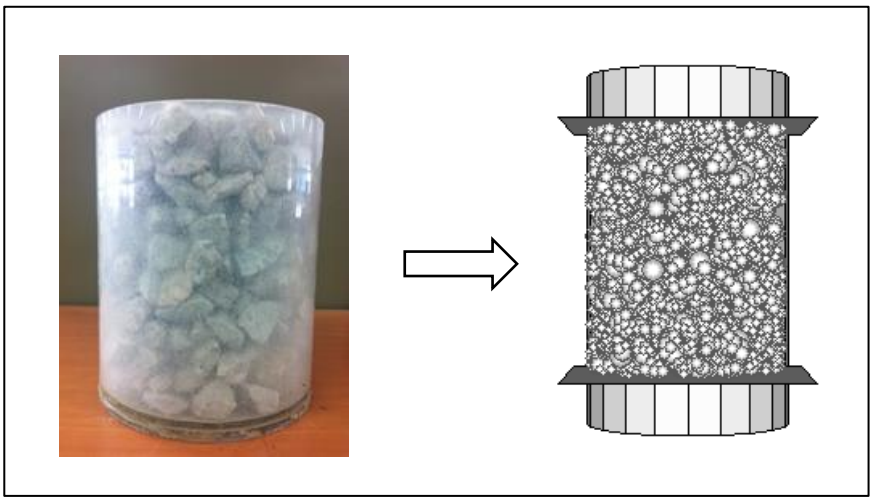

Figure 5.5 Illustration of compacted aggregate blend in the laboratory and the corresponding PFC3D model

The method to establish the PFC3D model of a compacted coarse aggregate blend is given in Chapter 3, in which 'servo-control' mechanism allows particles to be compacted through re-orientation. In the laboratory, coarse aggregate blend was compacted through rodding compaction method, in which the major compaction effect was re-orienting the aggregates to achieve a stable particle-to-particle framework, indicating the 'servo-control' mechanism applied in PFC3D model can appropriately simulate the packing condition in compacted coarse aggregate blend. Meanwhile, porosity is the ratio of voids within an assembly of particles by volume in a PFC3D model, which is a direct simulation parameter relating to voids content measured in the laboratory. The resultant porosity in the four types of models was obtained, with the difference as compared to VA_{DRC} value generally being within ± 2% error line (Figure 5.6), further indicating that PFC3D model is feasible in evaluating the packing condition in a compacted aggregate blend, of which voids content is a commonly-used indicator to represent the degree of aggregate interlocking.

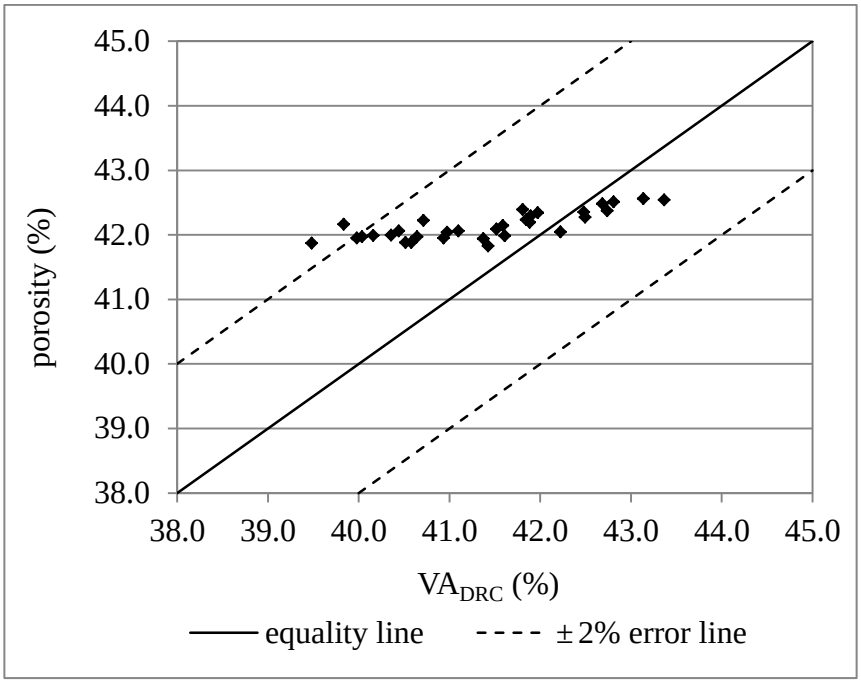

Figure 5.6 Relationship between porosity and VA_{DRC} value

Table 5.4 MCN_{cr} and MCN_{tot} for each model

G	MCN	Model-1	Model-2	Model-3	Model-4
G1	MCN_{cr}	4.17	2.29	2.46	4.54
	MCN_{tot}	5.51	5.41	5.46	5.39
G2	MCN_{cr}	1.39	2.98	4.43	3.90
	MCN_{tot}	5.40	4.64	5.52	5.37
G3	MCN_{cr}	2.55	3.76	2.36	3.56
	MCN_{tot}	5.44	5.39	5.45	5.39
G4	MCN_{cr}	0.71	4.13	4.18	2.48
	MCN_{tot}	5.38	5.42	5.37	5.42
G5	MCN_{cr}	1.42	2.09	4.54	4.63
	MCN_{tot}	5.06	5.37	5.45	5.15
G6	MCN_{cr}	3.61	2.02	4.77	3.31
	MCN_{tot}	5.33	5.41	5.43	5.40
G7	MCN_{cr}	0.94	4.25	3.71	4.90
	MCN_{tot}	5.19	5.44	5.42	5.42
G8	MCN_{cr}	2.99	2.92	3.14	2.96
	MCN_{tot}	5.24	5.37	5.45	5.44

Particle-to-particle contact can describe aggregate interlocking more directly and explicitly, but direct measurement of particle contact is hardly feasible. For each aggregate blend, the contact mechanism was simulated in PFC3D model to evaluate

the particle-to-particle interlocking through the simulation parameter, mean coordination number (MCN), which denotes the average number of effective contacts around each particle.

For each model, MCN values for coarser fraction as well as for the whole assembly were obtained and denoted respectively as MCN_{cr} and MCN_{tot} (Table 5.4). For MCN_{cr}, only effective contacts among the coarser particles were taken into account. For example, in Model-1, neither contact among finer fraction (i.e. 13.2-9.5 mm particles) nor between coarser and finer particles (i.e. between 19.0-9.5 mm and 13.2-9.5 mm particles) was taken into account for the MCN_{cr} value (Figure 5.7).

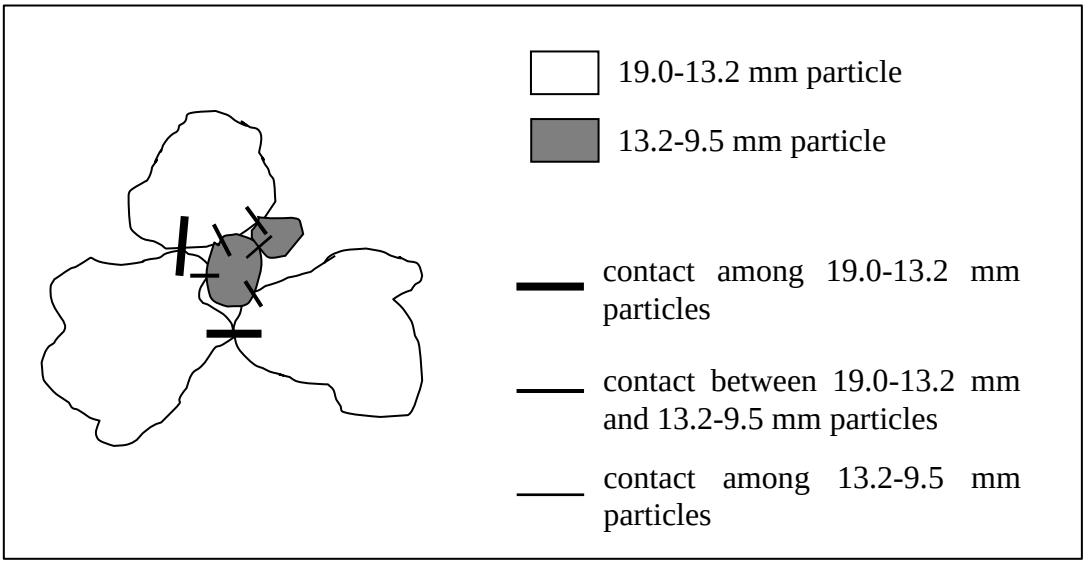

Figure 5.7 Sketch of the contacts in Model-1

The MCN_{tot} value in each model was greater than 4.0, indicating a generally stable interlocking was achieved, given that coordination number of at least 4.0 is required for a particle to retain stability in 3-dimension (Itasca 2008). For each aggregate gradation, MCN_{cr} value was lower than MCN_{tot} value, indicating the particle-to-particle skeleton created by coarser particles being separated by the finer particles. For each kind of PFC3D model, the difference between MCN_{cr} value and MCN_{tot} value was dependent on the amount of finer fraction, and a higher content of finer fraction resulted in a larger difference between the two types of MCN values (Figure 5.8).

Additionally, the packing condition in coarser fraction in each model can be indicated by MCN_{cr} value as well. MCN_{cr} value of around 2.0 would be associated with the establishment of chain by coarser particles, given that the configuration of chain involves a series of elements being connected one after another, resulting in each element amongst the chain possessing two contacts with the adjacent elements (Wikipedia 2015). Upon MCN_{cr} value being larger than 2.0, a network of coarser particles shall begin to be established till MCN_{cr} value achieved 4.0 (Figure 5.9). In contrast, coarser particle tended to be scattered in the matrix of finer fraction if MCN_{cr} value was less than 2.0.

In the portion of main coarse particles, corresponding to Model-1 and Model-2, adequate packing condition was achieved as MCN_{cr} value was at a relatively intermediate value (e.g. 2.0-4.0), implying the coarser and finer fractions in the model had sufficient interaction. Moreover, three conditions might occur upon the presence of various amounts of finer fraction (Figure 5.10).

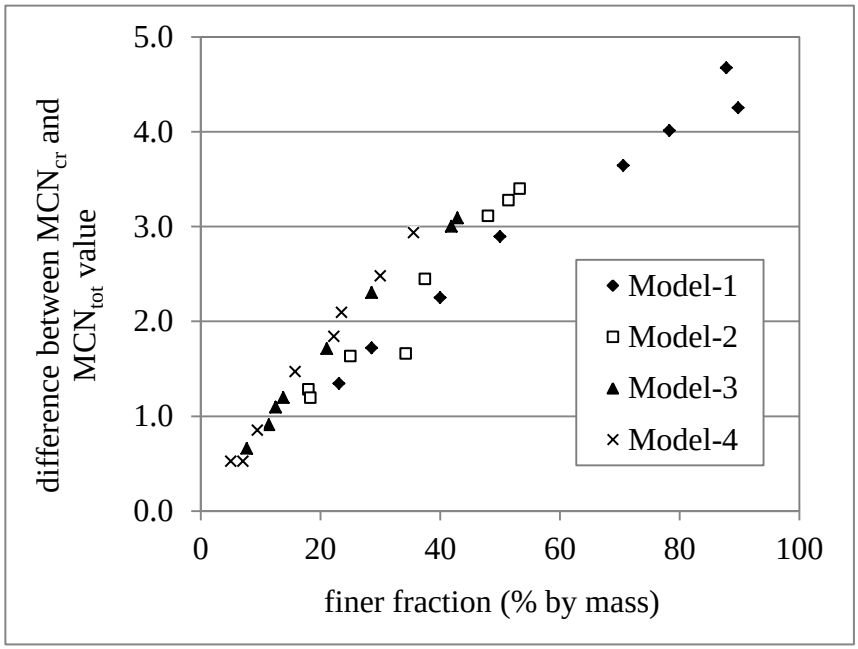

Figure 5.8 Relationship between finer fraction and the difference between two types MCN values

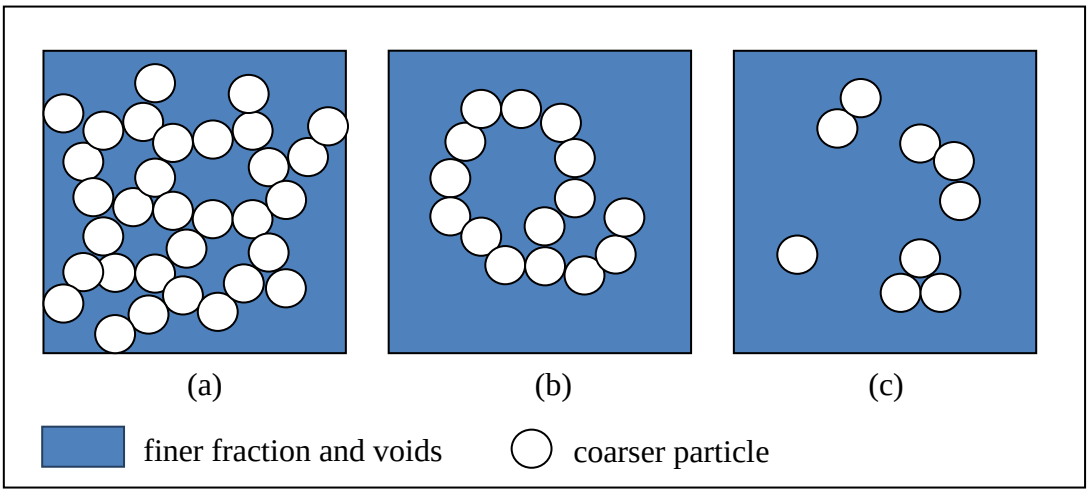

Figure 5.9 Sketch of packing condition in coarser fraction with MCN_{cr} value of : (a) greater than 2.0, (b) around 2.0, and (c) less than 2.0

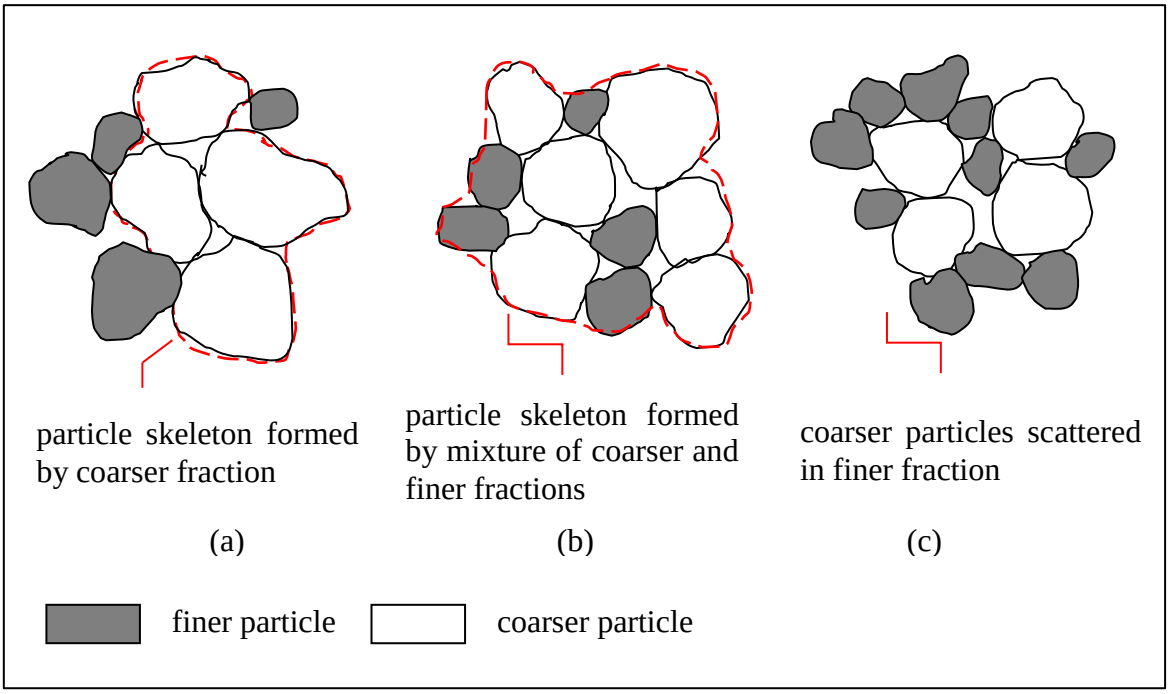

Figure 5.10 Sketch of the interaction between coarser and finer fractions in a model

(a) Gradation with a high MCN_{cr} value (close to 4.0)

For an aggregate blend at a high MCN_{cr} value, which reflected a stable skeleton (i.e. MCN value of at least 4.0), particle-to-particle framework created by coarser fraction can remain almost intact as finer fraction was added (Figure 5.9(a)), hence the network of coarser particles was well developed. This condition occurred in the case of low amount of the finer fraction, accompanied with minimal interference of

finer fraction to the coarser skeleton. For example, in Model-1, low amount of finer fraction in G1, namely 23.1% by mass, resulted in a high MCN_{cr} value of 4.17, indicating non-disruptive interaction between the coarser and finer fractions.

(b) Gradation with an intermediate MCN_{cr} value (2.0-4.0)

An intermediate MCN_{cr} value indicated disruptive interaction among the coarser and finer fractions, thereby forming a disrupted particle skeleton Figure 5.9(b)). In another word, particle skeleton formed by coarser fraction was disrupted by the newly-added finer fraction, but coarser particles were generally still in good contact in chain form, corresponding to an MCN value of at least 2.0. Specifically, according to the PFC3D model, adequate interaction in Model-1 and Model-2 occurred as MCN_{cr} value was within the range of 2.0-4.0, such as G3, G6, and G8 for Model-1, according to their VA_{DRC} of being the lowest values obtained in laboratory measurement (Table 5.2).

(c) Gradation with a low MCN_{cr} value (< 2.0)

At a low MCN_{cr} value (i.e. lower than 2.0) the particle skeleton created by coarser fraction was severely shoved apart by a high content of finer fraction (Figure 5.9(c)), and it was hard for coarser particles to form a chain. In the extreme, in Model-1 of G4, MCN_{cr} value was as low as 0.71 whence finer fraction accounted for 87.8% by mass in the model, implying particles in coarser fraction were hardly in direct contact with each other and were scattered amongst the particle assembly of finer fraction.

In Model-3, an interceptor portion was added. Similar to VA_{DRC} value, the porosity did not exhibit any clear relationship with finer fraction content. An intermediate content of interceptor particles is suggested regardless of the possibility of resultant high porosity in Model-3 or high VA_{DRC} value in Blend-3. Firstly, a low content of particles within a specific size range might cause problems in structural stability. Secondly, a high content of interceptor particles tended to reduce the size of voids created by the coarser particles. In general, the role of ‘interceptor’ was that of shoving apart the backbone created by the larger aggregates due to the ‘interceptor’

size being too large to fit in the voids generated by larger aggregates, this being consistent with the findings by Vavrik et al. (2002).

Furthermore, particle-to-particle framework was generally established in Blend-4 as quasi-fine portion was added, and finer particles in the aggregate gradation (i.e. smaller than 2.36 mm) functioned as filling the voids rendered in the framework, especially for open-graded design of PAM with low content of passing 2.36 mm aggregates. The MCN_{cr} value can indicate the interacting condition between quasi-fine portion and coarser fraction as well. For aggregate gradations with the MCN_{cr} value greater than 3.0, a lower value of voids content (i.e. VA_{DRC} value) was observed with the increased quasi-fine fraction. Especially, particle skeleton can be formed almost by coarser fraction in G1, G5 and G7, indicated by the MCN_{cr} value higher than 4.0, while the quasi-fine fraction by mass was relatively low (i.e. less than 10%). In contrast, particle-to-particle skeleton formed by coarser fraction was partially jeopardised by a high content of quasi-fine portion in G4 and G8, which was greater than 30% by mass.

Additionally, it should be noted that the interlocking mechanism primarily relies on line contacts rather than a point contact. However, a higher MCN_{cr} value still indicates a stable aggregate-on-aggregate interlocking in the coarse fraction that can enhance PAM's resistance to permanent deformation.

5.3 Packing condition in PAM specimens

In PAM specimens, coarse aggregates plays the role of creating particle-to-particle framework while fine fraction and asphalt mastic fill in the air voids and provide stability in the mixture. The remaining air voids content should be adequate so as to engender the essential performance of permeable mixture, namely drainage, which however is usually at the cost of reduced mixture strength.

A low content of fine aggregates is required for PAM to achieve adequate air voids content. It is found that air voids content reduced with the increase in the content of passing 2.36 mm aggregates (Figures 4.1~4.4) regardless of the difference in gyration compaction level (GCL) or asphalt binder type (ABT), indicating their role

in filling the voids. On the other hand, increasing the content of passing 4.75 mm aggregates generally decreased the air voids content up to the content of 30% (Figures 4.5~4.8). It is consistent with the finding that 4.75-2.36 mm aggregates played the role as quasi-fine in a mixture. The aggregate backbone created by the coarser aggregates tended to be partially shoved apart by quasi-fine aggregates (i.e. 4.75-2.36 mm aggregates) due to the relatively larger size than that of fine aggregates (i.e. passing 2.36 mm aggregates) and/or its high content in aggregate mixture, which was implied by VA_{DRC} measurement (Figure 5.4).

Moreover, for the aggregate gradations with the same content of passing 2.36 mm aggregates, PAM generally possessed the higher air voids content if the corresponding VA_{DRC} value in Blend-4 (i.e. containing 19.0-2.36 mm particles) was higher. Table 5.5 gives an example as the total air voids (TAV) content for each aggregate gradation was gained from PAMs fabricated with PG 76 asphalt at GCL of P600_N50, and similar trend could also be observed in PAMs with different ABT or GCL, indicating that a higher air voids content retained by coarser particles tended to result in a higher TAV content in PAM at the same amount of fine aggregates.

Table 5.5 TAV content and retained voids content in the PAMs (fabricated at P600_N50 with PG 76 asphalt)

G	PS2.36 * (%)	TAV (%)	VA_{DRC} (%)
G1	5	25.0	40.5
G2		24.3	40.2
G3	10	19.1	40.1
G4		18.6	39.8
G5	15	16.0	41.4
G6		14.1	39.5
G7	20	11.6	41.1
G8		11.7	40.0

* PS2.36= content of aggregate passing 2.36 mm, porosity is the value in Model-4, and VA_{DRC} is the value in Blend-4.

On the aspect of stone-on-stone framework in a compacted PAM specimen, two kinds of VCA parameters were measured in the laboratory, namely VCA_{mix} and

VCA_{DRC}. The VCA ratio (i.e. VCA_{mix}/VCA_{DRC}) was subsequently obtained to assess the packing condition in an asphalt mixture, and VCA ratio of less than 1.0 is suggested for adequate stone-on-stone backbone (Kandhal 2002). Based on the BS of 2.36 mm, denoted as BS2.36, VCA ratio was gained for each aggregate gradation (Table 5.6).

It was found that VCA ratio was influenced by the three packing factors, namely aggregate gradation (G), gyration compaction level (GCL), and asphalt binder type (ABT). For a certain aggregate gradation design, further compacted PAM, which was reflected by a lower VCA ratio, could be achieved by higher GCL (e.g. P600_N50) and/or modified asphalt (e.g. PG 76 asphalt), which agreed with the findings from experiments in Chapter 4.

In terms of aggregate gradation, all the eight aggregate gradations could achieve adequate packing condition, as reflected by the VCA ratio less than 1.0 (Table 5.6). Furthermore, according to Alvarez et al. (2010a), VCA ratio of 0.9 is recommended over the initial threshold value of 1.0, so as to ensure fully developed stone-on-stone packing structure in the PAM. Thereby, the content of fine aggregates equalling to or higher than 20% (e.g. G7 and G8) should be avoided in open-graded design for PAM, which is consistent with the recommendation in PAM design by Rajib et al. (2000). Moreover, for PAMs with fine aggregates content less than 15%, reference GCL of P600_N50 is suggested over lower gyration compaction level.

Table 5.6 VCA ratio of BS2.36

G	PAMs with Pen 60/70			PAMs with PG 76		
	P600_N50	P300_N100	P300_N50	P600_N50	P300_N100	P300_N50
G1	0.86	0.92	0.95	0.87	0.88	0.91
G2	0.83	0.90	0.91	0.83	0.88	0.92
G3	0.88	0.92	0.95	0.85	0.90	0.94
G4	0.87	0.91	0.95	0.85	0.89	0.91
G5	0.88	0.94	0.97	0.87	0.90	0.93
G6	0.90	0.94	0.97	0.88	0.92	0.95
G7	0.93	0.96	0.99	0.90	0.93	0.98
G8	0.94	0.97	1.00	0.93	0.94	0.99

5.4 Summary

Packing condition in the PAMs with eight gradation designs in Chapter 4 was analysed by means of laboratory measurements as well as DEM simulation, especially in the aspect of the development of stone-on-stone framework created by the coarse aggregates.

In the laboratory, the packing condition for each of the eight aggregate gradations was assessed through VA_{DRC} value, based on four types of aggregate blends: (a) Blend-1, containing 19.0-9.5 mm aggregates, (b) Blend-2, containing 19.0-6.3 mm aggregates, (c) Blend-3, containing 19.0-4.75 mm aggregates, and (d) Blend-4, containing 19.0-2.36 mm aggregates. In DEM simulation, four corresponding types of PFC3D models were established for the eight aggregate gradations, namely Model-1~Model-4, while the feasibility of the PFC3D model was verified in terms of porosity.

According to the laboratory measurement of VA_{DRC} value in each aggregate blend for the eight aggregate gradations, aggregates larger than 2.36 mm can be categorised into three types based on the effect on aggregate packing, which is further analysed by the contacting mechanism in PFC3D model, as summarised in the following:

(a) main-coarse

Main-coarse contains aggregates of 19.0-6.3 mm, providing coarse particles in the stone-on-stone framework, and the relatively densest aggregate structure can be achieved by proper proportioning (i.e. the ratio among 19.0-13.2 mm, 13.2-9.5 mm, and 9.5-6.3 mm aggregates) while MCN_{cr} in Model-1 and/or Model-2 is an intermediate value, namely 2.0-4.0, indicating adequate interaction between coarser and finer fractions. The reduction in voids content is realised by the rearrangement of stone-on-stone contact.

(b) interceptor

Interceptor contains aggregates of 6.3-4.75 mm, in which no clear relationship exists between the VA_{DRC} value and interceptor content, probably due to the role of

interceptor aggregates being to separate the stone-on-stone backbone created by larger aggregates. The content of interceptor aggregates is suggested to be intermediate in order to balance the requirements of both stability in aggregate gradation and voids size retained in the framework.

(c) quasi-fine

Quasi-fine contains aggregates of 4.75-2.36 mm, in which a higher quasi-fine content tended to decrease VA_{DRC} value, whilst an overly high content (e.g. larger than 25% in an aggregate blend) could shove apart the stone backbone formed by the coarser aggregates, corresponding to the MCN_{cr} value being lower than 3.0 as in Model-4 (in which 4.75-2.36 mm aggregates are the finer fraction), indicating the stone-on-stone backbone created by larger aggregates is partially jeopardised by the high content of quasi-fine aggregates.

In terms of packing condition in the PAM specimens, it was assessed through VCA ratio. Reference GCL of P600_N50 was recommended for PAM fabrication to achieve adequate aggregate interlocking. In terms of open-graded design, fine aggregates content lower than 20% was found necessary in generating fully developed skeleton by coarse aggregates. Regarding PAM design for low-strength pavement application, given that requirement in function (e.g. adequate drainage) is prior to mechanical strength, the content of fine aggregates and relevant aggregate gradation should be designed according to practical situation, and appropriate compaction level and asphalt binder type shall be selected so as to achieve adequate mixture strength.

Chapter 6 Design and evaluation of PAM for low-strength pavement application in Singapore

6.1 Introduction

Benefits of PAMs in the practical application include providing safe driving condition due to the excellent performance in drainage, lowering noise level, and generating cooling effect etc., which are strongly attributed to the typical open-graded design and resultant high air voids content. In terms of application, most PAM design are currently aimed at motor vehicle roads, such as expressways, arterial roads and collector roads, and principal attention is focused on providing adequate strength to withstand designed traffic volume, rather than ensuring the essential function such as drainage. For Singapore, large requirements in building low-strength pavements are engendered by the increasing trend in developing non-motorised traffic facility. Moreover, Singapore is a tropical country with frequent thunderstorms during the monsoon periods, rendering high requirement in effective drainage for pavement surface. Hereby, design of well performing PAM for specific application, namely low-strength pavement application in the tropical area, is timely and worthy of intensive research.

According to the findings in previous chapters, appropriate PAM design (including designing aggregate gradation, selecting asphalt binder and gyration compaction level) shall be conducted, so as to achieve adequate drainage capability, mixture strength, and aggregate interlocking. In particular, given that aggregate gradation is a significant design factor in terms of PAM's air voids content and permeability, it shall be appropriately designed based on the practical rainfall situation in Singapore. Subsequently, the properties and packing conditions in designed PAMs shall be evaluated.

6.2 PAM design for specific application

According to the experimental results of the preliminary PAM designs, PAM's functional performance (i.e. permeability) and mechanical properties (e.g. resistance to Cantabro abrasion and Marshall stability) were both affected by air voids content, while water-accessible air voids (WAAV) content was approximately linearly increased with total air voids (TAV) content. Higher permeability was usually companied with poorer ravelling resistance and weaker mixture strength. Furthermore, PAM's air voids content is dependent on aggregate gradation (G), gyration compaction level (GCL), and asphalt binder type (ABT).

In terms of asphalt binder, as compared with the corresponding PAM of the same aggregate gradation and gyration compaction level, usage of modified asphalt (namely PG 76 asphalt) was capable of enhancing PAM's resistance to Cantabro abrasion and Marshall stability, and generating PAMs that can meet the lower limits in UC-ALV (i.e. 20%), AC-ALV (i.e. 30%) and UC-MS (i.e. 4.0 kN) at the relatively lower content of passing 2.36 mm aggregates (e.g. 10%). Thereby PG 76 asphalt binder was suggested to be applied in PAM to obtain adequate ravelling resistance and mixture strength.

In terms of PAM's functional property, sufficient permeability shall be achieved by proper air voids content. Among the three design factors, aggregate gradation, especially with respect to the content of fine fraction, namely aggregates passing 2.36 mm sieve, could influence TAV content and/or WAAV content most distinctively, followed by gyration compaction level and asphalt binder type. Reference gyration compaction level, namely P600_N50, was selected so as to obtain stable packing condition.

Based on the regression equation between TAV content and permeability for PAM with PG 76 asphalt binder (Equation 4.4), TAV content of 22.0% should be obtained in PAM design to meet the drainage requirement in Singapore, namely 130 $\times 10^{-3}$ cm/s. Subsequently, according to the regression relationship between TAV content and the content of fine fraction in open-graded design for PAMs with PG 76

asphalt binder at P600_N50 (Equation 6.1), which was obtained through the data in Figure 4.3, proper content of fine fraction was suggest to be lower than 7.2%.

$$y = -0.8571x + 28.25 \quad (6.1)$$

y = TAV content, %;

x = content of passing 2.36 mm aggregates, % by mass.

Therefore, potential PAM for low-strength pavement application in Singapore is designed as the asphalt mixture fabricated at P600_N50 with PG 76 asphalt binder and the fine fraction in open-graded design is selected as 7%.

Furthermore, as aggregates in the coarse fraction are divided into three parts according to the effect in packing structure, namely main-coarse, interceptor, and quasi-fine, four PAMs with different packing structures created by the coarse aggregates were designed as following (Table 6.1 and Figure 6.1).

(a) G_cont: the coarse fraction was relatively continuously distributed, namely the shape of the coarse fraction was similar to Fuller's curve;

(b) G_coarse: the content of 'main-coarse' aggregates (i.e. aggregates larger than 6.3 mm) was very high, which was up to 80%;

(c) G_inter: the content of 'interceptor' aggregates was high, which equalled to 40%, engendering a 'S-shape' curve in the coarse fraction of aggregate gradation (Figure 6.1); and

(d) G_fine: the content of 'quasi-fine' aggregates (i.e. aggregates of 4.75-2.36 mm) was high, which equalled to 38%.

Table 6.1 Aggregate gradation designs for four newly-designed PAMs

G	passing percentage by mass (%), on each sieve (mm)										
	19	13.2	9.5	6.3	4.75	2.36	1.18	0.6	0.3	0.15	0.075
G_cont	100	77	59	40	30	7	6.6	6.2	5.8	5.4	5
G_coarse	100	70	45	20	12						
G_inter	100	85	70	58	18						
G_fine	100	90	80	60	45						

For each of the four PAM aggregate gradation designs, the content of aggregate fillers was kept as 5%, and particles with size of 2.36-0.075 mm were uniformly distributed. The asphalt binder content (ABC) was selected as 4% for all the four PAMs so that the thickness of asphalt film can achieve at least 10 μm and draindown of asphalt mastic was hardly observed in draindown test at the selected ABC, indicating draindown was not an issue herein.

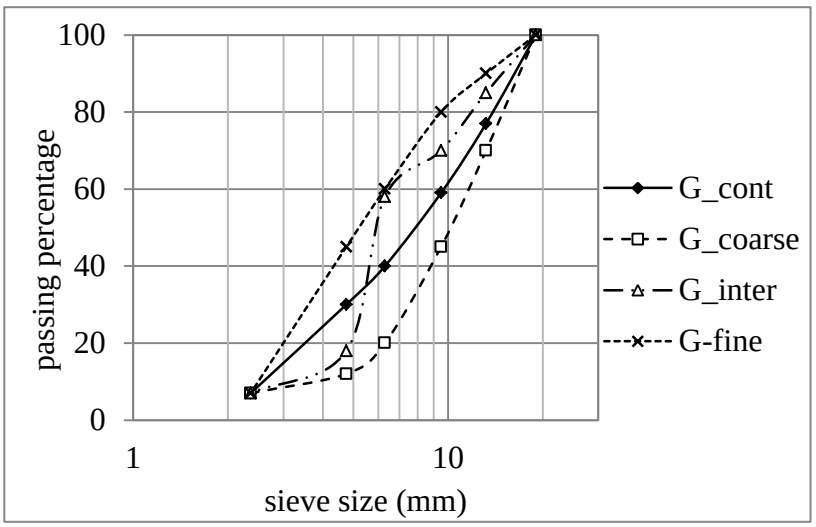

Figure 6.1 Profiles of the coarse fractions in four PAMs

6.3 Properties of designed PAMs

Upon the potential PAMs for the specific application (i.e. low-strength pavement application in tropical area) being designed with four different packing structures created by the coarse fraction, the basic properties, including volumetric properties, permeability, and mechanical properties, were measured in the laboratory via the methods as mentioned in Chapter 3, and three replicates were conducted for each performance test.

6.3.1 Air voids content and permeability

Due to the different interlocking structure created by the coarse aggregates in the four PAMs, different air voids content and permeability were obtained (Table 6.2), while WAAV ratio, indicating the content of WAAV in TAV by percentage, was obtained through Equation (6.2). As the coarse fraction contained more main-coarse

aggregates and interceptor aggregates, namely the cases of G_coarse and G_inter, more air voids contents (i.e. TAV and WAAV contents) were generated in these PAMs as compared with the other two PAM designs. Meanwhile, higher WAAV ratios were obtained in G_coarse and G_inter, namely effective air voids were created at higher ratios among the total air voids, and hereby the resultant coefficients of permeability (*k* values) were higher as well.

However, comparing G_coarse and G_inter, the one that possessed relatively higher WAAV content and WAAV ratio, namely G_coarse, showed relatively lower permeability. This can be explained that the high content of interceptor aggregates in G_inter generated air voids with sizes that were relatively more uniformly distributed and consequently water can flow through the specimen more fluently, as consistent with the findings by Poulikakos and Partl (2010) that PAM with better functionality can be achieved with air voids of more homogeneous structure.

Additionally, although the contents of fine fraction in the four PAM designs were the same, namely 7%, only G_coarse and G_inter could meet the suggested permeability in Singapore, namely being higher than 130 $\times 10^{-3}$ cm/s.

$$WAAV\ ratio = \frac{WAAV\ content}{TAV\ content} \times 100\% \tag{6.2}$$

Table 6.2 Results of air voids content and permeability

	TAV (%)	WAAV (%)	WAAV ratio (%)	*k* ($\times 10^{-3}$ cm/s)
G_cont	21.6 (±0.6)	15.8 (±0.7)	72.9 (±2.2)	107.4 (±10.6)
G_coarse	23.7 (±0.8)	19.2 (±1.1)	80.9 (±3.1)	155.8 (±13.0)
G_inter	23.6 (±0.9)	17.7 (±1.1)	75.1 (±3.4)	160.9 (±11.2)
G_fine	22.3 (±0.7)	15.9 (±1.1)	71.0 (±3.3)	126.4 (±11.7)

6.3.2 Marshall test

UC-MS values of the four PAM designs could all meet the requirement for low-strength pavement application, namely being greater than 4.0 kN, and the difference in UC-MS among the four PAM designs was relatively slight with the MS values of G_cont and G_fine being a little higher as compared with the other two designs (Table 6.3), which was heavily attributed to the relatively low air voids content.

Meanwhile, the designed PAMs shall be applicable to motorised roads by enhancing the Marshall stability to 9.0 kN, the lower limit of Marshall stability for normal roads (LTA 2010), which might be achieved via increased asphalt binder content.

In the aspect of moisture conditioning, the values of retained MS remained high for most PAM designs, and each design even possessed MC-MS value higher than 4.0 kN, indicating moisture exposure was not a debilitating issue.

Table 6.3 Results of Marshall test

	UC-MS (kN)	MC-MS (kN)	retained MS (%)
G_cont	6.5 (± 0.9)	6.1 (± 0.5)	93.5
G_coarse	6.0 (± 1.3)	5.9 (± 0.5)	98.1
G_inter	6.0 (± 0.7)	5.1 (± 0.3)	83.8
G_fine	6.3 (± 0.9)	5.9 (± 0.4)	92.8

6.3.3 ITSM test

Whereas Marshall test estimated the peak load that can be carried by specimen during constant loading, ITSM test measures asphalt mixture's capability in recovering the deformation upon external loading/unloading. It can be seen that G_coarse and G_fine possessed lower UC-ITSM and MC-ITSM values as compared with the other two PAM designs, implying that the resilient behaviour is weaker for high content of main-coarse aggregates or quasi-fine aggregates in the coarse fraction (Table 6.4). After moisture conditioning, retained ITSM value in G_fine was the lowest among the four designs, with MC-ITSM value in G_inter being close to G_cont and G_coarse, which may be ascribed to the higher air voids content in G_inter.

Table 6.4 Results of ITSM test

	UC-ITSM (MPa)	MC-ITSM (MPa)	retained ITSM (%)
G_cont	1899.5 (± 194.7)	1631.2 (±170.8)	85.9 (± 0.8)
G_coarse	1669.4 (± 76.1)	1427.5 (± 74.2)	85.6 (± 4.9)
G_inter	2373.8 (± 321.9)	1558.3 (± 118.3)	66.3 (± 6.1)
G_fine	1560.3 (± 123.7)	1146.8 (± 160.6)	73.2 (± 4.6)

6.4 Packing condition in designed PAMs

6.4.1 Particle-to-particle contact in compacted coarse aggregates

For each of the four PAM designs, a PFC3D model of the compacted coarse aggregates (namely compacted assembly containing 19.0-2.36 mm particles) was established via the method in Chapter 3. For the PFC3D model of each PAM design, mean coordination number (MCN) in different components of the coarse fraction was obtained, including MCN among:

(a) main-coarse particles: 19.0-6.3 mm;

(b) interceptor particles: 6.3-4.75 mm;

(c) quasi-fine particles: 4.75-2.36 mm;

(e) main-coarse and interceptor particles: 19.0-4.75 mm; and

(f) total particles: 19.0-2.36 mm, namely all the particles in coarse fraction.

In each component, MCN was obtained as taking into account only of the effective contacts between particles within the relevant components. For example, as calculating MCN in main-coarse particles, only effective contacts between particles within size of 19.0-6.3 mm were taken, and contacts involving particles outside of that main-coarse component (i.e. 6.3-2.36 mm) were not included.

Table 6.5 MCN in different components of the coarse fraction

PAM design	individual component			main-coarse & interceptor (19.0-4.75 mm)	total (19.0-2.36 mm)
	main-coarse (19.0-6.3 mm)	interceptor (6.3-4.75 mm)	quasi-fine (4.75-2.36 mm)		
G_cont	2.48	1.14	2.68	3.16	5.41
G_coarse	4.16	1.40	1.36	4.76	5.26
G_inter	1.61	2.95	1.53	4.38	5.39
G_fine	1.37	1.10	3.26	2.33	5.41

It is accepted that stable contact is achieved when MCN value is no lower than 4.0 and chain contact is usually realised for MCN value being higher than 2.0, as mentioned in Chapter 5. It can be seen that MCN in the total coarse fraction in each model was larger than 4.0 (Table 6.5), namely each particle in the model could be on the average supported by four contacts at least, indicating the stable condition in each PFC3D model.

Among the four PAM designs, G_coarse possessed the highest MCN value in main-coarse component, followed by G_cont, G_inter, and G_fine, and the trend was the same as the content of main-coarse aggregates in each PAM design. In G_coarse, the content of main-coarse aggregates in the gradation was as high as 80% while the content of interceptor and quasi-fine was as low as 13%, and consequently the corresponding contents of main-coarse particles and smaller particles (i.e. the combination of interceptor and quasi-fine particles) were 86.0% and 14.0% in the PFC3D model of compacted coarse fraction, respectively, given that 7% fine particles were not generated in the model. Thereby the main-coarse particles were easy to contact with each other after compaction with few particles being separated by smaller ones (i.e. interceptor and quasi-fine particles), resulting in extremely high MCN value in main-coarse component, namely 4.16. In contrast, MCN values in main-coarse component for G_inter and G_fine were lower than 2.0, indicating main-coarse particles alone could hardly form chain contact. Similarly, G_fine's MCN value in quasi-fine component was the highest, strongly attributed to the high content of quasi-fine in the aggregate gradation (i.e. 38%), and followed by G_cont, G_inter, and G_coarse with the descending content of quasi-fine particles.

In terms of MCN value in interceptor compnent, PFC3D model of G_inter possessed the highest value due to the highest content of interceptor particles. However, there was no trend of higher interceptor content being associated with higher MCN value in the interceptor component among the other three PAM designs as found in MCN values in main-coarse and quasi-fine components. It might be attributed to the uncertain role of interceptor aggregates in the coarse fraction. Interceptor particles could form particle-to-particle framework well with main-coarse, such as the MCN values in 'main-coarse & interceptor' component

being higher than 4.0 in the PFC3D models of G_coarse and G_inter. On the other hand, in the PFC3D model of G_fine, MCN value of 'main-coarse & interceptor' component was as low as 2.33 due to the high content of quasi-fine particles.

Furthermore, stable contact rate (SCR) and chain contact rate (CCR) in different component of the coarse fraction were obtained through Equations (6.3) and (6.4), respectively. For each PFC3D model of the PAM design, the development of particle-to-particle skeleton was shown clearly (Tables 6.6 and 6.7, Figures 6.2 and 6.3). In the total component of coarse fraction, particles in each PF3D model of the four PAM designs can well form chain contact, implied by the CCR value close to 100% with the corresponding SCR value being lower. For G_coarse and G_inter, most stable contact and chain contact were formed by main-coarse and interceptor particles while the effect of quasi-fine particles in strengthening contact was much lower. For G_fine, SCR and CCR values in the total coarse fraction were much higher than that in 'main-coarse & interceptor' component. Furthermore, contact ratio (SCR and/or CCR) in the separate component of quasi-fine particles was much higher than the other separate components (namely main-coarse component and interceptor component), indicating that most contact in the coarse fraction was generated within quasi-fine particles while larger particles were scattered in the matrix of quasi-fine particles.

$$SCR = \left(1 - \frac{N_{float}}{N}\right) \times 100 \tag{6.3}$$

N_{float} = number of floating particles (i.e. the ones with coordination number lower than 4.0) in relevant part;

N = total number of particles in relevant part.

$$CCR = \left(1 - \frac{N_{no\_chain}}{N}\right) \times 100 \tag{6.4}$$

N_{no_chain} = number of particles without chain contact (i.e. the ones with coordination number lower than 2.0) in relevant part.

Table 6.6 SCR in different parts of the coarse fraction

PAM design	individual component			main-coarse & interceptor (19.0-4.75 mm)	total (19.0-2.36 mm)
	main-coarse (19.0-6.3 mm)	interceptor (6.3-4.75 mm)	quasi-fine (4.75-2.36 mm)		
G_cont	23.2	2.5	26.6	34.9	73.2
G_coarse	58.4	2.9	3.6	63.6	64.9
G_inter	9.2	32.7	5.8	61.4	76.6
G_fine	5.0	2.5	39.9	19.4	76.9

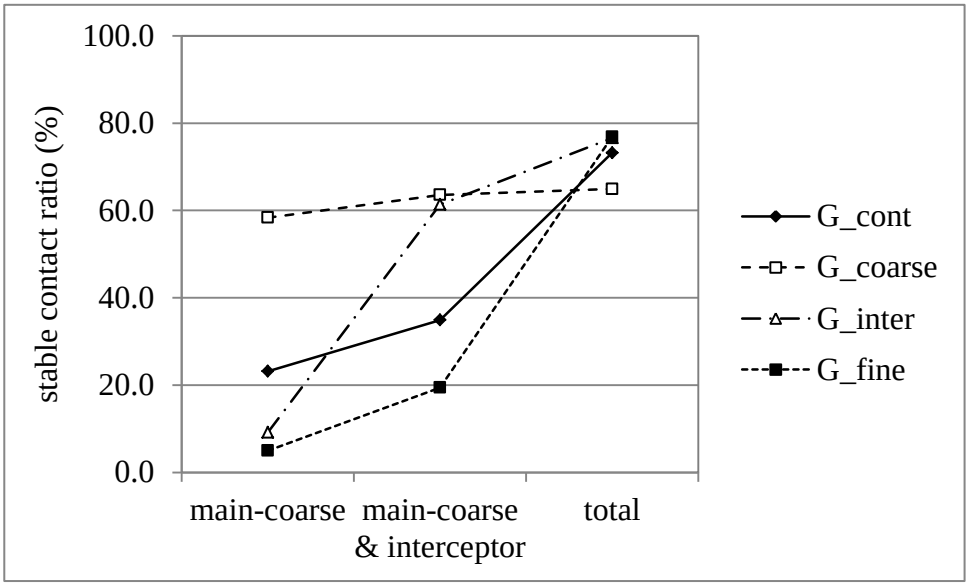

Figure 6.2 Development of SCR in the coarse fraction

Table 6.7 CCR in different parts of the coarse fraction

PAM design	individual component			main-coarse & interceptor (19.0-4.75 mm)	total (19.0-2.36 mm)
	main-coarse (19.0-6.3 mm)	interceptor (6.3-4.75 mm)	quasi-fine (4.75-2.36 mm)		
G_cont	69.4	26.6	74.5	81.2	99.5
G_coarse	94.9	29.1	29.3	97.2	98.4
G_inter	47.4	82.4	37.7	96.5	99.6
G_fine	39.8	28.1	86.2	67.2	99.8

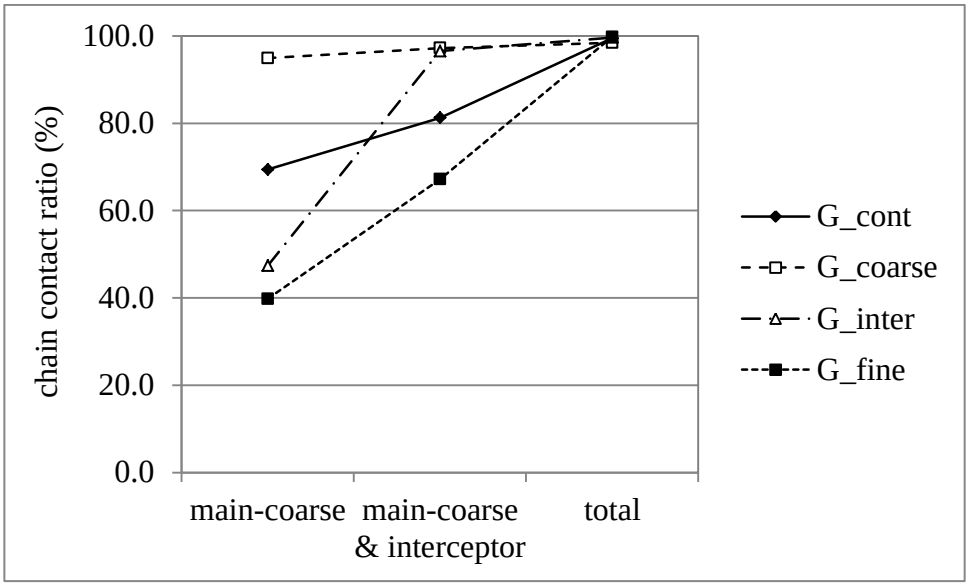

Figure 6.3 Development of CCR in the coarse fraction

6.4.2 Distribution of contact force in compacted PAM specimen

For each of the four PAM designs, a PFC3D model to simulate compacted PAM specimen was established as well (Figure 6.4). The procedure in modelling was similar as that mentioned in Chapter 3, except that:

(a) the size of modelled sample was set as the actual compacted PAM specimen with diameter of 100 mm;

(b) the total mass of coarse particles was set as 930 g according to the PAM design;

(c) target pressure on the top plate was set as 600 kN during compaction procedure in DEM using ‘servo-control’ mechanism, as the reference compaction pressure used in the laboratory; and

(e) fine particles with the size of 2.36-0.075 mm, whose content was 2% in aggregate gradation for all the four PAM designs, were modelled using spherical balls of diameter of 1 mm in the PFC3D model.

It should be noted herein that asphalt mastic, namely the mixture of fillers and asphalt binder, was not added into the model. Also, fine particles with the size of 2.36-0.075 were modelled as the spherical particles with the fixed diameter of 1.0 mm, namely the size is close to the intermediate value, rather than according to the

actual size distribution. This simplification in DEM simulation is based on the following consideration:

(a) The computation efficiency, which is regarded a significant issue in DEM simulation, is directly dependent on the number of contact points in a model (Itasca 2008). Thereby, though the content of fine fraction is low in open-graded design, extremely large number of particles will be created if fine fraction is modelled due to the fine size, leading to extraordinary increase in contact points and consequently drastically decreasing computation efficiency. Therefore, it is widely accepted to set a lower limit for aggregate size in modelling asphalt mixture in PFC3D, such as 2.36 mm, 2.0 mm, or 1.18 mm (You et al. 2008; Liu et al. 2009; Micaelo et al. 2011; Yu and Shen 2012; Cai et al. 2013).

(b) PFC3D model is applied aimed at evaluating the establishment and development of packing structure in PAM. On the aspect of PAM, stone-on-stone skeleton formed by the coarse aggregates is the major source of aggregate packing, which strongly influences the PAM's properties. On the other hand, the content of fine fraction and asphalt mastic is relatively much lower and the function is partially filling the voids created by the coarse aggregates rather than creating packing framework, thereby the relative modelling part is simplified so as to highly improve computation efficiency without critically compromising the analysis of the packing structure in PAM.

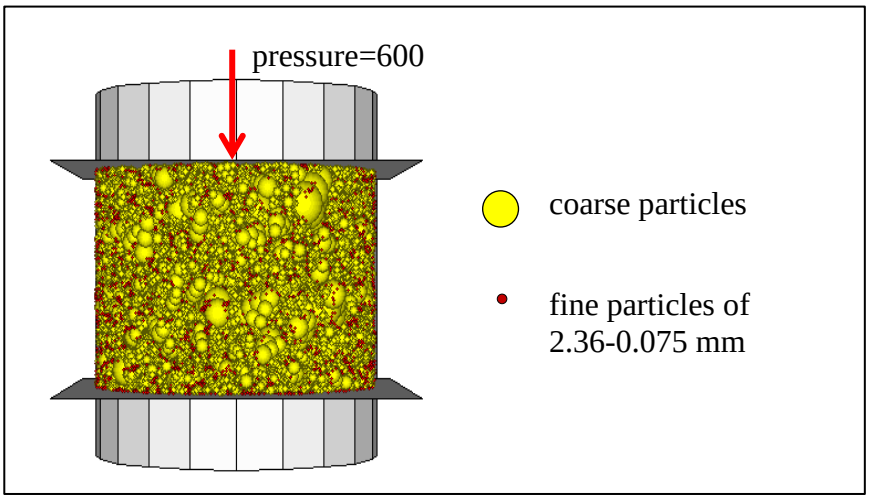

Figure 6.4 Modelled compacted PAM spcimen for G_cont

The estimated total air voids (TAV) content in each PAM design can be obtained by subtracting the content of asphalt mastic volume from the porosity in the corresponding PFC3D model of compacted PAM specimen, as shown in Equation (6.5). The volume of asphalt mastic (namely the mixture of asphalt binder and fillers) in the compacted PAM specimen was gained through the density measured in the laboratory, which equalled to 1.49 g/cm^3.

$$estimated\ TAV = porosity - \frac{V_{mastic}}{V_{container}} \tag{6.5}$$

V_{mastic} = volume of asphalt mastic in the compacted PAM specimen;

$V_{container}$ = volume of the container in PFC3D model after compaction.

Table 6.8 Measured and PFC3D-estimated TAV contents in each PAM design

PAM design	measure TAV (%)	PFC3D-estimated TAV (%)
G_cont	21.6 (±0.6)	20.1
G_coarse	23.7 (±0.8)	24.6
G_inter	23.6 (±0.9)	22.7
G_fine	22.3 (±0.7)	21.7

It can be seen that estimated TAV contents obtained in the PFC3D models of the four PAM designs, which contained the same fine fraction and asphalt binder, can well reflect the order of TAV content as measured in the laboratory, namely G_coarse possessed the highest TAV, followed by G_inter, G_fine, and G_cont (Table 6.8). Some factors to explain the difference between estimated and measured TAV contents are listed in the following:

(a) Breakage might occur during compaction in the laboratory using gyration compactor while particles in PFC3D were stiff and no breakage or deformation was allowed, resulting that estimated TAV being higher than measured TAV;

(b) Pressure on top plate in the PFC3D can be stably controlled at 600 kPa, while compacted PAM specimen was compacted at pressure of 600 kPa in the laboratory through a fixed gyration counts of 50, and subsequently full compaction might not

be accomplished, hence generating measured TAV in compacted PAM specimen being higher than estimated TAV;

(c) Asphalt mastic was partially absorbed into the minor voids in aggregate surface in reality, which was not reflected in PFC3D model, resulting in the measured TAV being higher than estimated TAV; and

(d) Fine particles with size of 2.36-0.075 mm were simulated in the PFC3D model using spheres with fixed diameter of 1.0 mm, resulting in unclear effect on the voids content.

In the aspect of contact force, the distribution of contact force in the PFC3D model is illustrated in Figure 6.5 with all the objects (i.e. balls and walls) being spatially displaced to observe the force chains more clearly. A force chain generated between a pair of contacted particles refers to the normal force transmitted between them; its thickness indicates the magnitude of the force whereby the thicker the force chain is the larger the force being transmitted (Itasca 2008). Usually thick and thin force chains are respectively created by coarse and fine particles in a compacted assembly of particles.

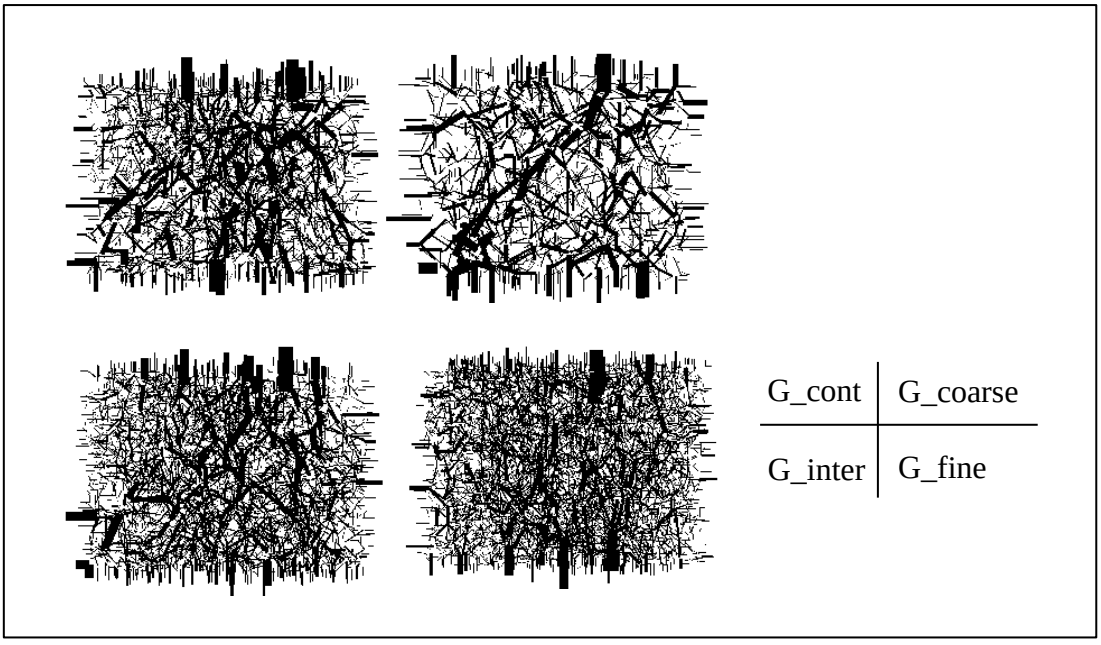

Figure 6.5 Distribution of contact force in four PAM designs

It can be seen that the structure of force chains developed in G_coarse was mostly composed by thick force chains with the total number of force chains being the fewest among the four PAM models. Namely, forces were mostly carried by the large-size particles (e.g. main-coarse particles) in G_coarse and less force can be further transmitted to small-size particles (e.g. quasi-fine and fine particles), resulting in the least stable framework among the four PAM designs. In contrast, the structure of force chains in G_fine was mostly created by the thin force chains in a dense pattern, while that in G_inter was somewhat looser. For G_cont model, due to the relatively continuous aggregate gradation in the coarse fraction, a stable structure was well developed by the combination of thick and thin force chains.

Furthermore, mean particle force (MPF) among the coarse fraction in the PFC3D model was obtained as well through Equation (6.6). Two kinds of MPF values were gained in different parts of the coarse fraction, namely exclusive and inclusive MPF, denoted as MPF_{ex} and MPF_{in}, respectively. For MPF_{ex}, only contact forces across effective contacts between relevant particles were accounted. In contrast, force chains between particles within and without relevant component were accounted as well in MPF_{in}. For example, MPF_{ex} of main-coarse component included contact forces across main-coarse particles exclusively, while contact forces transferred between main-coarse and interceptor particles were also taken into account when calculating MPF_{in} of main-coarse. Meanwhile, MPF among the total coarse fraction, denoted as MPF_{tot}, was obtained as well.

$$MPF = \frac{1}{N_p}\left(\sum_{N_p} PF\right) \tag{6.6}$$

PF = sum of relevant forces transferred to the particle;

N_p = number of particles.

For each PAM model, MPF_{ex} or MPF_{in} in main-coarse component was the highest, and became reduced gradually upon taking finer particles (i.e. interceptor and quasi-fine particles) into account (Table 6.9), indicating the supportive effect of finer particles on the coarser fraction.

Subsequently, for different components of the coarse friction (namely 'main-coarse' component and 'main-coarse & interceptor' component), MPF increase ratio was obtained through Equation (6.7) to assess the supportive effect of finer particles (Table 6.10).

$$MPF\ increase\ ratio = \frac{MPF_{in} - MPF_{ex}}{MPF_{ex}} \times 100 \tag{6.7}$$

Table 6.9 MPF values in different components of the coarse fraction

PAM design	MPF_{ex} (N)		MPF_{in} (N)		MPF_{tot} (N)
	main-coarse (19.0-6.3 mm)	main-coarse & interceptor (19.0-4.75 mm)	main-coarse (19.0-6.3 mm)	main-coarse & interceptor (19.0-4.75 mm)	main-coarse & interceptor & quasi-fine (19.0-2.36 mm)
G_cont	134.075	99.022	184.834	118.655	41.135
G_coarse	235.183	170.166	251.023	173.19	97.935
G_inter	97.035	75.997	171.502	81.776	58.333
G_fine	68.096	55.631	131.913	80.098	37.626

Table 6.10 MPF increase ratio between MPF_{ex} and MPF_{in} in different components of the coarse fraction

PAM design	MPF increase ratio (%) in	
	main-coarse (19.0-6.3 mm)	main-coarse & interceptor (19.0-4.75 mm)
G_cont	37.9	19.8
G_coarse	6.7	1.8
G_inter	76.7	7.6
G_fine	93.7	44.0

In G_coarse model, MPF_{ex} and MPF_{in} values in 'main-coarse' component were the highest among the four PAMs while the MPF increase ratios in both 'main-coarse' and 'main-coarse & interceptor' components were the lowest, indicating forces transferred among the main-coarse particles were the largest in G_coarse and the supportive effect of finer fraction was the weakest, which agreed with the findings in terms of SCR and CCR values in the previous PFC3D model of compacted coarse aggregates, namely interlocking structure was almost developed by main-coarse particles in G_coarse. Due to the deficiency in force transfer by interceptor and quasi-fine particles in the coarse fraction, relatively weak strength, as reflected

by low Marshall stability (i.e. 6.0 kN), was observed for G_coarse PAMs in the laboratory.

Similarly, in G_inter model, supportive effect by 'quasi-fine' part was low as well, which is implied by the low value of MPF increase ratio in 'main-coarse & interceptor' part, and forces were mostly transferred among 'main-coarse & interceptor' part.

In contrast, in G_fine model, MPF increase ratios in both 'main-coarse' and 'main-coarse & interceptor' components were the highest among the four PAMs, while the MPF_{ex} and MPF_{in} values in various components of the coarse fraction were the lowest. It indicates the strong support by the 'quasi-fine' component, namely force transferred in 'main-coarse' and 'interceptor' components can mostly be well dispersed by 'quasi-fine' particles, ascribing to the high content of quasi-fine particles. On the other hand, due to the low content of main-coarse and interceptor aggregates, stable framework and/or chain contacts were established at the lowest level among the four PAMs according to SCR and CCR values in the previous PFC3D model of compacted coarse aggregates. Consequently, relatively high Marshall stability (i.e. 6.3 kN) was found in G_fine's PAM specimens, probably due to the good capability in transferring forces among the particle-to-particle structure with the relatively densest thin force chains among the four PAM designs.

In the PAM design with relatively continuous aggregate gradation in the coarse fraction, namely G_cont, a stable interlocking structure was observed. Based on MPF increase ratios in different components of the coarse fraction (namely 37.9% and 19.8% in 'main-coarse' component and 'main-coarse & interceptor' component, respectively), it can be seen that principal support was provided mostly by the finer particles in the coarser fraction. Correspondingly, in terms of effective contacts, SCR and CCR values developed in the coarse fraction in G_cont, which were shown in the previous PFC3D models of compacted coarse aggregates, were relatively intermediate among the four PAM designs. Thereby, a well-developed framework was observed in G_cont, as reflected by (a) adequate coarse particles to carry most of the force, avoiding the large forces exerting on small particles directly, and (b) thin force chains generated by finer particles in the coarse fraction to well

disperse the forces across coarser particles. Consequently, among the four PAM designs, the highest Marshall stability (i.e. 6.5 kN) was found in G_cont's PAM specimens.

6.4.3 Packing degree in PAM

VCA ratio is usually used to assess the packing degree in a PAM specimen. A corresponding simulation parameter, porosity_CP ratio, can be obtained through Equation (6.8) as well, reflecting the packing degree of the coarse fraction in a compacted PAM.

$$porosity\_CP\ ratio = \frac{porosity\_CP(MS)}{porosity\_CP(CAB)} \tag{6.8}$$

$porosity\_CP(MS)$ = porosity within the coarse particles in the PFC3D model of compacted PAM specimen, as shown in Figure 6.4;

$porosity\_CP(CAB)$ = porosity within the coarse particles in the PFC3D model of compacted coarse aggregate blend, as shown in Figure 5.5.

Table 6.11 VCA ratio and porosity_CA ratio of the four PAMs

PAM design	VCA ratio (%)	porosity_CP ratio (%)	difference (%)
G_cont	0.85	0.79	6.9
G_coarse	0.86	0.88	2.0
G_inter	0.86	0.84	2.4
G_fine	0.84	0.82	2.6

VCA ratio and porosity_CP ratio, gained through the measurement in the laboratory and DEM simulation, respectively, are given in Table 6.11. It can be seen that the difference between VCA ratio and porosity_CP ratio was relatively small except for G_cont, which was up to 6.9%. The compaction effect provided in the PFC3D model of compacted coarse aggregate blend was not high enough for a blend with continuous aggregate gradation like G_cont, resulting in the porosity_CP ratio

being lower than VCA ratio. On the other hand, a compaction procedure that provided higher compaction effect in PFC3D model, namely a surcharge (i.e. 10% of the total gravitational force) being applied on the top plate and subsequently being released stably, was carried out for G_cont. The resultant porosity_CP ratio was 0.84, and the difference as compared to VCA ratio was lowered to 0.65%, with the contacting conditions obtained through the two methods being similar in terms of MCN, SCR, and CCR. In general, both VCA ratio and porosity_CP ratio can be used to assess the packing degree of the stone-on-stone framework created by the coarse aggregates, and much tedious work in the laboratory can therefore be avoided when assessing the packing degree via DEM simulation. Meanwhile, for PAM with relatively continuously aggregate gradation in the coarse fraction, a compaction procedure provides relatively higher compaction effect is suggested.

6.5 Summary

Potential PAMs for low-strength pavement application in Singapore were designed in this chapter and the resultant properties and packing conditions were evaluated subsequently.

Firstly, according to the findings in previous chapters, PG76 asphalt and reference gyration level (i.e. P600_N50) were selected in PAM design so as to achieve relatively improved mixture strength and packing condition. Based on the gradation-permeability relationship, content of fine fraction was selected as 7% in open-graded design to meet the requirement in permeability in Singapore. Upon the different effect on the development of packing structure, aggregates in the coarse fraction were divided into three types, namely main-coarse, interceptor, and quasi-fine. Thereby four PAMs were designed, encompassing different packing structures created by the coarse aggregates: (a) G_cont, the coarse fraction was generally continuously distributed, (b) G_coarse, content of main-coarse aggregates (i.e. 19.0-6.3 mm) in the coarse fraction was high, (c) G_inter, content of interceptor aggregates (i.e. 6.3-4.75 mm) in the coarse fraction was high, and (d) G_fine, content of quasi-fine aggregates (i.e. 4.75-2.36 mm) in the coarse fraction was high.

Higher air voids content was generated as the content of main-coarse and/or interceptor aggregates was higher in PAM designs, such as G_coarse and G_inter, and WAAV ratio was larger as well, namely inter-connected air voids were generated at a higher rate within the total air voids, leading to higher permeability. Moreover, PAMs with more intermediate-size aggregates (e.g. interceptor aggregates) tended to generate air voids with the sizes more uniformly distributed in the PAM specimen, leading to more effective permeability. In terms of mechanical strength, UC-MS values in all the four PAM designs were higher than the lower limit suggested for low-strength pavement application (i.e. 4.0 kN), so were the MS values after moisture conditioning.

Packing condition in the designed PAMs was subsequently evaluated and it is found that DEM simulation can explicitly show the establishment and development of packing structure in PAMs. Firstly, a PFC3D model of compacted aggregate blend was established for each PAM design to assess the packing structure in compacted coarse aggregates. Based on the resultant simulation parameters, namely MCN, SCR, and CCR, it is found that stable contact and chain contact were gradually developed with assistance of finer fraction in the coarse fraction. Secondly, a PFC3D model of compacted PAM specimen was established for each PAM design. Based on the resultant simulation parameters, namely MPF and MPF increase ratio, it is found that large forces carried by the large-size particles (e.g. main-coarse and interceptor parts) were partially transferred by the support of finer fraction (i.e. quasi-fine part).

In both kinds of PFC3D model, it shows that packing structures in G_coarse and G_inter were mainly created by main-coarse and interceptor particles; whereas in G_fine, large-size particles in the coarse fraction tended to be scattered in the matrix of quasi-fine particles. In G_cont, a relatively stable interlocking structure was observed, reflected by the large force being mainly carried by the large-size particles and sufficient support being provided by the finer particle. Furthermore, a simulation parameter, porosity_CP ratio, was proposed to assess the packing degree in a compacted PAM specimen, possessing the similar meaning to VCA ratio obtained in the laboratory.

Chapter 7 Evaluation of PAM's performance in ravelling and clogging

7.1 Introduction

PAM is favourable in the application in wet environment due to the excellent performance in drainage, however ravelling and clogging are the two major issues directly related to the functional service life of PAM pavements. Revelling refers to finer particles being stripped from pavement surface due to degraded adhesiveness in the asphalt mastic, which might be caused by moisture, ageing or oxidation. Clogging is related to the inter-connected air voids within PAM being blocked by dust and/or debris, thereby leading to impaired drainage.

In this chapter, two kinds of experiment, namely ravelling resistance test and clogging resistance tests, were designed in three testing scenarios, namely unconditioned, ageing-conditioned, and moisture-conditioned. The results and discussion of the experimental results on the four designed PAMs (namely G_cont, G_coarse, G_fine, and G_inter) are subsequently presented.

7.2 Evaluation of PAM's performance in ravelling

7.2.1 Design of ravelling resistance test

Cantabro abrasion test is a conventional method to assess PAM's performance in resisting ravelling. To simulate the effect of ravelling, the specimen undergoes 300 revolutions in a Los Angeles (LA) machine at 25 ºC at a speed of 30-33 rpm, and the abrasion loss value (ALV) is represented as the mass loss during abrasion in percent.

However, given that most abrasion effect involved in Cantabro abrasion test is the impact between specimen and drum wall of the LA machine, which is overly severe

as compared with the practical abrasion effect on low-strength pavement surface, a reduced abrasion effect has been suggested (Dong et al. 2013). In this research, ALV values were recorded at intervals of 50 revolution counts.

Three testing scenarios were carried out:

- unconditioned

  Test was conducted as specimen was cooled down to room temperature (i.e. 25 °C) after fabrication;
- ageing-conditioned

  Specimen was conditioned in an oven at 60 ± 1 °C for seven days and cooled down later before testing; and
- moisture-conditioned

  Specimen was conditioned in a water bath at 60 ± 1 °C for 24 hours and subsequently was put in a ventilated room for one day so as to evaporate most of the moisture retained in the specimen.

The testing results are represented as unconditioned abrasion loss value (UC-ALV), ageing-conditioned abrasion loss value (AC-ALV), and moisture-conditioned abrasion loss value (MC-ALV), respectively.

7.2.2 Results and discussion of ravelling resistance test

In all the three testing scenarios, ALV value for each PAM design increased consistently with the revolution count (Figures 7.1-7.3). In the case of unconditioned Cantabro abrasion test, all four PAM designs can meet the 20% requirement in UC-ALV's upper limit. The PAM design with a high content of quasi-fine aggregates in the coarse fraction, namely G_fine, showed the strongest resistance to Cantabro abrasion among the four designs, and its final UC-ALV value after the total 300 revolutions was lower than 10%, followed by G_inter, G_cont, and G_coarse. This suggests that stronger resistance to Cantabro abrasion can be achieved with higher content of relatively finer aggregates (namely quasi-fine aggregates and interceptor aggregates) in the coarse fraction, while PAM

designs with more main-coarse aggregates, such as G_coarse, showed weaker resistance in maintaining integrity of the specimens during Cantabro abrasion.

Due to the high air voids content in PAM, ageing and oxidation in asphalt binder tended to occur more rapidly as compared to dense asphalt mixture, resulting in larger reduction in the adhesiveness of asphalt mastic and weaker resistance to abrasion (Herrington et al. 2005; Alvarez et al. 2010b). In the case of ageing-conditioned Cantabro abrasion test, AC-ALV values in all PAM designs were lower than the 30% upper limit. For G_coarse and G_inter, AVL values after ageing conditioning were slightly larger than that in the unconditioned scenario, and the corresponding increases were 6.3% and 13.4%, respectively. For G_cont, the resistance to Cantabro abrasion after ageing condition was well retained as that in unconditioned scenario.

On the other hand, AC-ALV value of G_fine was almost 1.9 times higher than its UC-ALV value, indicating ageing conditioning was more severe for PAMs with a high content of quasi-fine aggregates in coarse fraction as compared with the packing structures created in the other three PAM designs. This is probably due to the relatively thinnest asphalt film in G_fine, given that the total surface area of aggregates in G_fine was the largest for the high content of quasi-fine aggregates in the aggregate gradation and the asphalt binder content was the same (namely 4%) among the four PAMs. Consequently, adhesiveness in asphalt binder degraded most in G_fine during ageing conditioning and engendered high AC-ALV value, as consistent with the findings by Suresha et al. (2010).

In the case of moisture-conditioned Cantabro abrasion test, the PAM specimens of all the four designs were harshly degraded after 300 revolutions, with MC-ALV values being larger than 70%, indicating that moisture exposure is a serious issue in Cantabro abrasion. On the other hand, MC-ALV at low revolution counts, such as 50, 100, or 150 revoluations, can be applied in assessing PAM's resistance to ravelling, given that the breakage effect of Cantabro abrasion would be much more severe as compared with the practical ravelling effect on the pavement surface. It can been seen that, for all the four PAM designs, MC-ALV values were lower than 20% at 50 revolutions and started to become higher than 40% at 150 revolutions.

On the other hand, the relatively low content of asphalt binder might contribute to the weak resistance to Cantabro abrasion in moisture conditioning. Hence, a higher asphalt binder is suggested to better balance asphalt and filler contents and to prevent the early distress in PAM pavements. Meanwhile, along the whole process of Cantabro abrasion, MC-ALV in G_fine was the lowest, followed by G_inter, G_cont, and G_coarse, which is similar to the case in unconditioned scenario.

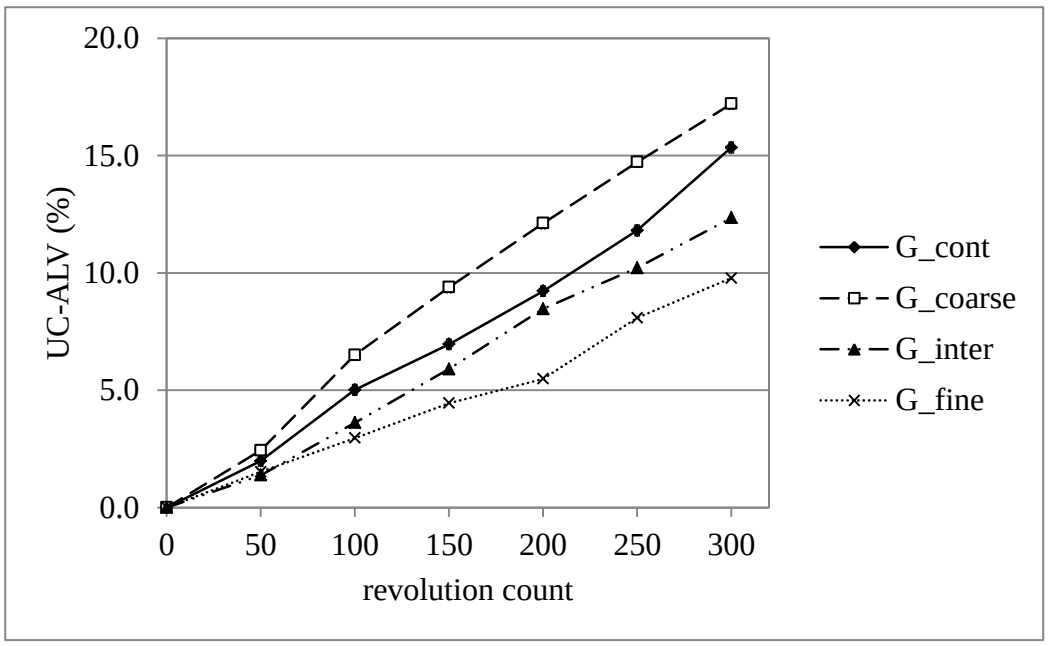

Figure 7.1 Results of Cantabro abrasion test with no conditioning

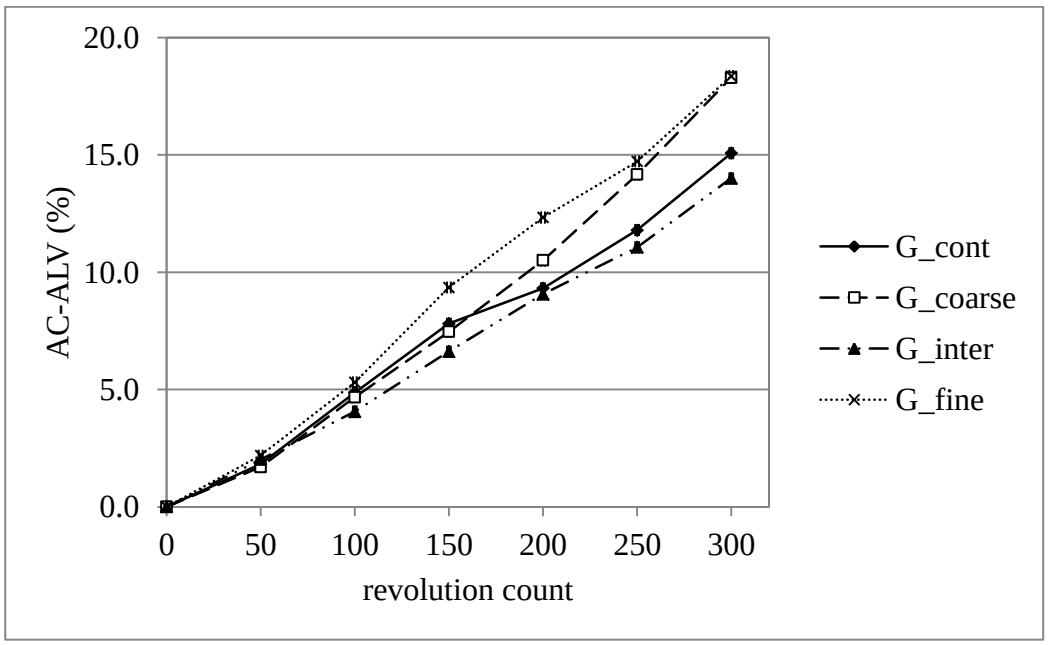

Figure 7.2 Results of Cantabro abrasion test after ageing conditioning

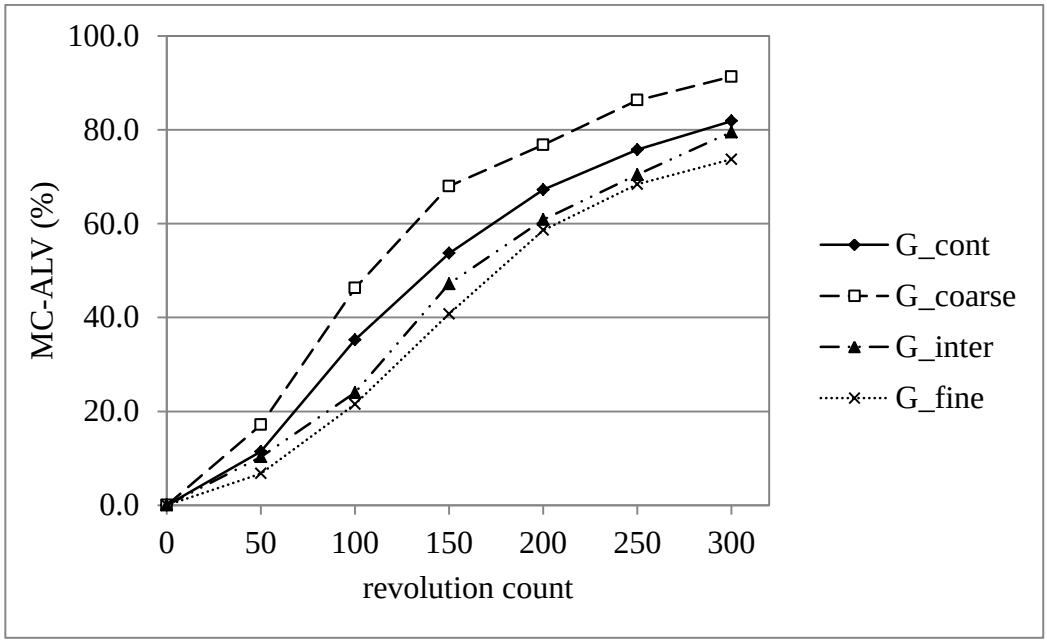

Figure 7.3 Results of Cantabro abrasion test after moisture conditioning

On the whole, PAM's resistance to Cantabro abrasion is strongly related to the packing structures created by coarse aggregates. In unconditioned and moisture-conditioned scenarios, PAM specimens with a higher content of quasi-fine or interceptor aggregates showed stronger resistance during the process of Cantabro abrasion. Meanwhile, PAM's resistance to abrasion was affected by the adhesiveness of asphalt binder as well. In ageing-conditioned scenario, thinner asphalt film tended to be oxidised more rapidly and resulted in weaker resistance to abrasion, as shown in the PAM specimens of G_fine design.

7.3 Evaluation of PAM's performance in clogging

7.3.1 Design of clogging resistance test

Clogging is another critical problem with PAM, referring to the deterioration in permeability due to dust and/or debris blocking the air voids in PAM. However, there is no widely-accepted test which has been approved for evaluating PAM's performance in resisting clogging. Based on previous research work (Fwa et al. 1999; Tan et al. 2000), a process of clogging/de-clogging was designed, and the effect on PAM's permeability was measured so as to evaluate PAM's performance in resisting clogging.

Two batches of granite dust with different size distributions were applied as clogging material (CM), namely CM1 and CM2, possessing the maximum particle size of 600 μm and 300 μm, respectively (Figure 7.4).

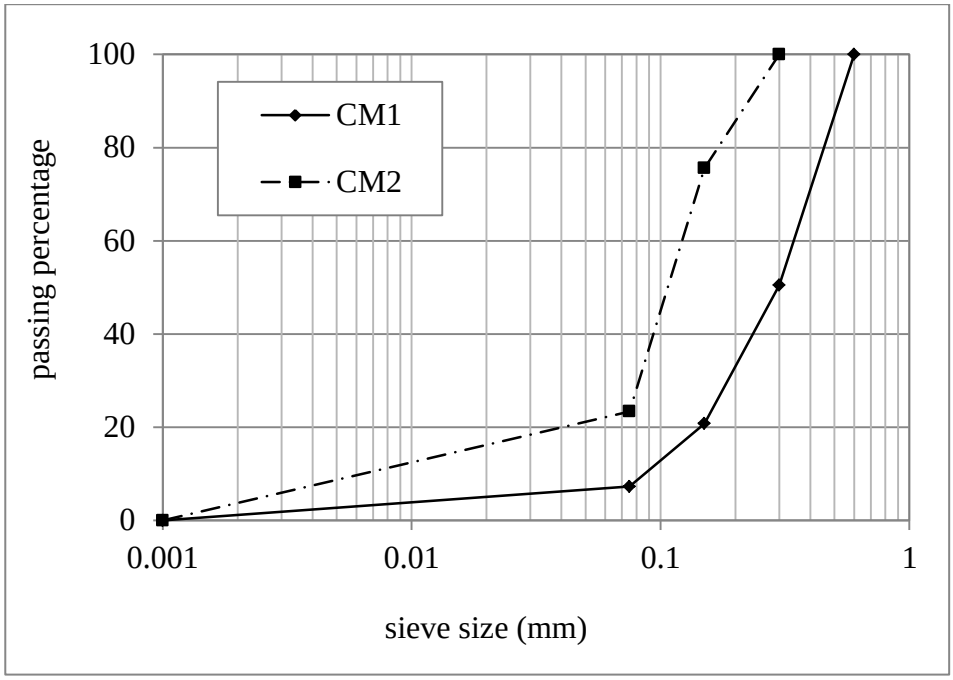

Figure 7.4 Gradation of the two clogging materials

The testing procedure is as follows:

(a) place PAM specimen in the permeability testing apparatus;

(b) clogging/de-clogging cycle

- *clogging process:* scatter 5 *grams* CM on the specimen surface uniformly and subsequently apply 100 *ml* water to make CM penetrate into the specimen, and permeability is measured after clogging;
- *de-clogging process:* apply 2,000 *ml* water through the specimen as a de-clogging process and measure the permeability meanwhile, and repeat the de-clogging process 5 times to record the permeability recovery;

(c) repeat clogging/de-clogging cycle 5 times.

Three testing scenarios were involved in clogging resistance tests as well, namely unconditioned, ageing-conditioned, and moisture-conditioned, and the conditioning

methods for ageing and moisture cases were the same as that in ravelling resistance test. Retained permeability (i.e. retained *k* value) was calculated along the process of clogging/de-clogging process through Equation (7.1).

$$retained\ k = \frac{k_2}{k_1} \times 100\% \tag{7.1}$$

k_1 = the initial coefficient of permeability, namely the one without conditioning or clogging/de-clogging;

k_2 = the coefficient of permeability after conditioning or clogging/de-clogging.

7.3.2 Results and discussion of clogging resistance test

Two kinds of clogging material, namely CM1 (<600 μm) and CM2 (<300 μm) were applied to assess PAM's resistance to clogging, namely the capability in retaining permeability, in the unconditioned scenario. It can be seen that permeability decreased upon clogging, and gradually recovered partially during the process of de-clogging, which was simulated via flushing with 2,000 *ml* water (Figures 7.5-7.12). As compared with CM1, permeability tended to be recovered to a higher degree for each PAM design using CM2, given that finer size particles are easier to be flushed out from the PAM specimens. Considering that permeability tended to be largely recovered after clogging/de-clogging process with CM2 as clogging material, CM1 with coarser particles was applied to assess PAM's resistance to clogging in the more severe ageing-conditioned and moisture-conditioned scenarios. The results are given in Figures 7.13-7.20.

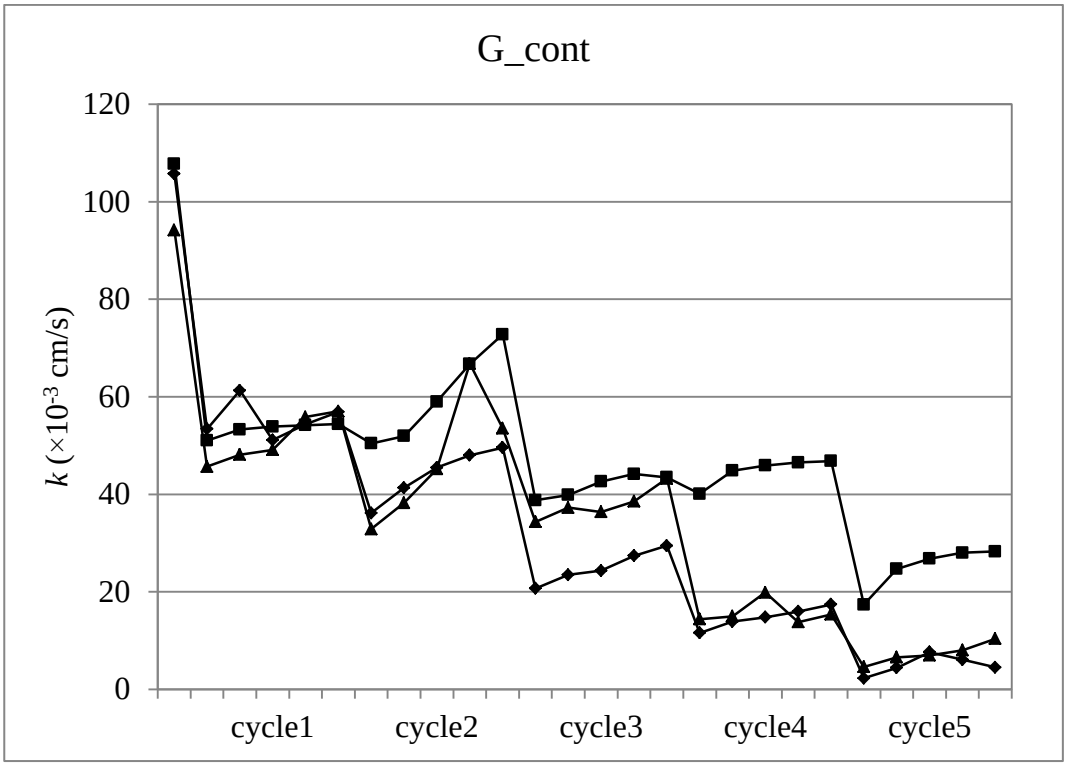

Figure 7.5 Results of clogging resisting test for G_cont design with no conditioning (using CM1)

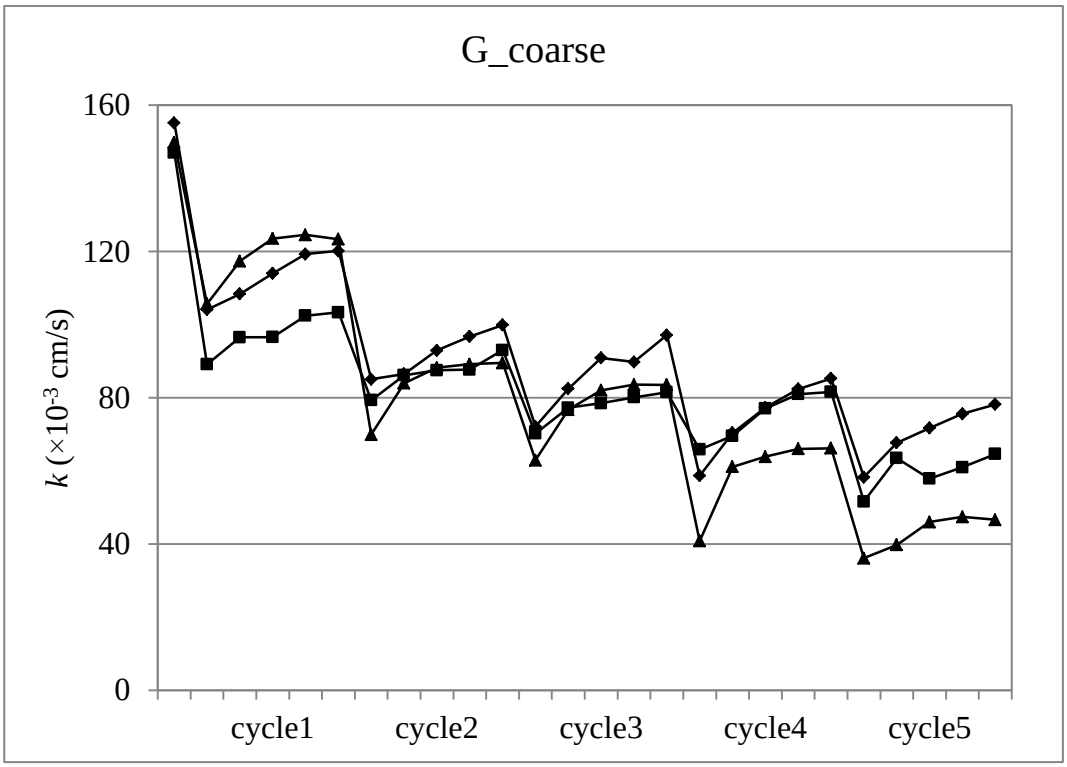

Figure 7.6 Results of clogging resisting test for G_coarse design with no conditioning (using CM1)

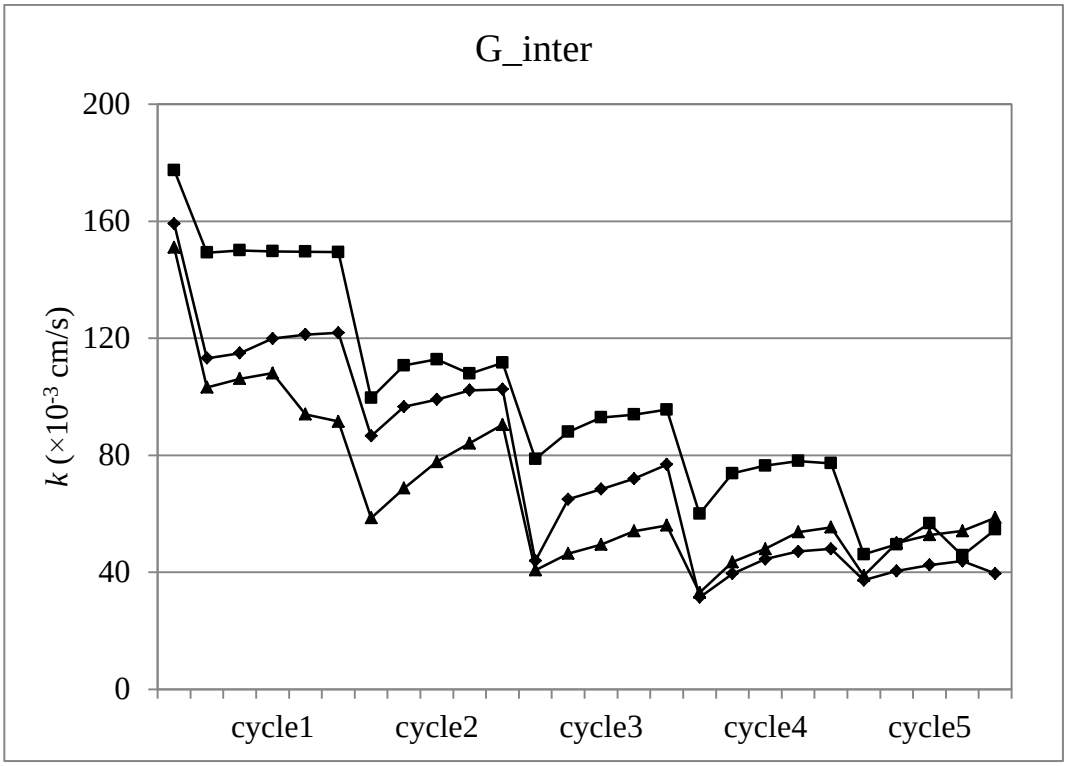

Figure 7.7 Results of clogging resisting test for G_inter design with no conditioning (using CM1)

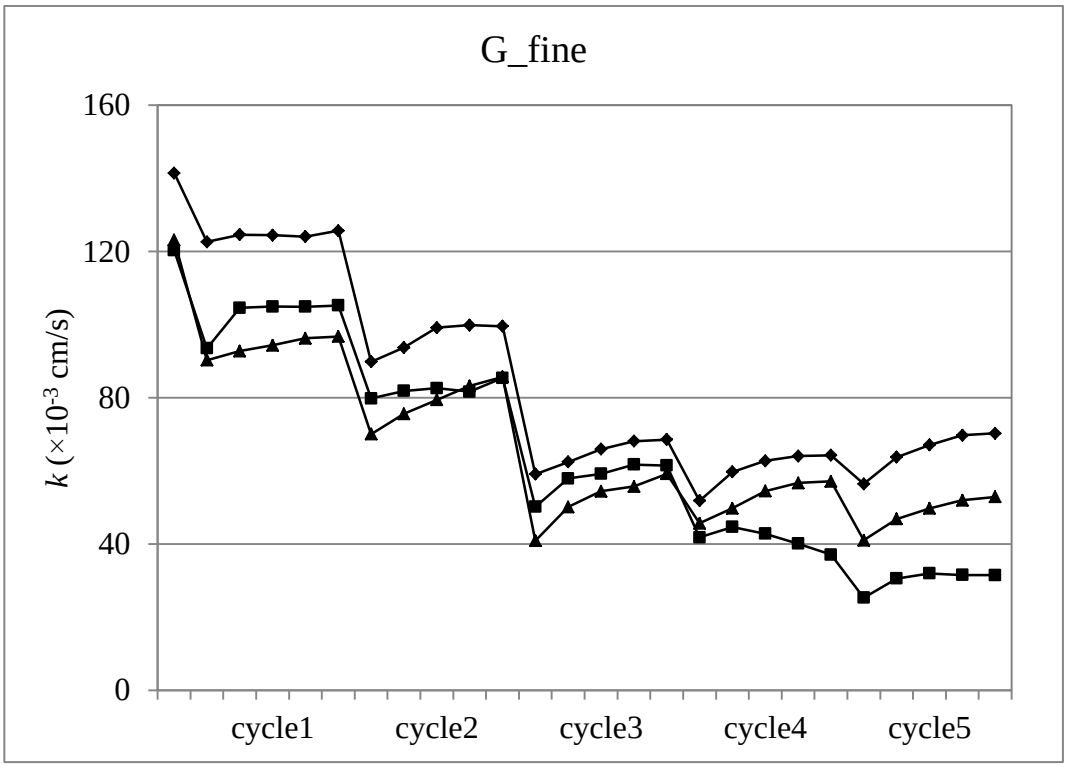

Figure 7.8 Results of clogging resisting test for G_fine design with no conditioning (using CM1)

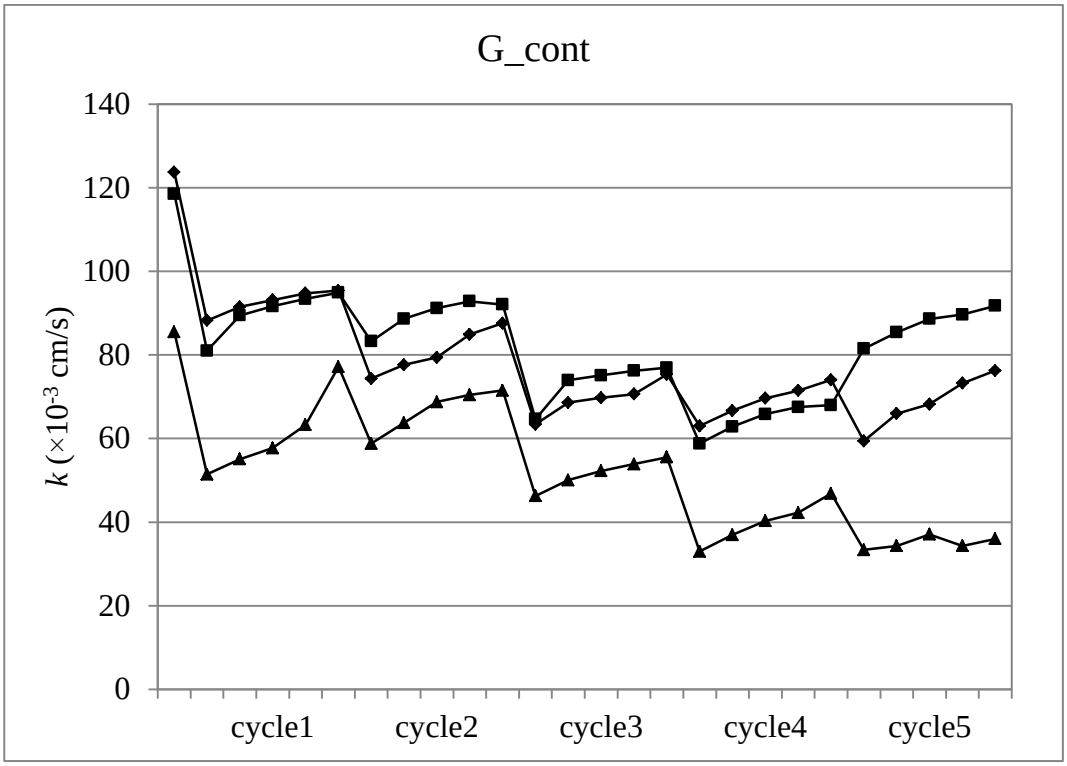

Figure 7.9 Results of clogging resisting test for G_cont design with no conditioning (using CM2)

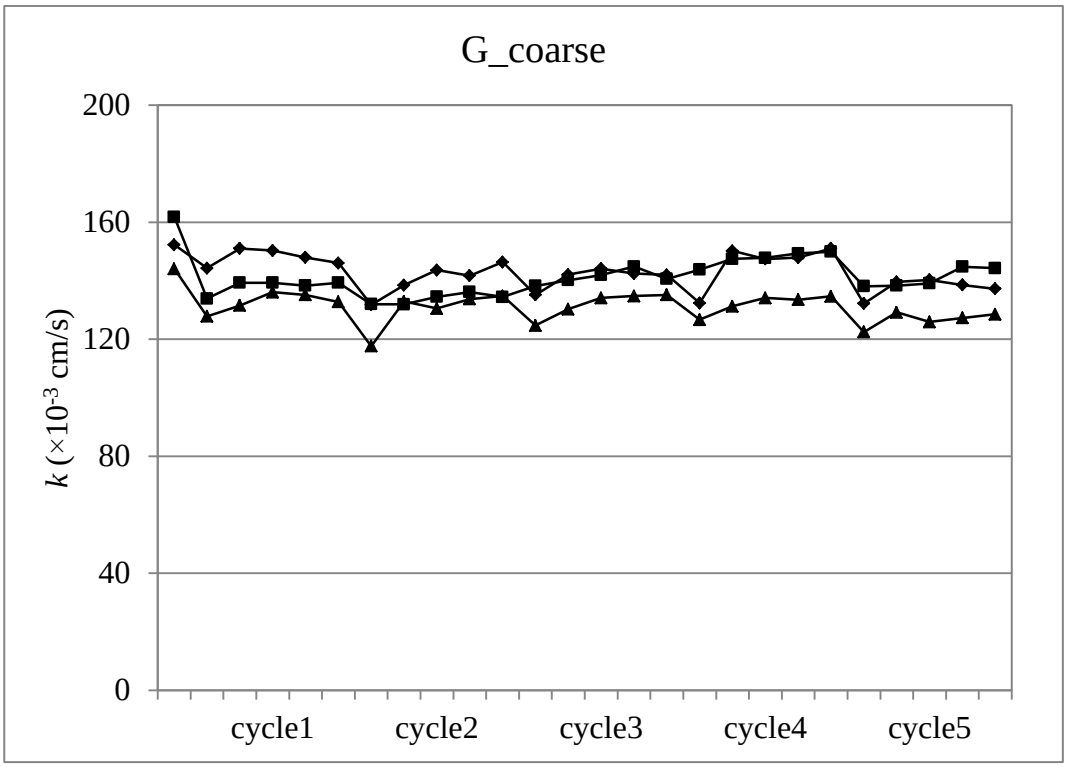

Figure 7.10 Results of clogging resisting test for G_coarse design with no conditioning (using CM2)

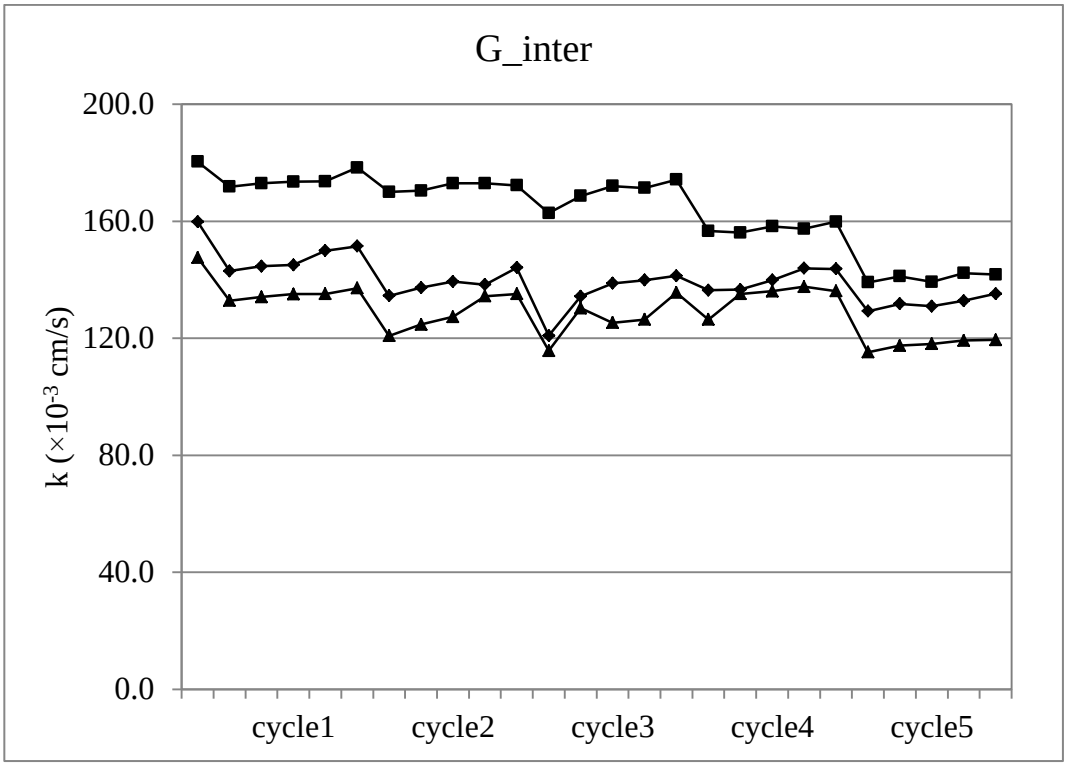

Figure 7.11 Results of clogging resisting test for G_inter design with no conditioning (using CM2)

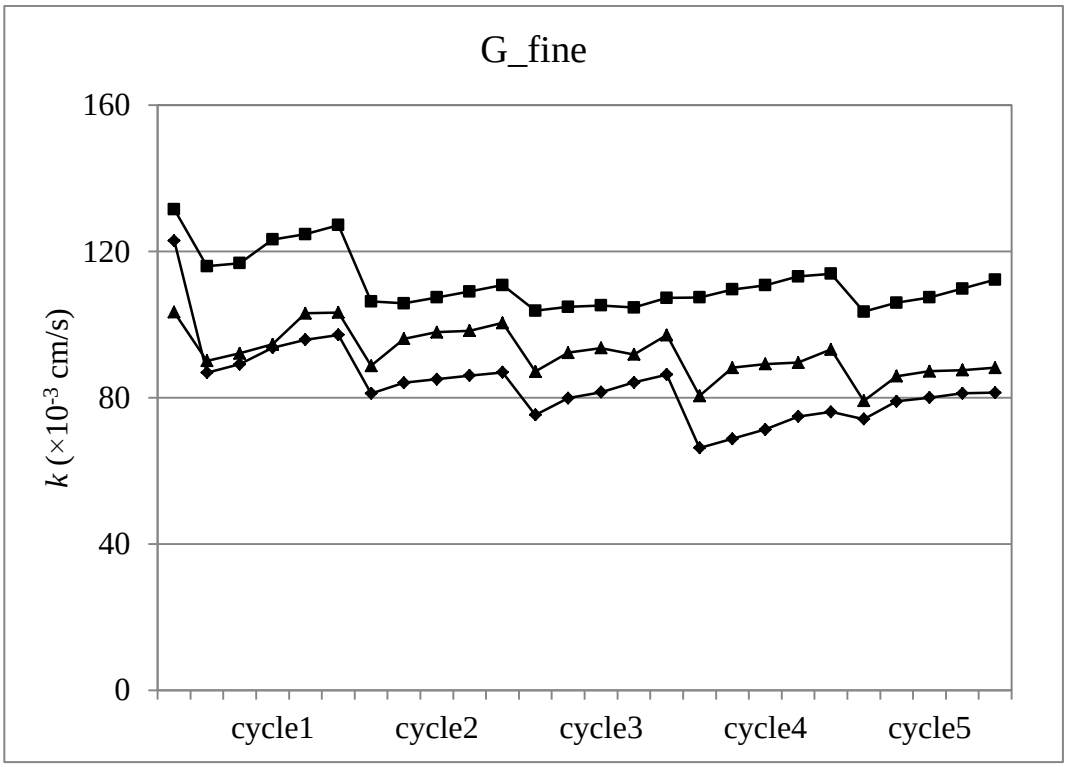

Figure 7.12 Results of clogging resisting test for G_fine design with no conditioning (using CM2)

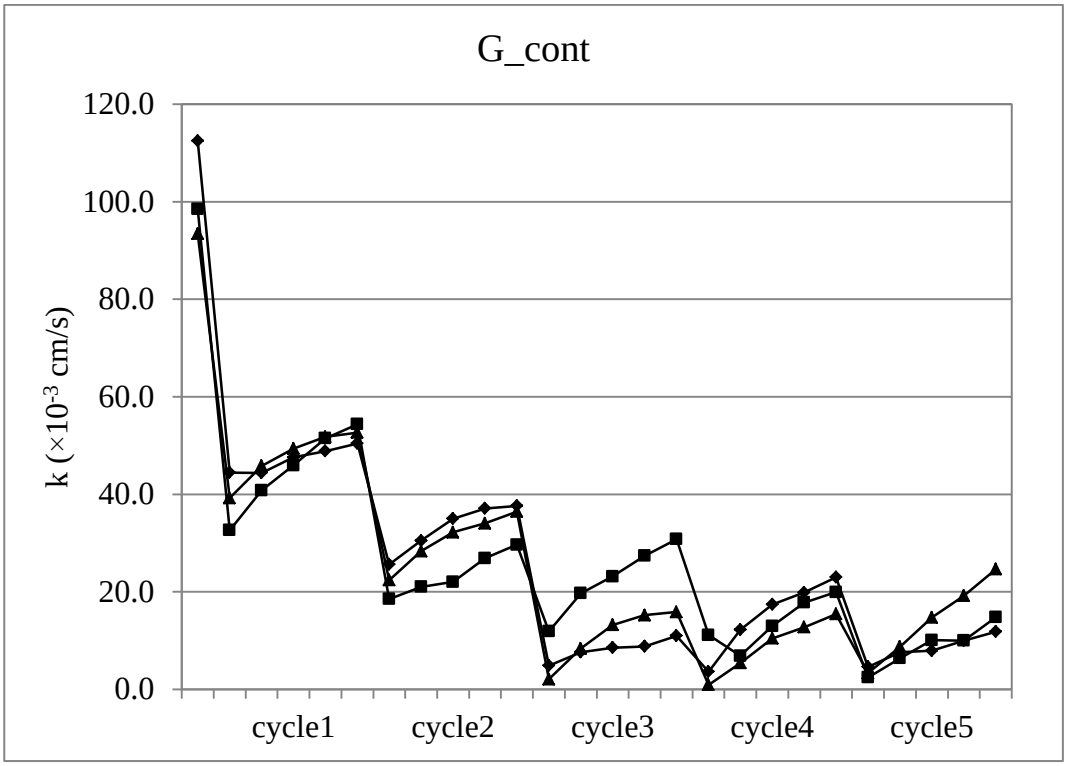

Figure 7.13 Results of clogging resisting test for G_cont design after ageing conditioning (using CM1)

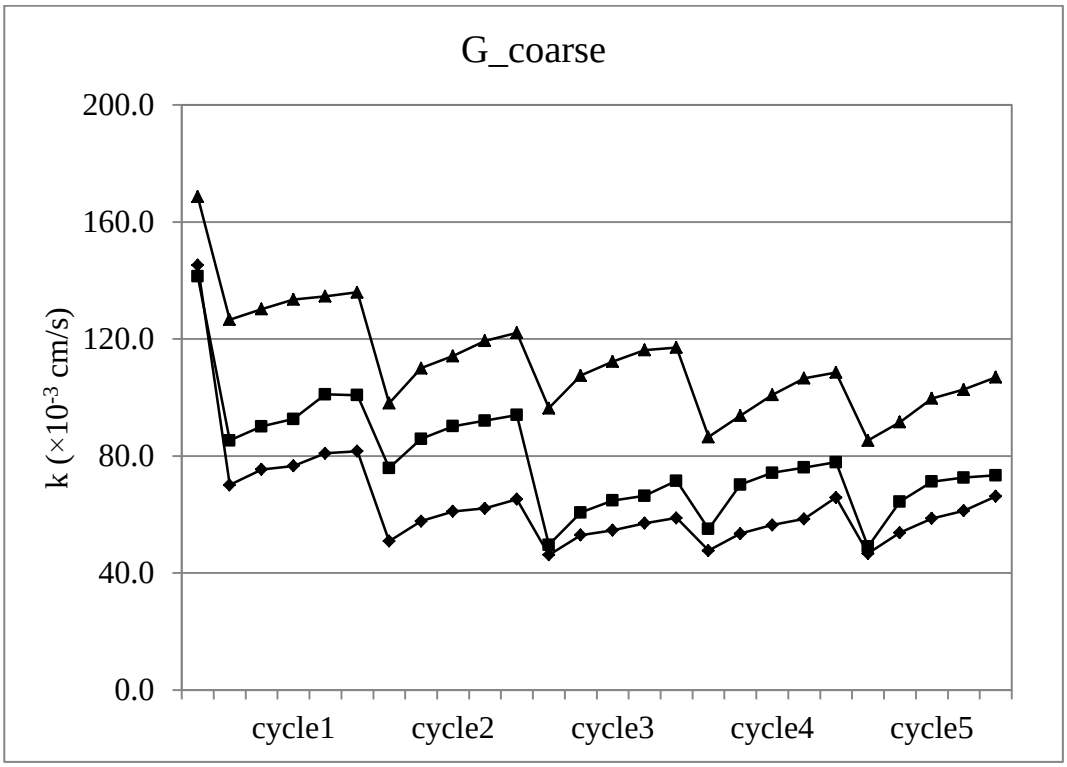

Figure 7.14 Results of clogging resisting test for G_coarse design after ageing conditioning (using CM1)

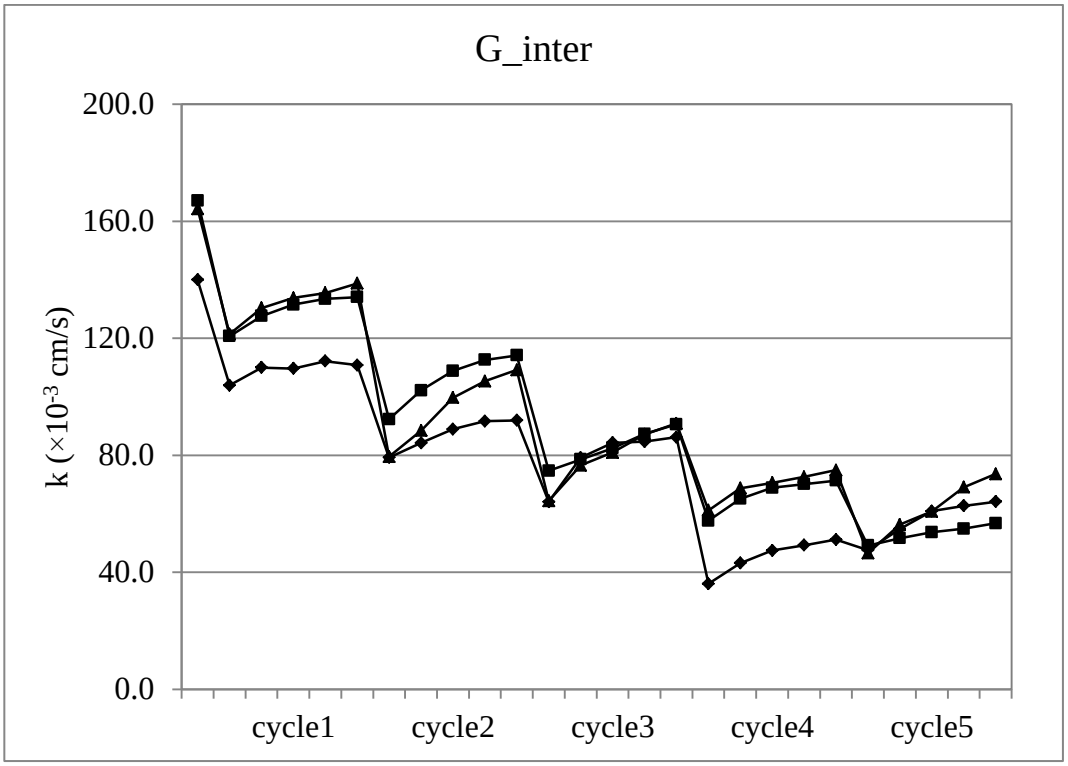

Figure 7.15 Results of clogging resisting test for G_inter design after ageing conditioning (using CM1)

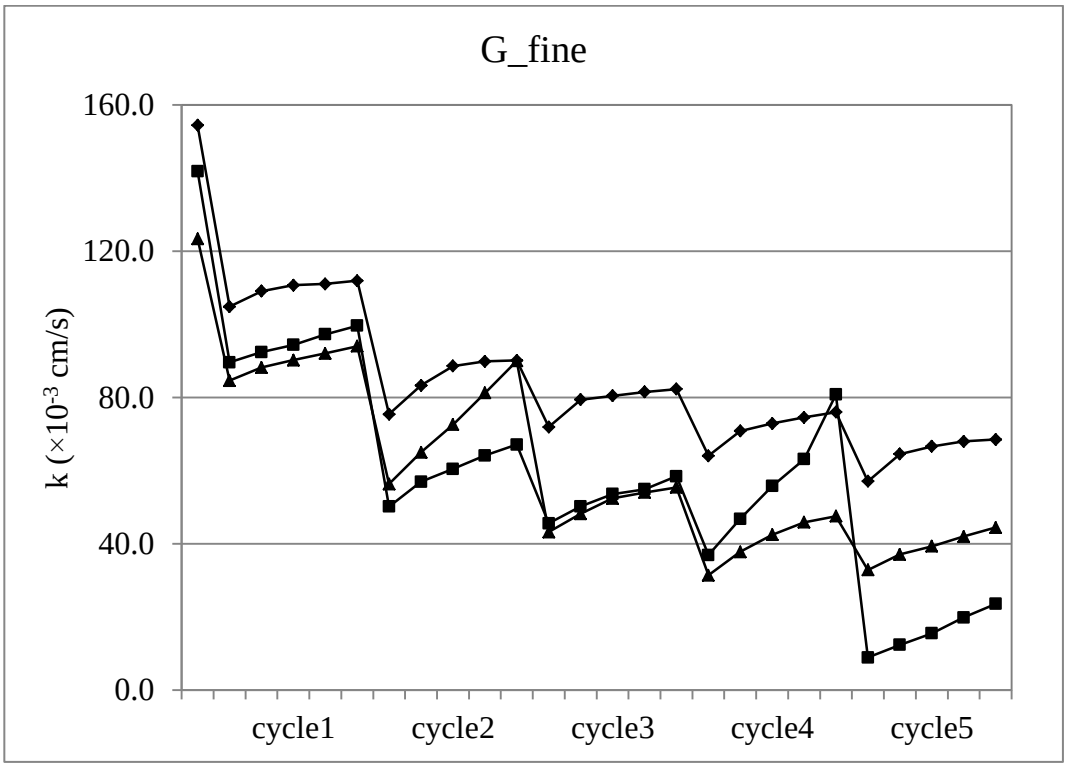

Figure 7.16 Results of clogging resisting test for G_fine design after ageing conditioning (using CM1)

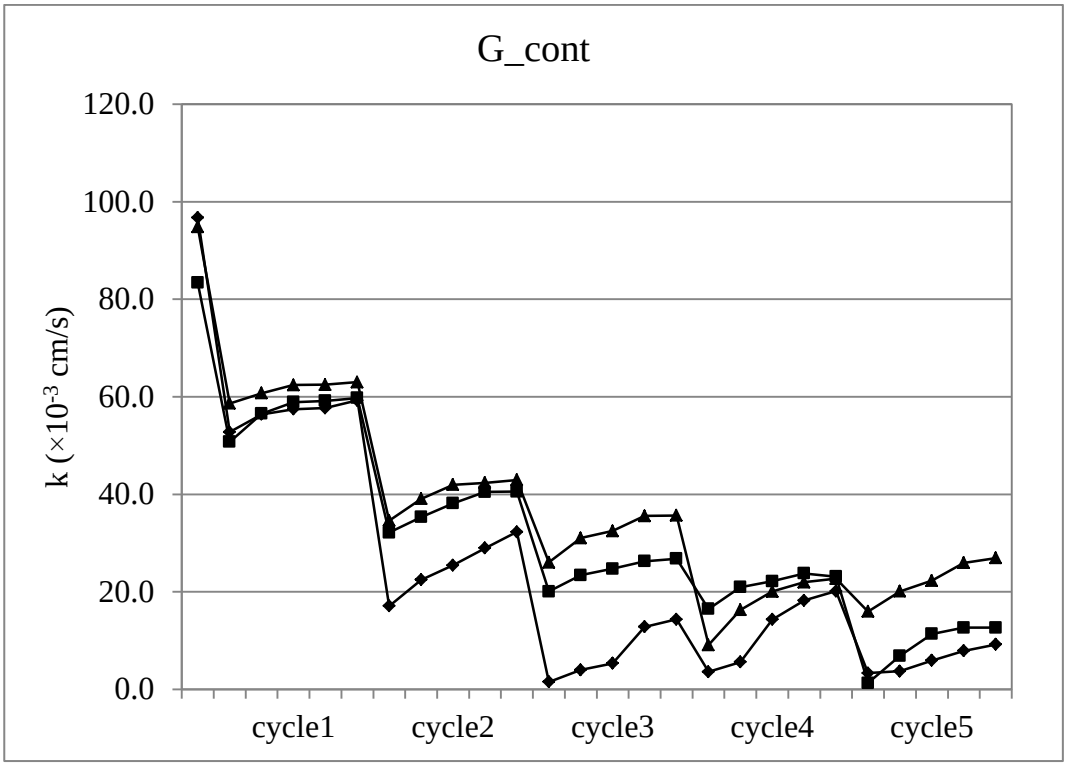

Figure 7.17 Results of clogging resisting test for G_cont design after moisture conditioning (using CM1)

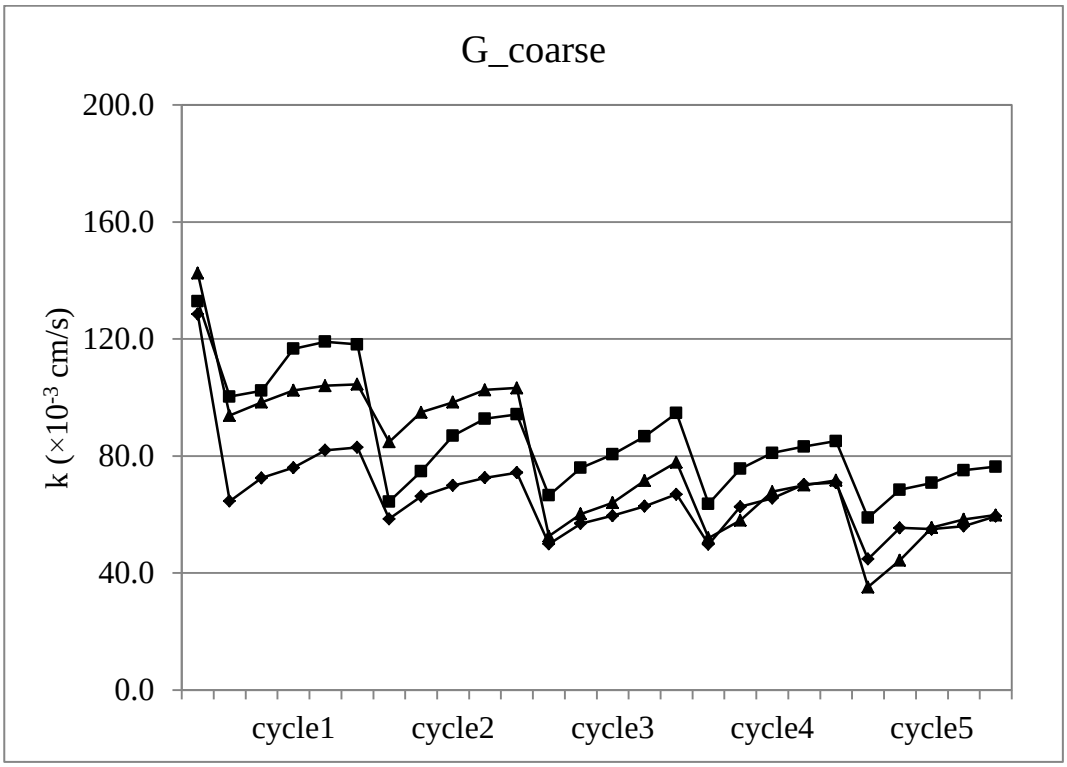

Figure 7.18 Results of clogging resisting test for G_coarse design after moisture conditioning (using CM1)

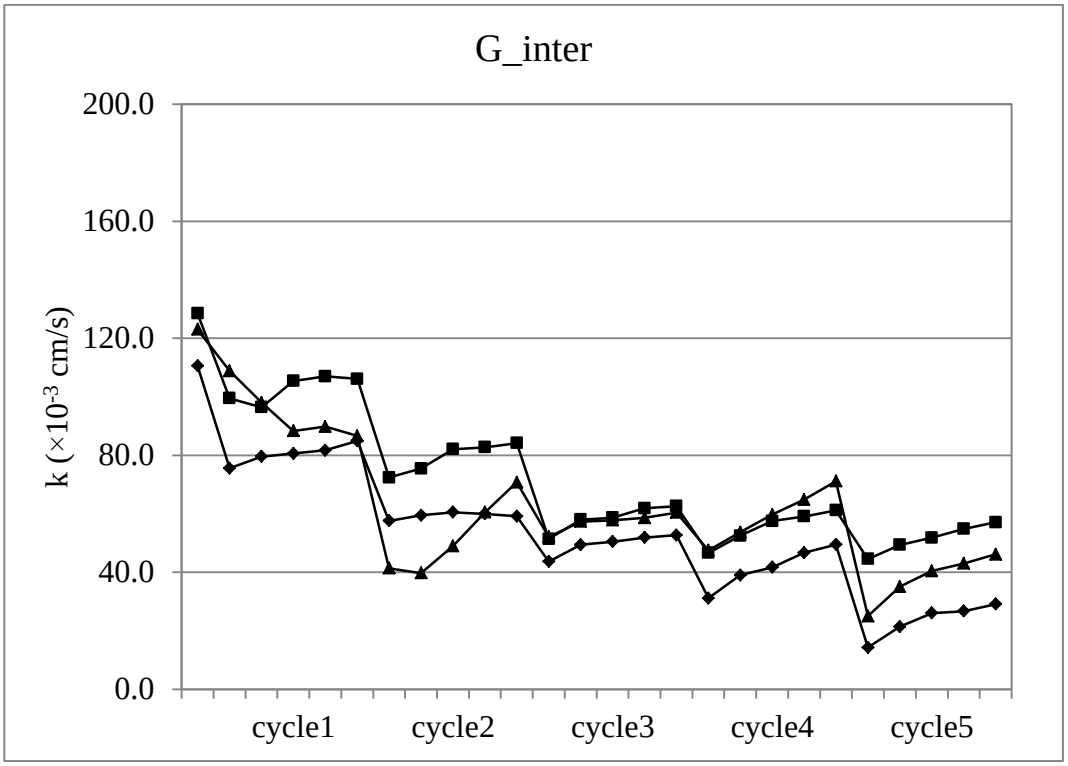

Figure 7.19 Results of clogging resisting test for G_inter design after moisture conditioning (using CM1)

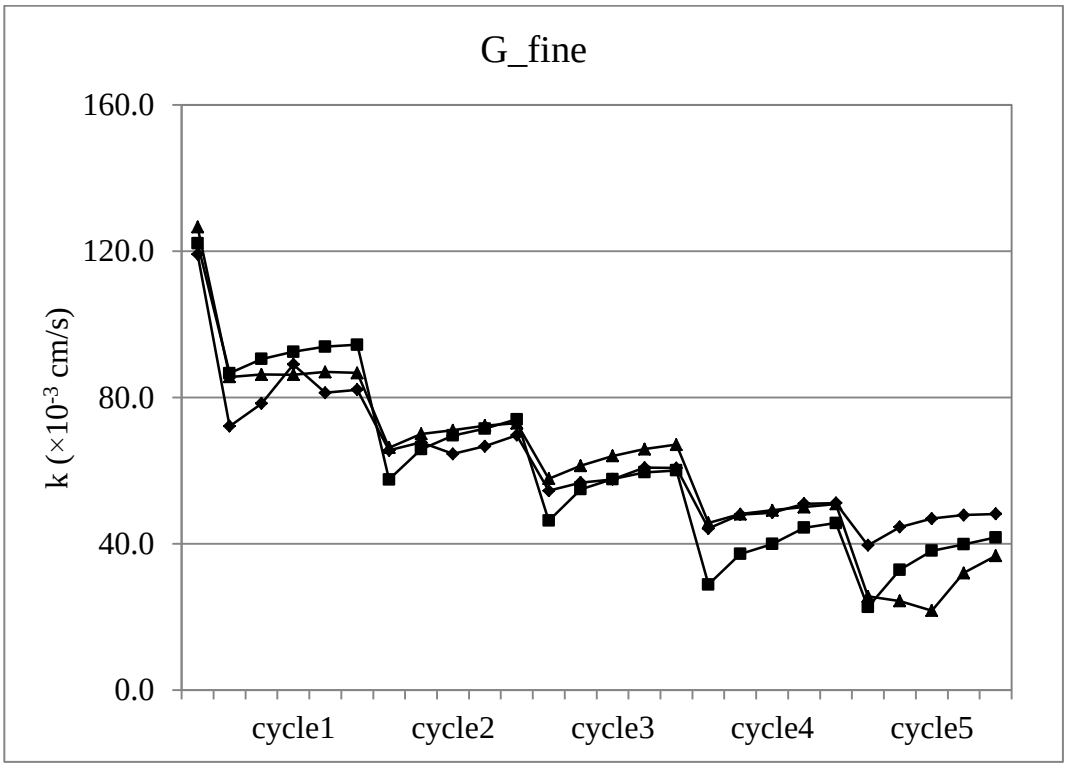

Figure 7.20 Results of clogging resisting test for G_fine design after moisture conditioning (using CM1)

It can be seen that after ageing-conditioning (without clogging/de-clogging process), retained *k* values all remained very high in the four PAM designs as compared with the retained *k* values after moisture-conditioning (Table 7.1), indicating moisture exposure had the more severe effect in impairing PAM's drainage capability. However, in each PAM design, the development of *k* value along the process of clogging/de-clogging process was similar to that in unconditioned scenario, resulting in the final *k* values (after five cycles of clogging/de-clogging process) being very similar among all three scenarios. In terms of *k* value after conditioning (i.e. ageing conditioning or moisture conditioning), G_coarse still possessed the highest permeability, followed by G_inter, G_fine, and G_cont, which is similar to the case in unconditioned scenario. It is indicated that, as compared with PAMs containing more quasi-fine aggregates in coarse fraction, PAMs with higher content of main-coarse aggregates and/or interceptor aggregates possessed better resistance to clogging, namely a higher permeability is achieved over clogging/de-clogging process, which is probably attributed to the air voids of larger size and at higher content that are generated by the larger aggregates in the PAM specimens.

Table 7.1 Results of retained permeability

PAM design	clogging material	condition-ing	retained *k* (%)		*k* ($\times 10^{-3}$ cm/s)
			after conditioning	after five cycles	after five cycles
G_cont	CM1	no	/	13.8 (±9.2)	14.4 (±17.1)
	CM2	no	/	60.4 (±14.4)	68.0 (±10.1)
	CM1	ageing	93.1 (±3.2)	15.9 (±5.5)	17.1 (±7.7)
	CM1	moisture	76.4 (±3.7)	13.7 (±6.6)	16.2 (±23.5)
G_coarse	CM1	no	/	41.8 (±8.0)	63.1 (±82.2)
	CM2	no	/	89.5 (±0.4)	136.7 (±12.9)
	CM1	ageing	94.3 (±3.2)	50.8 (±8.4)	82.2 (±7.9)
	CM1	moisture	86.1 (±2.0)	41.7 (±5.0)	65.2 (±6.4)
G_inter	CM1	no	/	31.5 (±5.7)	50.9 (±64.8)
	CM2	no	/	81.4 (±2.5)	132.1 (±8.2)
	CM1	ageing	98.1 (±4.1)	40.6 (±4.6)	64.8 (±11.5)
	CM1	moisture	75.8 (±4.6)	27.6 (±6.8)	44.1 (±9.4)
G_fine	CM1	no	/	39.6 (±9.9)	51.5 (±45.5)
	CM2	no	/	79.0 (±9.0)	93.9 (±15.9)
	CM1	ageing	99.5 (±2.7)	31.9 (±11.0)	45.5 (±4.7)
	CM1	moisture	92.1 (±3.3)	31.7 (±3.4)	42.2 (±13.2)

The aggregates used in this research possess high LA abrasion value, which might be broken down in case of heavy trafficked roads, leading to particle loss, ravelling and closing up the air voids, while they might still be feasible for low-strength application for pedestrian/cyclist pathways.

Additionally, it is suggested to regularly remove the dust and/or debris on the surface of or inside the PAM pavements by means of relevant cleaning machines, such as high-pressure jets of water and vacuum suction, so as to maintain acceptable drainage performance especially during monsoon periods.

7.4 Summary

Two types of experiment are designed in this chapter to measure PAM's resistance to ravelling and clogging in three testing scenarios, namely unconditioned, ageing-conditioned, and moisture-conditioned.

In the aspect of ravelling resistance, all the four designed PAMs (G_cont, G_coarse, G_fine, and G_inter) can meet the requirements suggested for unconditioned and ageing-conditioned Cantabro abrasion tests. In the case of moisture-conditioned scenario, more severe breakage occurred after the process of abrasion (over 300 revolutions), and the results indicated moisture conditioning impaired the adhesiveness between aggregates and asphalt mastic more harshly than ageing conditioning. In unconditioned and moisture-conditioned scenarios, PAM specimens of G_fine design, namely the aggregate gradation containing more quasi-fine aggregates, possessed the strongest resistance to Cantabro abrasion, followed by G_inter, G_cont, and G_coarse. In the case of ageing conditioning, weight loss in G_fine specimen during Cantabro abrasion was largely increased as compared with that in unconditioned case, being attributed to the large reduction in adhesiveness of asphalt binder due to the thinner asphalt film.

In addition, a lower revolution count is suggested for assessing PAM's resistance abrasion, such as 50, 100, or 150 revolutions, since the abrasion in Cantabro abrasion is much more severe than practical ravelling in the field.

On the aspect of clogging resistance, retained permeability after moisture conditioning in each PAM design was lower than that after ageing conditioning, indicating moisture is a more serious condition for PAM's clogging resistance as compared to ageing, which is similar to ravelling resistance. G_coarse showed the highest permeability along the clogging/de-clogging process among the four PAM designs, which was attributed to the higher content of large-size air voids created by high content of large-size aggregates (namely main-coarse aggregates) in coarse fraction.

The overview performance of the four designed PAMs is given in Table 7.2. The four PAM designs all showed adequate mechanical strength in terms of Marshall stability. In terms of permeability, PAMs with higher content of air voids content, namely G_coarse and G_inter, possessed sufficient initial permeability, while G_inter showed stronger resistance to ravelling in the three testing scenarios. Thereby, PAM with fine fraction at 7% and 'S-shape' in the gradation curve of coarse fraction, namely with high content of interceptor aggregates, and fabricated with modified asphalt (such as PG76 asphalt) at reference gyration level (namely P600_N50), is recommended for the low-strength pavement application in Singapore.

Table 7.2 Overview performance of the four PAM designs*

PAM design	initial permeability	Marshall stability	ravelling resistance			clogging resistance		
			no_c	age_c	moi_c	no_c	age_c	moi_c
G_cont	×	√	Δ	√	×	×	×	×
G_coarse	√	√	Δ	√	×	√	√	√
G_inter	√	√	√	√	×	√	√	Δ
G_fine	×	√	√	√	×	√	Δ	Δ

* '√'=good, 'Δ'=fair, '×'=poor, no_c=without conditioning, age_c=after ageing condition, and moi_c=after moisture conditioning

As compared to ageing, moisture is a more severe condition for PAM's resistance to ravelling and clogging. Thus additives to enhance PAM's resistance to moisture-related damage are recommended.

Chapter 8 Conclusions and future work

8.1 Summary of the main findings

The main objective of this research work is to obtain suitable PAM design for pedestrian/cyclist pathways in Singapore, covering five specific research issues: the impact of design factors on PAM's properties, the role of coarse aggregates in PAM's packing condition, design of potential PAMs for the specific application, simulation parameters in assessing PAM's packing structure, and experimental methods in the aspects of ravelling and clogging. The key findings concluded in this thesis are summarised as follows.

The impact of design factors on PAM's properties

To investigate the impact of design factors on PAM's properties, three critical design factors, namely aggregate gradation (G), gyration compaction level (GCL), and asphalt binder type (ABT), were selected, generating a total of 48 PAMs designed at eight Gs (denoted as G1~G8), three GCLs (denoted as P600_N50, P300_N100, and P300_N50, meaning compaction pressure at 600 kPa of 50 counts, 300 kPa of 100 count, 300 kPa of 50 counts, respectively), and two ABTs (i.e. Pen 60/70 and PG 76 asphalt binders).

On the aspect of PAM's air voids content, both total air voids (TAV) content and water-accessible air voids (WAAV) content were dependent on the three design factors. Less dense structure in PAM can be achieved by lower GCL and/or using Pen 60/70 asphalt binder. Especially, air voids content increased with the reduction in the content of aggregates finer than 2.36 mm, while no consistent relationship was formed for the content of aggregates finer than 4.75 mm, indicating it is more suitable to regard 2.36 mm as the breaking sieve (BS) size herein, instead of 4.75 mm.

PAMs' performance in permeability was enhanced with the increase in air voids content, and there is no obvious trend that WAAV content possessed a stronger relationship with the coefficient of permeability, *k*, as compared to TAV content, since WAAV content is approximately linearly related to TAV content.

Weaker performance in the mechanical tests, namely Cantabro abrasion test, Marshall test, and indirect tensile stiffness modulus (ITSM), was found in the PAMs with lower content of passing 2.36 mm aggregates and/or compacted at lower GCL. However, application of modified asphalt, namely PG 76 asphalt, can improve PAM's strength and durability, and the corresponding performance after moisture-conditioning and age-conditioning as well.

On the whole, PAM's properties, namely permeability and mechanical performance, are significantly influenced by the three factors (namely G, GCL, and ABT) and the interactions between them as well, while expected air voids content is easier to be achieved by proper open-graded design, given aggregate gradation is a relatively unstructured factor.

The role of coarse aggregates in PAM's packing condition

Packing structure in asphalt mixture is principally provided by the particle-to-particle framework created by the coarse aggregates, especially for PAM in which content of fine fraction is much lower. Packing condition in the coarse fraction of the eight selected gradation designs were evaluated by both means of laboratory measurements and DEM simulation. In the laboratory, four kinds of aggregate blends were prepared with finer aggregates being added stepwise, denoted as Blend-1~Blend-4. In DEM simulation, corresponding PFC3D models were established, which were Model-1~Model-4.

Based on the analysis of the effect on the packing condition, coarse aggregates within different size ranges were divided into three types:

(a) main-coarse (i.e. 19.0-6.3 mm aggregates), as providing coarse particles in the stone-on-stone framework and the densest aggregate structure can be achieved by

proper proportioning (i.e. the ratio among 19.0-13.2 mm, 13.2-9.5 mm, and 9.5-6.3 mm aggregates);

(b) interceptor (i.e. 6.3-4.75 mm aggregates), in which no clear relationship exists between the interceptor content and voids content in the compacted aggregate blend, and the size being not fine enough to fit in the voids created by coarser fraction; and

(c) quasi-fine (i.e. 4.75-2.36 mm aggregates), in which a higher quasi-fine content tended to decrease voids content in the compacted aggregate blend, whilst an overly high content (e.g. larger than 25% in an aggregate blend) could shove apart the stone backbone formed by the coarser aggregates.

Subsequently, the development of packing structure in the coarse fraction was evaluated in the corresponding PFC3D models, and it is found that the simulation parameter, mean coordination number (MCN), is useful in describing the particle-to-particle contacting mechanism. Among an assembly of particles, a stable packing structure can be presented by a MCN value larger than 4.0 and a chain contact pattern can be indicated by a MCN value around 2.0.

Design of potential PAMs for the specific application

According to the preceding findings, PG76 asphalt and reference gyration compaction level (namely P600_N50) were selected in PAM design so as to achieve relatively improved mixture strength and packing condition. Based on the gradation-permeability relationship, content of fine fraction was selected as 7% in open-graded design to meet the requirement in permeability in Singapore, namely 130 $\times 10^{-3}$ cm/s. Given the three types of coarse aggregates in the packing condition, namely main-coarse, interceptor, and quasi-fine, four PAMs were designed: (a) G_cont, the coarse fraction was generally continuously distributed, (b) G_coarse, main-coarse aggregates were dominant in the coarse fraction, (c) G_inter, interceptor aggregates were dominant in the coarse fraction, and (d) G_fine, quasi-fine aggregates were dominant in the coarse fraction.

In terms of the essential function of PAM, namely effective drainage, G_coarse and G_inter performed better in permeability test, which was attributed to the relatively

higher air voids content, resulting from the higher content of main-coarse and/or interceptor aggregates. Meanwhile the WAAV ratios were relatively larger in G-coarse and G_inter as well, meaning inter-connected air voids were generated at a higher rate within the total air voids, contributing to the higher permeability. In addition, G_inter possessed higher permeability than G_coarse, which was due to the air voids with size being more uniformly distributed in the PAM specimens, resulting from the high content of intermediate-size aggregates (e.g. interceptor aggregates). On the aspect of application, all the four PAMs met the requirement in mixture strength for low-strength pavement application, namely possessing the UC-MC values no lower than 4.0 kN, as were the MS values after moisture conditioning.

Simulation parameters in assessing PAM's packing structure

For the four PAM designs, two types of PFC3D models were established, namely PFC3D model of compacted coarse aggregates and PFC3D model of compacted PAM specimen. Through the simulation parameters in PFC3D model of compacted coarse aggregates, namely MCN, SCR, and CCR, it is found that stable contact and chain contact were gradually developed with assistance of finer fraction in the coarse fraction. Meanwhile the packing structure in G-coarse and G_inter were mainly created by main-coarse and interceptor particles; whereas in G_fine, large-size particles in the coarse fraction tended to be scattered in the matrix of quasi-fine particles; and a relatively stable interlocking framework was established in G_cont. These findings were further confirmed in the PFC3D model of compacted PAM specimen through the relevant simulation parameters of MPF and MPF increase ratio, and the contacting mechanism in terms of force transfer within the PFC3D specimen for each PAM design was explicitly shown through the profile of particle force distribution. Moreover, the packing degree in designed PAM can be well reflected by a simulation parameter, porosity_CP ratio, which possesses the similar meaning to VCA ratio via laboratory measurement.

Experimental methods in the aspects of ravelling and clogging

To evaluate the PAMs' performance in terms of the two critical aspects, namely ravelling and clogging, ravelling resistance test and clogging resistance test were

conducted on the four designed PAMs under three testing scenarios, namely unconditioned, ageing-conditioned, and moisture-conditioned.

In ravelling resistance test, all the four designed PAMs can meet the requirements for unconditioned and ageing-conditioned Cantabro abrasion tests. Nevertheless, much more severe breakage occurred on PAM specimens in moisture-conditioned scenario. Given that the abrasion in Cantabro abrasion is much drastically severe than the practical ravelling situation in the field, a lower revolution count is suggested for assessing PAM's ravelling resistance, such as 50, 100, or 150 revolutions. In general, PAM's resistance to Cantabro abrasion is dependent on the aggregate gradation and the adhesiveness of asphalt binder as well.

In terms of clogging resistance, G_coarse showed the highest permeability along the clogging/de-clogging process among the four PAM designs, which was attributed to the higher content of large-size air voids created by high content of large-size aggregates (namely main-coarse aggregates) in the coarse fraction. Similar to the situation in ravelling resistance test, moisture conditioning is a more severe scenario for PAM's performance in effective drainage, as compared to ageing conditioning.

On the whole, among the four PAM designs, PAMs with higher content of air voids content, namely G_coarse and G_inter, generally possessed higher performance in permeability and clogging resistance, while G_inter showed stronger resistance to ravelling in the three testing scenarios. Thereby, PAM with fine fraction at 7% and 'S-shape' in the gradation curve of coarse fraction, namely with high content of interceptor aggregates, and fabricated with modified asphalt (such as PG76 asphalt) at reference gyration compaction level (namely P600_N50), is recommended for the low-strength pavement application in Singapore.

8.2 Conclusions and contributions

The conclusions and contributions of this research work are summarised as follows:

(1) The impacts of design factors (G, GCL, and ABT) on the PAM's properties are investigated and the relationship between aggregate gradation and permeability is established.

(2) The aggregates in the coarse fraction can be divided into three components in studying their role in packing structure: main-coarse (19.0-6.3 mm aggregates), interceptor (6.3-4.75 mm aggregates), and quasi-fine (4.75-2.36 mm aggregates).

(3) The potential PAMs are designed for the low-strength pavement application in Singapore, and experimental methods in three testing scenarios (namely unconditioned, ageing-conditioning, and moisture-conditioning) are applied towards assessing PAM's resistance to ravelling and clogging, which are two major issues associated with PAM.

(4) PFC3D models are established to evaluate PAM's packing condition, which can be explicitly described by the simulation parameters (e.g. porosity, MCN, and MPC) in the aspect of contacting mechanism. A simulation parameter, porosity_CP ratio is proposed to assess the aggregate interlocking, which turns out to be useful in evaluating PAM's packing degree.

(5) For the low-strength pavement application in Singapore, an open-graded design with high content of interceptor aggregates in the coarse aggregates is recommended to achieve sufficient permeability and resistance to clogging. The application of modified asphalt and adequate gyration compaction level is necessary meanwhile to ensure adequate strength and durability, especially to safeguard against moisture/ageing effects.

8.3 Future work

Based on the research work presented in this thesis, several potential studies can be conducted to extend the current findings.

In Cantabro abrasion test, impact between the PAM specimen and the inside wall of LA machine is too severe as compared with practical abrasion experienced on pavement surface. Instead of reducing the revolution counts in Cantabro abrasion test, it is more proper to design new experimental method to assess PAM's resistance to ravelling, which might involve designing and fabricating new experiment set-up. Furthermore, the measure to enhance PAM's ravelling resistance is suggested, such as increasing the asphalt binder content. Meanwhile, upon the

enhancement of PAM in the aspect of ravelling resistance and Marshall stability, the designed PAM may also be recommended for heavy trafficked roads to broaden the application.

To better assess PAM's feasibility in Singapore, a tropical country experiencing high temperature all around the year, a new test method should be developed to assess PAM's capability in generating cooling effect.

On the aspect of clogging, cleaning machines should be developed to effectively remove the dust and/or debris that block the surface of PAM pavement, alleviating impairment of PAM's drainage functionality caused by gradual clogging.

On the aspect of DEM simulation, some simplifications have been made in this research to overcome the limitation in computation efficiency. With the development of high-speed computer, modified PFC3D model can be established to better simulate the practical condition in a compacted PAM specimen, consequently resulting in a more accurate knowledge of the packing structure. Meanwhile, relevant mechanical tests shall be simulated via PFC3D as well.

In terms of permeability, it should be cautioned that PAM's permeability as measured in the laboratory may not correlate well with pavement drainage in the field due to the varying environmental situations, clogging materials, and traffic conditions. In future work, it is desirable to undertake field validation by conducting in-field permeability tests and relevant clogging resistance tests on different types of trial pavement sections. For example, four types of test sites are suggested, denoted as L1~L4: L1, a parking lot with covered shelter; L2, a shared pedestrian-cycling pathway alongside a local access road; L3, a shared pedestrian-cycling pathway alongside an arterial road; and L4, the carriageway of an arterial road. Whereas L1 site has relatively the mildest environment (without exposure to rainfall or severe ageing from direct sunlight, and limited traffic flow), L2, L3, and L4 sites are exposed to progressively more dusts and debris (clogging materials) from the heavier traffic flows, especially the heavy trucks. In this way, the loading effect of the clogging materials can be compared. Evaluation tests are to be conducted for

different periods of the year that straddle different rainfall intensity, and hence the de-clogging effect of rainfall intensity can be established.

References

Abbas, A., Masad, E., Papagiannakis, A. T. and Shenoy, A. (2005). Modelling Asphalt Mastic Stiffness Using Discrete Element Analysis and Micromechanics Based Models. International Journal of Pavement Engineering, 6(2), 137-146.

Al-Jarallah, M. and Tons, E. (1981). Void Content Prediction in Two-Size Aggregate Mixes. Journal of Testing and Evaluation, 9(1), 1.

Alvarez, A. E., Martin, A. E. and Estakhri, C. (2008). Effects of Densification on Permeable Friction Course Mixtures. Journal of Testing and Evaluation, 37(1), 11-20.

Alvarez, A. E., Mahmoud, E., Martin, A. E., Masad, E. and Estakhri, C. (2010a) Stone-on-Stone Contact of Permeable Friction Course Mixtures. Journal of Materials in Civil Engineering, 22(11), 1129-1138.

Alvarez, A. E., Martin, A. E., Estakhri, C. and Izzo, R. (2010b). Evaluation of Durability Tests for Permeable Friction Course Mixtures. International Journal of Pavement Engineering, 11(1), 49-60.

American Society for Testing and Materials [ASTM] (2008). Standard Practice for Open-Graded Friction Course (OGFC) Mix Design (Vol. D7064-08). West Conshohocken, PA.

ASTM (2011a). Standard Test Method for Maximum Specific Gravity and Density of Bituminous Paving Mixtures (Vol. D2041-11). West Conshohocken, PA.

ASTM (2011b). Standard Test Method for Determination of Draindown Characteristics in Uncompacted Asphalt Mixtures (Vol. D6390-11). West Conshohocken, PA.

Asaeda, T. and Ca, V. T. (2000). Characteristics of Permeable Pavement during Hot Summer Weather and Impact on the Thermal Environment. Building and Environment, 35(4), 363-375.

Asphalt Institute [AI] (1996). Superpave Design Method. Lexington, KY : Asphalt Institute.

AI (1997). Mix Design Methods for Asphalt Concrete and Other Hot-Mix Types. Lexington, KY : Asphalt Institute.

Australian Asphalt Pavement Association [AAPA] (2004). National Asphalt Specification, 2nd Ed., Kew Victoria.

Australian Standard [AS] (1995). Methods of Sampling and Testing Asphalt – Determination of the Resilient Modulus of Asphalt – Indirect Tensile Method (Vol. 2891.13.1). Standards Association of Australia.

Bahia, H. U., Zhai, H., Bonnetti, K. and Kose, S. (1999). Non-Linear Viscoelastic and Fatigue Properties of Asphalt Binders. Journal of the Association of Asphalt Paving Technologists, AAPT, 68, 1-34.

Barrett, M. E. and Shaw, C. B. (2007). Benefits of Porous Asphalt Overlay on Storm Water Quality. Transportation Research Record: Journal of the Transportation Research Record Board 2025, 127-134.

Bendtsen, H. and Andersen, B. (2005). Noise Reducing Pavements-State of the Art in Denmark. (Rep. No. 141), Road Directorate, Danish Road Institute, Denmark Ministry of Transport, Hedehusene, Denmark.

Bohemen, H. D. V. and Janssen Van De Laak, W. H. (2003). The Influence of Road Infrastructure and Traffic on Soil, Water, and Air Quality. Environmental Management, 31(1), 50-68.

Brattebo, B. O. and Booth, D. B. (2003). Long-Term Stormwater Quantity and Quality Performance of Permeable Pavement Systems. Water Research, 37(18), 4369-4376.

Buttlar, W. G. and You, Z. (2001). Discrete Element Modeling of Asphalt Concrete: Microfabric Approach. Transportation Research Record, 1757, 111-118.

Cai, W. McDowell, G. R. and Airey, G. D. (2013). Discrete Element Modelling of Uniaxial Constant Strain Rate Tests on Asphalt Mixtures. Granular Matter, 15, 163-174.

Charbeneau, R. J., Klenzendorf, J. B. and Barrett, M. E. (2011). Methodology for Determining Laboratory and In Situ Hydraulic Conductivity of Asphalt Permeable Friction Course. Journal of Hydraulic Engineering, 137(1), 15-22.

Chen, J. (2010). Virtual Fatigue Tests of Asphalt Mixture Based on Discrete Element Method (in Chinese). PhD Thesis, Southeast University, Nanjing, China.

Chen, J. S., Sun, Y. C., Liao, M. C., Huang, C. C. and Tsou, K. W. (2013). Evaluation of Permeable Friction Course Mixes with Various Binder and Additives. Journal of Materials in Civil Engineering, 25(5), 573-579.

Chen, M. J. and Wong, Y. D. (2013). Porous Asphalt Mixture with 100% Recycled Concrete Aggregate. Road Materials and Pavement Design, 14(4), 921-932.

Chen, M. J. and Wong, Y. D. (2015). Porous Asphalt Mixture with a Combination of Solid Waste Aggregates. Journal of Materials in Civil Engineering, 27(6).

Cheung, C. Y. and Cebon, D. (1997). Thin Film Deformation Behaviour of Power-Law Creeping Materials. Journal of Engineering Mechanics, 123(11), 1138-1152.

Cho, N., Martin, C. D., Sego, D. C. and Jeon, J. (2010). Dilation and Spalling in Axially Compressed Beams Subjected to Bending. Rock Mechanics and Rock Engineering, 43, 123-133.

Coleri, E., Kayhanian, M., Harvey, J. T., Yang, K. and Boone, J. M. (2013). Clogging Evaluation of Open Graded Friction Course Pavements Tested under Rainfall and Heavy Vehicle Simulators. Journal of Environmental Management, 129, 164-172.

Cook, R. D., Malkus, D. S., Plesha, M. E. and Witt, R. J. (2002). Concepts and Applications of Finite Element Analysis. New York, NY : Wiley, 4th Ed.

Cundall, P. A. (1971). A Computer Model for Simulating Progressive, Large-scale Movements in Blocky Rock Systems. Paper presented at the The International Symposium on Rock Mechanics Nancy, France.

Cundall, P. A. and Strack, O. D. L. (1983). Modeling of Microscopic Mechanisms in Granular Material. Paper presented at the Mechanics of Granular Materials: New Models and Constitutive Relations, Ithaca, New York.

Dondi, G., Bragaglia, M. and Vignali, V. (2007). Flexible Pavement Simulation with Distinct Particle Element Method. Paper presented at 4th International SIIV Congress, Palermo.

Dong, Q., Wu, H., Huang, B., Shu, X. and Wang, K. (2013). Investigation into Laboratory Abrasion Test Methods for Pervious Concrete. Journal of Materials in Civil Engineering, 25(7), 886-892.

Drainasphaltschichten (2001). Standards for Porous Asphalt (SN 640 433b). Konzeption Anforderung, Ausführung.

Fabb, T. R. J. (1993). The Case for the Use of Porous Asphalt in the UK: Institute of Asphalt Technology.

Fabb, T. R. J. (1998). Porous Asphalt Surface Courses. In J. C. Nicholls (Ed.), Asphalt Surfacings. London: Spon Press.

Fang, K. T. and Ma, C. X. (2001). Orthogonal and Uniform Experimental Design (in Chinese). Beijing: Science Press.

Ferguson, B.K. (2005). Porous Pavements: Boca Raton, Fla: Taylor & Francis.

Florida Department of Transportation [Florida DOT]. (2004). Florida Method of Test for Measurement of Water Permeability of Compacted Asphalt Paving Mixture (FM5-565). Florida: Department of Transportation.

Fakhimi, A. and Gharahbagh, E. A. (2011) Discrete Element Analysis of the Effect of Pore Size and Pore Distribution on the Mechanical Behavior of Rock. International Journal of Rock Mechanics and Mining Sciences, 48(1), 77–85.

Fong, M. (2012). The Weather and Climate of Singapore. Singapore: Meteorological Service Singapore.

Foster, C. R. (1982). Development of Marshall Procedures for Designing Asphalt Paving Mixtures (Vol. No. NAPA IS84): National Asphalt Pavement Association.

Foster, C. R., Monismith, C. L., Benson, F. J., Britton, W. S. G., Hargett, E. R. and Kalcheff, I. V. (1970). Effects of Aggregate Size, Shape, and Surface Texture on the Properties of Bituminous Mixtures. Highway Researcg Board, Special Report 109, 1-32.

Fuller, W. B. and Thompson, S. E. (1907). The Laws of Proportioning Concrete. Journal of Transportation Division, American Society of Civil Engineering., 59. [Cited in AI, 1996].

Furnas, C. C. (1931) Grading Aggregates I-Mathematical Relations for Beds of Broken Solids of Maximum Density. U.S. Bureau of Mines. 23(9), 1052-1058.

Fwa, T. F., Tan, S. A. and Guwe, Y. K. (1999). Laboratory Evaluation of Clogging Potential of Porous Asphalt Mixtures. Transportation Research Record, 1681, 43-49.

Ghaboussi, J. and Barbosa, R. (1990). Three-Dimensional Discrete Element Method for Granular Materials. International Journal for Numerical & Analytical Methods in Geomechanics, 14(7), 451-472.

Golden, J. and Kamil, K. (2005). A Hot Night in the Big City: How to Mitigate the Urban Heat Island. Public Works.

Good, J. F. and Lufsy, L. A. (1965). Voids, Permeability, Film Thickness vs Asphalt Hardening. Proceeding of the Association of Asphalt Pavement Technologists, 34. [Cited in Huber, 1989].

Hardiman, H. (2004). Application of Packing Theory on Grading Design for Porous Asphalt Mixtures. Civil Engineering Demension, 6(2), 57-63.

Herrington, P.R., Reilly, S. and Cook S. (2005), Porous Asphalt Durability Test: Transfund New Zealand Research Report (No. 265). Opus International Consultants Ltd, Central Laboratories, Lower Hutt, New Zealand.

Holt, R. M., Kjolass, J. K., Larsen, I., Li, L., Gotusso Pilliteeri, A. and Sonsteo, E. F. (2005) Comparison between Controlled Laboratory Experiments and Discrete Particle Simulations of the Mechanical Behaviour of Rock. International Journal of Rock Mechanics and Mining Sciences, 42, 985-995.

Hsu, T. W., Chen, S. C. and Hung, K. N. (2011). Performance Evaluation of Asphalt Rubber in Porous Asphalt-Concrete Mixtures. Journal of Materials in Civil Engineering, 23(3), 342-349.

Huang, C. W., Al-Rub, R. K. A., Masad, E. A. and Little, D. N. (2011). Three-Dimensional Simulations of Asphalt Pavement Permanent Deformation Using a Nonlinear Viscoelastic and Viscoplastic model. Journal of Materials in Civil Engineering, 23(1), 56-68.

Huber, G. (2000). Performance Survey on Open-Graded Friction Course Mixes. National Cooperative Highway Research Program, A Synthesis of Highway Practice 284. Transportation Research Board, Washington, D.C.

Itasca (2008). PFC3D Version 4.0. Minneapolis, Minnesota: Itasca Consulting Group Inc.

Japan Highway Public Corporation (1994). Design and Execution Manual for Porous Asphalt, Haisuisei-hosou Sekkei Sekou Manual, Tokyo.

James, E. (2008). Literature Review on the Effect of Porous Asphlat Roads on Water Pollution Silvia Project Report (Vol. SILVIA-TRL-008-01-WP3-240703). London: TRL.

Jiang, Y. J., Ren, J. L., Xu, Y. S. and Li., D. (2011). Simulation Method of Mechanical Properties of Graded Broken Stone Based on Particle Flow Code (in Chinese). Journal of Tongji University, 39(5), 699-704.

Kandhal, P. S. and Mallick, R. B. (1998). Open Graded Asphalt Friction Course: State of Practice. Transportation Research Board. Washington, D.C.

Kandhal, P. (2002). Design, Construction, and Maintenance of Open-Graded Asphalt Friction Courses: Information series 115, National Asphalt Pavement Association, Lanhuam, MD.

Kanitpong, K., Atud, T. J. and Martono, W. (2007). Application process of hydrated lime to resist moisture damage and rutting in asphalt mixture and revision report. Journal of the Eastern Asia Society for Transportation Studies, 7, 2051-2061.

Khalid, H. and Jimenez, P. F. K. (1995). Performance Assessment of Spanish and British Porous Asphalts Performance and Durability of Bituminous Materials. London : Spon Press.

Kim, J., Roque, R. and Byron, T. (2009a). Viscoelastic Analysis of Flexible Pavements and Its Effects on Top-Down Cracking. Journal of Materials in Civil Engineering, 21(7), 324-332.

Kim, J., Tutumluer, E. and Kwon, J. (2009b). Nonlinear Pavement Foundation Modeling for Three-Dimensional Finite-Element Analysis of Flexible Pavements. International Journal of Geomechanics, 9(5), 195-208.

Kim, S., Roque, R. and Birgisson, B. (2006). Identification and Assessment of the Dominant Aggregate Size Range (DASR) of Asphalt Mixture. Journal of the Association of Asphalt Paving Technologists, 75, 789-814.

Kluck, E., van de Ven, M., Baggen, J. and Hofman, R. (2010). Environmental Life Cycle Cost for Durable Porous Surface Layers with Synthetic Binders. International Journal of Pavement Research and Technology, 3(3), 142-148.

Knut, V. and Juned, A. (2011). Cost-Benefit Analysis of Low-Noise Pavements: Dust into the Calculations. International Journal of Pavement Engineering, 12(1), 75-86.

Koh, P. P. and Wong, Y. D. (2012). The Evolution of Cycling in Singapore. Journeys, 9, 39-50.

Land Transport Authority [LTA] (2010). Engineering Group Materials & Workmanship Specification for Civil & Structural Works. Singapore: Land Transport Authority.

Lawrence, A. M., Tia, M., Ferraro, C. C. and Bergin, M. (2012). Effect of Early Age Strength on Cracking in Mass Concrete Containing Different Supplementary Cementitious Materials: Experimental and Finite-Element Investigation. Journal of Materials in Civil Engineering, 24(4), 362-372.

Lesueur, D. and Little, D. N. (1999). Effect of Hydrated Lime on Rheology, Fracture, and Aging of Bitumen. Transportation Research Record, 1661, 93-105.

Li, L. H. and Zhang, N. L. (2004) Road Constructional Materials (in Chinese). Beijing: China Communications Press.

Liu, Y., Dai, Q. and You, Z. (2009). Viscoelastic Model for Discrete Element Simulation of Asphalt Mixtures. Journal of Engineering Mechanics, 135(4), 324-333.

Liu, Y. and You, Z. P. (2011). Accelerated Discrete-Element Modeling of Asphalt-Based Materials with the Frequency-Temperature Superposition Principle. Journal of Engineering Mechanics, 137(5), 355-365.

Lu, M. and McDowell, G. R. (2007). The Importance of Modelling Ballast Particle Shape in the Discrete Element Method. Granular Matter, 9, 69-80.

Mangulkar, M. N. and Jamkar, S. S. (2013). Review of Particle Packing Theories Used for Concrete Mix Proportioning. International Journal of Scientific & Engineering Research, 4(5), 143-148.

Mansour, T. N. and Putman, B. J. (2013). Influence of Aggregate Gradation on the Performance Properties of Porous Asphalt Mixtures. Journal of Materials in Civil Engineering, 25(2), 281-288.

Matsushima, T. and Saomoto, H. (2002). Discrete Element Modeling for Irregularly-Shaped Sand Grains. In: Proceedings of the 5th European Conference: Numerical Methods in Geotechnical Engineering, Paris.

McDowell, G. R. and Ferellec, J. F. (2010) A Method to Model Realistic Particle Shape and Inertia in DEM. Granular Matter, 12, 459-467.

McGennis, R. B., Anderson, R. M., Kennedy, T. W. and Solaimanian, M. (1995). Background of Superpave Asphalt Mixture Design & Analysis (Vol. No. FHWA-SA-95-003): the Federal Highway Administration

Micaelo, R., Ribeiro, J., Azevedo, M. and Azevedo N. (2011). Asphalt Compaction Study: Micromechanical Modelling of a Simplified Lab Compaction Procedure. Road Materials and Pavement Design, 12(3), 461-491.

National Enivronment Agency [NEA] (2014). Weatherwise Singapore. [Online] http://app2.nea.gov.sg/training-knowledge-hub/publications/annual-weather-review Singapore: National Enivronment Agency. Retrieved 12-Sept, 2014.

NEA (2015). Weatherwise statistics. [Online] http://www.nea.gov.sg/weather-climate/climate-information/weather-statistics Singapore: National Enivronment Agency. Retrieved 24-March, 2015.

Nelson, P. M. and Abbott, P. G. (1990). Acoustical Performance of Pervious Macadam Surfaces for High-Speed Roads. Transportation Research Record, 1265, 25-33.

Nicholls, J. C. (1997). Review of UK Porous Asphalt Trials (Vol. TRL Report 264). London: Transport Research Laboratory.

Nicholls, J. C. and Carswell, I. G. (2001). The Design of Porous Asphalt Mixtures to Performance-related Criteria Crowthorne, Berkshire, England : Transport Research Laboratory, 2001.

Noramuena-Contreras, J., Izqierdo, E. A., Castro-Fresno, D., Partl, M. N. and Garcia, A. (2013). A New Model on the Hydraulic Conductivity of Asphalt Mixtures. Journal of Pavement Research and Technology, 6(5), 488-495.

Papagiannakis, A.T. and Masad, E.A. (2008) Pavement Design and Materials. Hoboken N J :Wiley & Sons.

Poulikakos L. D. and Partl M. N. (2010). Investigation of Porous Asphalt Microstructure using Optical and Electron Microscopy. Journal of Microscopy, 240, 145-154.

Putman, B. J. and Kline, L. C. (2012). Comparison of Mix Design Methods for Porous Asphalt Mixtures. Journal of Materials in Civil Engineering, 24(11), 1359-1367.

Punith, V. S., Suresha, S. N., Raju, S., Bose, S. and Veeraragavan, A. (2009) Laboratory Investigation of Open-Graded Friction-Course Mixtures Containing Polymers and Cellulose Fibers. Journal of Transportation Engineering, 138(1), 67-74.

Qian S., Ma, H., Feng, J., Yang, R. and Huang, X. (2014) Fiber Reinforcing Effect on Asphalt Binder under Low Temperature. Construction and Building Materials, 61, 120-124.

Qin, M. (2004). Study on Application of Modifiers to Performance of Porous Asphalt Mixture (in Chinese). Master Thesis, Southeast University, Nanjing.

Rajib, B. M., Prithvi, S. K., Cooley, L. A. and Donald, E. W. (2000). Design, Construction, and Performance of New-Generation Open-Graded Friction Courses: National Center for Asphalt Technology.

Robert, F. L. (1996). Hot Mix Asphalt Materials, Mixture Design, and Construction (2 ed.). Lanham, Md: NAPA Educational Foundation.

Roque, R., Huang, S. and Ruth, B. E. (1997). Maximizing Shear Resistance of Asphalt Mixtures by Proper Selection of Aggregate Gradation. The 8th International Society for Asphalt Pavements, Seattle, 249-268.

Ruiz, A., Aurelio, R., Perez, F. and Sanchez, B. (1990). Porous Asphalt Mixtures in Spain. Transportation Research Record, 1265, 87-94.

Rungruangvirojn, P. and Kanitpong, K. (2010). Measurement of visibility loss due to splash and spray: porous, SMA and conventional asphalt pavements. International Journal of Pavement Engineering, 11(6), 499-510.

Ruth, B. E., Roque, R. and Nukunya, B. (2002). Aggregate Gradation Characterization Factors and Their Relationship to Fracture Energy and Failure Strain of Asphalt Mixtures. Journal of the Association of Asphalt Paving Technologists, 71, 310-344.

Shashidhar, N., Zhong, X., Shenoy, A. V. and Bastian Jr, E. J. (2000). Investigating the Role of Aggregate Structure in Asphalt Pavements. Paper presented at the 8th annual symposium on aggregate, asphalt concrete, bases and fines, Denver.

Shen, S. H. and Yu, H. N. (2010). Determination of HMA Voids in Mineral Aggregate Based on the Analysis of Aggregate Gradation and Packing. Presented on 89th TRB Annual Meeting.

Shen, S. H. and Yu, H. N. (2011). Characterize Packing of Aggregate Particles for Paving Materials: Particle Size Impact. Construction and Building Materials, 25(3), 1362-1368.

Shuler, S. and Hanson, D. I. (1990). Improving Durability of Open-graded Friction Courses. Transportation Research Record, 1259, 35-41.

Smith, R. W., Rice, J. M. and Spelman, S. R. (1974). Design of Open-Graded Asphalt Friction Courses (Vol. FHWA-RD-74-2). Washington, D.C.: Federal Highway Administration.

Smith, W. O., Foote, P., D. and Busang, P. F. (1929). Packing of Homogeneous Spheres. Physical Review, 34, 1271-1274.

Starke, P., Gobel, P. and Coldewey, W.G. (2010). Urban Evaporation Rates for Water-permeable Pavements. Water Science & Technology, 62 (5), 1161-1169.

Suresha, S. N., George, V. and Shankar, A. U. R. (2009). Evaluation of Properties of Porous Friction Course Mixes for Different Gyration Levels. Journal of Materials in Civil Engineering, 21(12), 789-796.

Suresha, S. N., George, V. and Shankar, A. U. R. (2010). Effect of Aggregate Gradations on Properties of Porous Friction Course Mixes. Materials and Structures, 43, 789-801.

Tan, S. A., Fwa, T. F. and Guwe, V. Y. K. (2000). Laboratory Measurements and Analysis of Clogging Mechanism of Porous Asphalt Mixes. Journal of Testing and Evaluation, 28(3), 207-216.

Tappeiner, W. (1993). Open-Graded Asphalt Friction Course, Information Series 115, National Asphalt Pavement Association, Lanham, MD.

Tayfur, S., Ozen, H. and Aksoy, A. (2007). Investigation of Rutting Performance of Asphalt Mixtures Containing Polymer Modifiers. Construction and Building Materials, 21(2), 328-337.

Texas Department of Transportation [TxDOT] (2004). Standard Specifications for Construction and Maintenance of Highways, Streets, and Bridges Adopted by the Department of Transportation. Austin, TX.

Transit New Zealand (2007). Specification for Open Graded Porous Asphalt (SP/SP 11 070704). Ararau Aotearoa.

Vallerga, B. A. and Lovering, W. R. (1985). Evolution of the Hveem Stabilometer Method of Designing Asphalt Paving MIxture. Association of Asphalt Paving Technologists, 54.

van Bochove, G. G. (1996). Twinlay, a New Concept of Drainage Asphalt Concrete. Paper presented at the 1st Eurobitume and Euroasphalt Congress.

Vavrik, W. R. (2000). Asphalt Mixture Design Concepts to Develop Aggregate Interlock. PhD thesis, University of Illinois at Urbana-Champaign, Urbana, Illinois.

Vavrik, W. R., William, J. P., and Carpenter, S. H (2002). Bailey Method for Gradation Selection in HMA Mixture Design. Transportation Research Circular (No. E-C044).

Walpole, R. E., Myers, R. H., Myers, S. L. and Ye, K. (1998). Probability and Statistics for Engineers and Scientists (6^{th} ed.). Upper Saddle River, N. J.: Prentice Hall International Inc.

Waterson, D. E., Masad, E., Moore, K. A., Williams, K. and Cooley, L. A., Jr. (2004). Verification of Voids in Coarse Aggregate Testing: Determining Stone-On-Stone Contact Of Hot-Mix Asphalt Mixtures. Transportation Research Record, 1891, 182-190.

Watson, D. E., Moore, K. A., Williams, K. and Cooley Jr, L. A. (2003) Refinement of New-Generation Open-Graded Friction Course Mix Design, Transportation Research Record, 1832, 78-85.

White, T. D. (1985). Marshall Procedures for Design and Quality Control of Asphalt Mixtures. Association of Asphalt Paving Technologists, 54.

Wikipedia (2015). Chain. [Online] https://en.wikipedia.org/wiki/Chain Retrieved 24-July, 2015.

Wu, J. Wu., Collop, A. C. and McDowell, G. R. (2011). Discrete Element Modeling of Constant Strain Rate Compression Tests on Idealized Asphalt Mixture. Journal of Materials in Civil Engineering, 23(1), 2-11.

Yideti, T. F., Birgisson, B. Jelagin, D., and Guarin, A. (2013). Packing Theory-Based Framework to Evaluate Permanent Deformation of Unbound Granular Materials. International Journal of Pavement Engineering, 14(3), 309-320.

You, Z. P., Adhikari, S. and Dai, Q. L. (2008). Three-Dimensional Discrete Element Models for Asphalt Mixtures. Journal of Engineering Mechanics, 134(12), 1053-1062.

You, Z. P., Liu, Y. and Dai, Q. L. (2011). Three-Dimensional Microstructural-Based Discrete Element Viscoelastic Modeling of Creep Compliance tests for Asphalt Mixtures. Journal of Materials in Civil Engineering, 23(1), 79-87.

Yu, H. N. and Shen, S. H. (2012). Impact of Aggregate Packing on Dynamic Modulus of Hot Mix Asphalt Mixtures Using Three-Dimensional Discrete Element Method. Construction and Building Materials, 26, 302-309.

Yu, H. N. and Shen, S. H. (2013). A Micromechanical Based Three-Dimensional DEM Approach to Characterize the Complex Modulus of Asphalt Mixtures. Construction and Building Materials, 38, 1089-1096.

Zhang, M. M. and Hao, P. W. (2012). Effects of Parameters Designed by Bailey Method on the Property of Porous Asphalt Mixture. Advanced Materials Research 374-377: 1414-1419.

Zhu, Z. H. (2005). The Application of 'Bailey Method' in Porous Asphalt (in Chinese). Master Thesis, Taiwan National Cheng Kung University, Taiwan.

Zulkati, A., Wong, Y. D. and Sun, D. D. (2012a). Effects of Fillers on Properties of Asphalt Concrete Mixture. Journal of Transportation Engineering, 138(7), 902-910.

Zulkati, A., Wong, Y. D. and Sun, D. D. (2012b). Mechanistic Performance of Asphalt Concrete Mixture Incorporating Coarse Recycled Concrete Aggregate (RCA). Journal of Materials in Civil Engineering, 25(9), 1299–1305.